Physics and Physical Oceanography Technical Report
2000-2

Circulation Through the Narrows of St. John's Harbour: Summer 2000

Brad deYoung, Douglas J. Schillinger and Jack Foley

Department of Physics and Physical Oceanography
Memorial University of Newfoundland
St. John's, Newfoundland
A1B 3X7

Abstract

Current, temperature, and surface elevation are presented from St. John's harbour for 29 July to 18 September 2000. Three Acoustic Doppler Current Profiler's (ADCPs) and two S4 current meters were deployed in the Narrows of St. John's Harbour to measure the current velocities at the mouth of the harbour. The integrated, along-channel, interpolated current agrees well with the observed sea-surface elevation at tidal periods. It is therefore clear that the cross-channel measurements provide a good description of the current flow through the Narrows. At longer periods, beyond 2-4 days, the agreement between the integrated currents and the sea-surface elevation is not as good, for reasons that we do not understand. One ADCP, one S4 current meter, one RCM current meter, and 13 Vemco thermistors were deployed outside the Narrows to measure the flow of the Avalon current. Analysis of the temperature data shows strong coherence at longer periods, 2-4 days, between the temperature signals measured in the Narrows and those above 25 m depth outside the Narrows. The strongest tidal variation outside the Narrows is parallel to the alongshore direction, north-south. Within the channel, more than 90% of the current variance, at all periods, is directed along the channel.

Acknowledgements

We thank the St. John's Harbour Authority for permission to work in the Narrows again. In particular, we thank Dave Methven and the divers from the Ocean Sciences Centre for their support and for working in a difficult area. We acknowledge financial support from NSERC to BdeY.

Table of Contents

List of Tables

List of Figures

Introduction

The city of St. John's is located on the Northeast coast of the Avalon Peninsula on the Island of Newfoundland, Canada. The harbour mouth opens to the east, has a large sill and narrow entry to a shallow protected bay that has a somewhat deeper basin in the northeastern half of the harbour. The mean depth of the harbour is about 12-15 m, the sill depth is 13 m and the width of the harbour mouth is approximately 180 m. The deepest point of the harbour is about 33m. The channel leading to the sill, the Narrows, is approximately 800 m long and the harbour itself is about 1200m long. The harbour has a surface area of approximately 1.2 million square metres. We report on new measurements made in the Narrows, and just outside, that resolve some of the problems of an earlier study by deYoung et al. (2000). Due to the poor determination of the mean flow through the harbour mouth in deYoung et al. (2000), we deployed 5 instruments (indicated by red stars in Figure 1) 275 m east of the inner harbour mouth, which is demarcated by Chain Rock and Anchor Point. The distance across the Narrows following the curve subtended by the mooring locations is roughly 350 m. The cross sectional area of the Narrows at this point is approximately 5000 square metres.

In 1999 we deployed a pair of Acoustic Doppler Current Profilers (ADCPs) in the Narrows of St. John's Harbour in order to determine the characteristics of flow through the Narrows and to quantify the exchange and flushing rates of the Harbour (deYoung et al. 2000). While the project was somewhat successful, and much was learned about the dynamics of the currents in the Narrows, it was also clear that the single measurement of currents in the middle of the channel was inadequate. We integrated the along-channel, currents to determine the expected change in sea-level driven by the currents for comparison with the observed sea-level and found very poor agreement. This disagreement, and other analysis of the data, clearly showed that the cross-channel measurements were not representative of currents across the channel and that there had to be substantial cross-channel shear of the along channel currents. For this reason, we decided to repeat the 1999 experiment with additional instruments in an attempt to properly resolve the cross-channel current structure.

During the summer of 2000, three upward-looking Acoustic Doppler Current Profilers (ADCPs) and two S4 current meters were deployed in the Narrows (Figure 1, Table 1). In addition, one ADCP, one S4 and one RCM current meter were deployed outside the harbour mouth, along with thirteen Vemco thermistors (Inset Figure 1, Table 1). Our primary goal was to determine the circulation over the sill and the influence of external forcing, from the Avalon Channel, on the transport into and out of the Narrows. Temperature sensors were located on the each of the instruments. Surface height data recorded at the Coast Guard docks inside the harbour was obtained from the MEDS website (www.meds-sdmm.dfo-mpo.gc.ca/meds/Home_e.htm).

Mooring data is tabulated with statistics on the mean, standard deviation, maximum and minimum in each velocity component in Tables 2-9. The velocity data are presented graphically: time series at selected depths, power spectral density of the hourly time series, profile plots, tidal ellipse plots and low-pass filtered sub-tidal plots. We also calculated the flow along the channel using an inverse linear squared distance interpolation routine, using a grid size of 25 m by 1 m in the horizontal and vertical respectively. From this interpolation, the transport and change in height of the harbour water level in the harbour was calculated and compared to the observed surface elevation. Tidal analysis was conducted on both the velocity and height data. The results are presented graphically, with summary statistics in tabular format.

A Water Level Recorder measured the surface elevation in the Narrows at N5. These results are compared to both the MEDS data from inside the harbour and the calculated change in height from the current data.

Station Information

Near the sill, the channel entering St. John's Harbour is very narrow, measuring less than 200m across at the mouth. The instruments were deployed 275 m East of the mouth in the channel leading to the North Atlantic, which is called 'the Narrows'. We chose to centre the mooring line in the middle of the channel, halfway between the mouth and the entrance to the Harbour, to minimize the end-effects of the channel. Following the curve connecting instrument locations (Figure 1), the distance across the channel is

350 m. The ADCP's were each set to measure the current velocities in Earth co-ordinates with bin sizes of 1 m in the vertical. The S4's recorded the velocity at the depth at which they were deployed, and are assumed to reflect the average velocity in the 25 m by 1m bin in the two dimensional interpolation. The number of current measurements was meant to over-sample the region, in order to observe the complicated flow through the Narrows, which was hypothesized by deYoung et. al (2000). Our goal was to get a horizontal resolution of 60-70 m. Unfortunately, the ADCP at N2 was deployed closer than planned to N1. The depth for N2 was, however, very close to the intended depth and so the data from N2 was still very useful in spite of the mis-location of the ADCP. Given the channel geometry, we believed that most of the flow would be directed along the axis of the channel.

Table 1: Mooring Locations

Mooring	Latitude	Longitude	Bin Width (m)	Depth (m)	Sampling Interval (minutes)
N1 (s1555)	47 33.9	54 41.1	N/A	7.2	20
N2 (a718)	47 33.9	54 41.1	1	21.2	20
N3(a879)	47 33.9	54 41.0	1	22.5	20
N4(a1316)	47 34.0	54 41.0	1	17.9	20
N5(s1561) (tg133)	47 34.0	54 41.0	N/A	12.7	20
H1 (oasis)	47 34.15	52 39.75	N/A	109	10
H1 (s1559)	47 34.15	52 39.75	4	22	20
H2(r128)	47 34.15	52 38.64	N/A	77	20

The nomenclature for referencing the moorings is N for the Narrows, and H for outside the harbour. The letter/number combination after the mooring number presented in Table 1 is a letter representing the device type (a for ADCP; s for S4; r for RCM; tg for tidal gauge) and the serial number of the instrument.

Data Analysis

Data collected during the deployment and recovery of the instruments were first clipped from all the records. Isolated incidents of bad data points were eliminated using a simple linear interpolation scheme. The wind speed data had only one bad data point, while all other data did not record nonsensical data.

We determined the along-channel and cross-channel axes through a covariance analysis to locate the angle that minimized the variance along one component of a set of perpendicular axes. The current data from outside the Narrows did not yield consistent results with each depth. The instruments in the Narrows showed both a depth dependence and a location dependence for the angle required to minimize the variance. While the values determined by the covariance analysis indicated a rotation of approximately 30 degrees was required, the dependence on both depth and location prevented a single best angle of rotation to be determined by trial and error. Instead, a rotation angle of 10 degrees was used, and was determined from the line connecting the planned locations of the instruments (purple line in Figure 1).

For the data collected by the ADCPs, the surface was located by examining the backscatter intensity contours and identifying the depth bin with the most intense backscatter signal. Additional depth bins were discarded on the basis of shear in the velocity profile. For the ADCP at N2, N3, and N4 this resulted in the additional exclusion of two depth bins below the bin that recorded the maximum backscatter intensity, while H1 excluded 5.

For tidal analysis, we applied the harmonic analysis routines of Foreman (1977), which require that the time series be in hourly intervals. To this end, data for the tidal analysis were first filtered using a third order low-pass Butterworth filter with a pass band of 3 hours and a stop band of period 2 hours in order to remove high frequency fluctuations in the data. The data were then subsampled at 1-hour intervals as required by the tidal analysis software. For consistency with the results from Foreman's analysis, the entire data set was smoothed with the low-pass filter and subsampled at hourly intervals. The MEDS data and wind speed data were sampled at one hour intervals and did not require this filtering process.

Although the length of the record allows for the determination of several additional constituents, only five primary constituents are included: MSf, O_1, K_1, M_2 and S_2. The calculation was performed using a Rayleigh scaling factor 3.0. Both the axes of the representative tidal-ellipses and the corresponding Greenwich phase describe the main constituents of the tidal currents. The inclination of the ellipse indicates the angle the semi-major axis makes with the positive x-axis (10^{o} clockwise rotation from Earth axes). A positive value for the length of the semi-major axis indicates that the current rotates counter clockwise around the tidal ellipse, while a negative value indicates a clockwise rotation.

In addition to the summary information provided from the harmonic analysis, the time series were filtered using a least squared method to remove tidal signals at the MSf, O_1, K_1, M_2 and S_2 frequencies. In addition to removing the tidal signals, the velocity fluctuations at the inertial period (approximately 16 hours for this latitude) were removed using complex demodulation. The residual of this filter was then low-pass filtered with a third order Butterworth filter with a cut-off period of 1.6 days.

Interpretation

The strongest tidal signal from each of the current meters is the M_2 tide. This is evident from the tabulated data Tables 9-15) as well as the tidal ellipse figures (Figures 7-9, 41). The M_2 signal is strongest along the In/Out axes of the Narrows, and the North/South axes outside the Narrows. In addition, the M_2 signal decreases with depth at each of the current meter locations. There is little change in phase with depth except near the very bottom. The K_1 tidal signal does not show any consistent inclination with depth, nor much change in magnitude with depth. The K_1 tidal constituent is weak relative to the M_2 and it may be that the weakness of the K_1 is the reason for the lack of vertical structure.

The time series plots for currents in the Narrows (e.g. Figure 2) shows that while the tide dominates the sea surface elevation the current record is strongly influenced by the lower frequencies and the importance of the tidal signal is less obvious. The wind stress time series shows the typical spiky character of all wind data with low-frequency events at periods of 2-5 days.

The power spectral density at N2 (Figure 11), N3 (Figure 12) and N4 (Figure 13) show that the M_2 tidal spike, at roughly 2 cycles per day (cpd), is strongly surface intensified as indeed is also true at lower frequencies below 1 cpd. Energy at the lower frequencies below 1 cpd extends deeper into the water column. At N3 and N4, the power spectrum is fairly uniform with depth below 0.5 cpd. Comparison of the plots shows that M_2 tidal energy is greatest on the southern side of the channel. There is more energy at the lowest frequencies, below 0.5 cpd, on the northern side of the channel.

Observations made in 1999 (deYoung et al. 2000) revealed strong inflow at 2-4 days period that extended from the bottom to the surface. There was, however, only a single current measurement made in the middle of the channel and deYoung et al. questioned whether the observations at that single point were indeed representative of the transport through the channel. With the additional instruments deployed this year, it is now apparent that the 2-4 day inflow events do show significant cross-channel structure. The strong outflow event on 18 August that extends from the bottom to the surface at N4 is limited to the bottom 5 metres at N3 and is not at all apparent at N2. Immediately following this event there is the strong inflow which is limited to the top 10 m of the water at N2, extends from 17m depth to the surface at N3 and is almost completely absent at N4. In general the inflow events are strongest in the centre of the channel, and weakest on the north side of the channel which exhibits more outflow events, and more outflow on average, than does the centre of the channel or the southern side.

The mean currents are strongest nearest the surface, just under 2 cm/s at N1 and 4 cm/s at N3. The profiles of the mean along-channel velocity (Figures 21-23) reveal a strong inflow at depths from 5-10m, and only weak outflow near the surface and the bottom. This profile shape looks very similar to the profiles observed in 1999 (see Figure 9 in deYoung et al. 2000). In that study, a single ADCP in the centre of the channel at the western end of the Narrows showed outflow at the surface and the bottom and inflow centred at about 6 m depth. We integrated the full cross-channel velocity to determine the mean velocity depth-by-depth to determine the true depth-averaged cross-channel velocity, which should integrate to zero from the bottom to the surface, but clearly does not (Figure 24). The discrepancy suggests that we may not have adequately measured the low-frequency velocity, even with an array of three ADCP's and two S4 current meters.

By using the measured data in the Narrows, a two dimensional approximation of the flow is determined using grid spacing of 25 m by 1 m. The mean current shows the importance of the inflow events apparent in Figures 18 and 19, with the mean inflow peaking at depths between 8 and 10 metres. As with the 1999 data set, there is still a problem with the mean transport skewed towards inflow suggesting that the inflow events are over-represented and that the outflow, which appears to be concentrated on the northern side of the channel, may not have been properly observed. The peak of the mean inflow is in the channel (Figure 25) with most of the inflow on the northern side of the channel. Mean outflow only occurs near the bottom in the centre of the channel and near the surface on the southern side of the channel.

Sample snapshots of the velocity through the channel are developed by interpolation of the velocity field across the channel (Figures 26-30). These figures show the difference in structure across the channel on ebb and flood tide. Figure 28 shows the state of the ebb and flood tides on day 225. This figure reveals that during the ebb tide there is strong inflow on the northern side of the channel with the outflow associated with the ebbing tide concentrated on the bottom, not the surface as one might expect, on the southern side of the channel. During the flood tide the strongest inflow is on the southern half of the channel and during the peak flood tide there is strong outflow at the bottom in the centre of the channel. Figures 26 and 30 show that the structure of the ebbing and flooding tide is not fixed; there are times when the strong ebb tide does generated strong surface outflows, in general on the northern side of the channel, and that not all flood tides lead to bottom intensified outflows.

Coherence squared analysis of temperature shows that the strongest coherence is between neighbouring moorings, not surprisingly, and that the greatest overall coherence occurs between N2 and N3, in the centre of the channel, where there is strong coherence at pretty much all frequencies between 0 and 4 cpd (Figure 31).

Moorings were deployed outside the Narrows (Figure 1) to provide information about the external forcing that would be likely to influence the flow through the Narrows. The temperature time series from the nearshore mooring (Figure 33) shows an increase in temperature later in the record at depths of 20-35 m. This warming is not the result of surface heating that develops during the fall, since in fact the reverse occurs and cooling

begins to become more important as the fall progresses, but rather a downward mixing of warm surface water. In addition, there are many wind-forced events apparent in the time-series that show durations of 2-3 days.

Coherence squared between the near-surface temperature (at 22 m depth) outside at H1 and N1-N5 reveals very little coherence at the tidal period, not surprising since there is little evidence of a baroclinic tide at H1 (Figure 41), but significant coherence at lower frequencies, below 0.5 cpd (Figure 34). This low-frequency coherency supports the idea that the low-frequency inflow events are externally forced. Further analysis is required to determine the nature of this forcing and the source of the external low-frequency signal.

Figure 36a shows the surface elevation plots for a 10 day period measured in the harbour (MEDS, dashed line) and in the Narrows by the water level recorder (WLR, solid line). There are clear periods where the two records do not match (day 210, 216-219), indicating that this might be a choked system. In other words, the height in the Narrows is not completely representative of the height in the harbour. This lack of continuity is more clear in the sub-tidal plots of surface elevation in the Figure 37b. Here, there is both a time lag of approximately one day, as well as periods of complete mismatch.

By integrating the flow field, and multiplying by the cross sectional area of each bin, the flow through the Narrows is calculated. Scaling this transport by the appropriate sampling time (one hour intervals), the change in surface elevation is determined. This change in elevation is compared to the change in elevation observed by both the MEDS and WLR in Figure 37a. To get this figure, the subtidal transport was first subtracted from the raw transport. We can see that over this 10 day period, the change in surface elevation at tidal frequencies is well determined. However, examining Figures 37b and c show that at the sub-tidal frequencies there is a large transport into the harbour which is not observed by either the WLR or the MEDS.

The currents outside the harbour are surface intensified with most of the variance directed along the direction of the topography parallel to the coastline (Figure38 and 39). Thus most of the variance is in the north-south direction with peak component speeds of greater than 25 cm/s at 22 m depth at mooring location H1 (see Figure 1). The low-passed current time-series (Figures 42 and 43) show substantial energy at 2-5 day periods

as is common everywhere in the coastal oceans of the Northwest Atlantic (deYoung et al. 1993). Power spectral plots (Figures 46-47) show much flatter low-frequency spectra than are found in the Narrows of the Harbour with little evidence for a distinct peak at the semi-diurnal tidal frequency. The low-frequency currents also show relatively little depth dependence at the outer H2 mooring (Figure 48).

Rotary spectral analysis comparing the wind speed to the current speed does not yield any significant results. There is no coherence between either component of wind speed and either component of current velocity. This is not surprising and is consistent with similar analysis carried out by deYoung et al. (1993) in Conception Bay. Rotary cross-spectral analysis between the near-surface S4 at 22 m depth at H1 and the currents observed at N3 show that there is significant coherence squared, greater than – 7, at the bottom and near the surface, at positive frequencies below 0.5 cpd but no significant coherence at any other depths and frequencies. There is therefore some support, in the straight temperature coherence analysis and the rotary current coherence analysis, that external forcing from outside the Narrows, at long periods is responsible for the observed low-frequency current inflows observed in the Narrows.

Comparisons of the temperature and velocity outside the Narrows, at H1, with temperature and velocity inside the Narrows confirm the results of the time series analysis. Temperature time series show changes in temperature of 2-3 ^{o}C over periods of a day or less, e.g. between days 223 and 224 (Figure 54). These temperature changes must result from the advection of water from outside the Harbour, or vertical movement of water associated with upwelling or Kelvin wave dynamics. Plots of velocity components at N3 and outside the Narrows at H1, reveal that the peak outflow events in the Narrows, positive velocities, are associated with strong northeasterly velocities outside the Narrows, e.g. at days 218 and 224 in Figures 54 and 55. The strong outflows in the Narrows are limited to near-bottom intensified currents with strong inflows nearer or at the surface. Such events are observed early in the period (days 215-225 in Figures 54 and 55) and later as well (days 230-240 in Figures 56 and 57). The strong coherence between the temperature and velocity outside and inside the Narrows confirms that the low-frequency exchange of water into and out of the Harbour is determined by external forcing. This analysis does not confirm the dynamical character of this response although

earlier work in Conception Bay (deYoung et al. 1993) has shown that most of the low-frequency response in the coastal waveguide is wind-forced upwelling-downwelling activity.

The backscatter plots (Figures 50-53), corrected for spherical spreading and chemical absorption, show that there is substantial cross-channel variability in the backscatter intensity although it is clear that the big events, e.g. late in July, are strongly coherent within the Narrows. Big events of backscatter that occur outside the Narrows, e.g. just before 18 August, do not appear to have much impact on the Narrows, i.e. the backscatter events in the Narrows are not externally generated.

References

deYoung, B., Otterson, T. and R. Greatbatch. 1993. The local and non-local response of Conception Bay to wind forcing. *J. Phys. Ocean*., 23, 2636-2649.

deYoung, B., Schillinger, D.J., Zedel, L, and Jack Foley. 2000. Circulation Throught the Narrows of St. John's Harbour: Summer and Fall 1999. *Physics and Physical Oeanography Technical Report 2000-1*, Memorial University of Newfoundland, St. John's Newfoundland.

Davidson, F. , Greatbatch, R. and B. deYoung. 2000. Asymmetry in the response of a stratified coastal embayment to wind forcing. *J. Geophys. Res*. (in press).

Foreman, M. 1977. Manual for Tidal Heights Analysis and Prediction, *Pacific Marine Science Report 78-6*, Institute of Ocean Sciences, Patricia Bay, Victoria B.C.,

Tabulated Data

Table 2: Summary statistics for S4 current velocities at N1. Std is one standard deviation**.**

Depth (m)	Component	Mean (cm/s)	Std (cm/s)	Max (cm/s)
7.2	u	0.80	2.40	13.78
	v	0.23	1.41	7.13

Table 3: Summary statistics for ADCP current velocities at N2. . Std is one standard deviation**.**

Depth (m)	Component	Mean (cm/s)	Std (cm/s)	Max (cm/s)
18	u	0.25	3.01	11.79
	v	-0.86	2.00	10.72
17	u	0.19	2.43	9.94
	v	-0.07	1.27	4.31
16	u	0.03	2.28	8.25
	v	-0.01	1.31	6.53
15	u	-0.14	2.22	9.06
	v	0.16	1.47	5.24
14	u	-0.26	2.24	7.81
	v	0.52	1.82	8.43
13	u	-0.63	2.17	9.89
	v	0.24	1.91	8.70
12	u	-0.72	2.14	9.47
	v	0.38	1.37	5.55
11	u	-0.98	2.17	8.36
	v	0.54	1.72	7.33
10	u	-1.30	2.24	9.21
	v	0.57	1.46	6.64
9	u	-1.51	2.27	9.06
	v	0.68	1.51	6.29
8	u	-1.61	2.36	11.35
	v	0.91	1.68	7.92
7	u	-1.86	2.52	12.05
	v	0.87	1.83	8.64
6	u	-1.75	2.98	15.59
	v	0.83	1.98	10.40
5	u	-1.31	3.48	17.16
	v	0.71	2.17	10.01
4	u	-0.29	4.05	16.60
	v	0.29	2.41	13.88
3	u	1.79	5.08	18.07
	v	0.44	2.60	13.04

Table 4: Summary statistics for the ADCP current velocities at N3. Std is one standard deviation**.**

Depth (m)	Component	Mean (cm/s)	Std (cm/s)	Max (cm/s)
20	u	2.06	4.56	18.42
	v	-1.37	2.96	11.35
19	u	2.03	4.63	20.29
	v	-1.25	2.81	12.61
18	u	1.60	4.60	22.49
	v	-1.08	2.64	11.22
17	u	1.08	4.55	18.59
	v	-1.01	2.46	10.77
16	u	0.37	4.44	19.33
	v	-0.80	2.28	9.26
15	u	-0.48	4.28	18.17
	v	-0.55	2.08	10.15
14	u	-1.30	4.05	15.75
	v	-0.34	1.91	9.67
13	u	-2.07	3.75	13.94
	v	-0.07	1.83	7.96
12	u	-2.89	3.50	13.16
	v	0.21	1.82	9.10
11	u	-3.59	3.55	16.02
	v	0.52	1.95	9.22
10	u	-4.21	3.53	17.67
	v	0.79	2.04	9.71
9	u	-4.60	3.50	17.79
	v	0.96	2.20	11.03
8	u	-4.53	3.55	16.64
	v	1.08	2.30	10.47
7	u	-4.23	3.57	15.52
	v	1.13	2.28	9.55
6	u	-3.38	3.83	13.80
	v	1.12	2.29	10.95
5	u	-2.22	4.31	19.04
	v	0.95	2.41	12.20
4	u	-0.98	5.08	27.01
	v	0.72	2.83	18.20

Table 5: Summary statistics for the ADCP current velocities at N4. Std is one standard deviation**.**

Depth (m)	Component	Mean (cm/s)	Std (cm/s)	Max (cm/s)
11	u	-1.71	2.55	10.00
	v	-0.27	1.81	7.63
10	u	-2.10	2.87	12.20
	v	-0.02	1.80	7.03
9	u	-2.55	3.11	12.60
	v	0.29	1.78	8.43
8	u	-2.85	3.26	13.50
	v	0.48	1.73	7.84
7	u	-3.05	3.43	16.10
	v	0.56	1.76	8.35
6	u	-2.93	3.46	15.00
	v	0.61	1.83	7.96
5	u	-2.53	3.48	18.30
	v	0.58	1.79	8.48
4	u	-1.79	3.47	15.00
	v	0.56	1.85	8.91
3	u	-0.74	3.60	15.00
	v	0.33	1.91	9.67

Table 6: Summary statistics for the S4 current velocities at N5. Std is one standard deviation**.**

Depth (m)	Component	Mean (cm/s)	Std (cm/s)	Max (cm/s)
12.7	u	-0.24	1.81	14.80
	v	-0.34	1.09	5.94

Table 7: Summary statistics for the current velocities at H1. S4 measured at 22 m, RCM at 77 m. Std is one standard deviation**.**

Depth (m)	Component	Mean (cm/s)	Std (cm/s)	Max (cm/s)
77	u	-0.54	2.09	11.00
	v	-0.09	2.79	15.80
22	u	0.48	4.81	17.40
	v	0.94	8.23	32.60

Table 8: Summary statistics for the ADCP current velocities at H2. Std is one standard deviation**.**

Depth (m)	Component	Mean (cm/s)	Std (cm/s)	Max (cm/s)
96	u	-0.50	3.07	13.49
	v	-0.76	3.52	19.35
92	u	-0.32	3.06	14.46
	v	-0.64	3.59	17.36
88	u	-0.18	2.97	13.19
	v	-0.49	3.50	16.19
84	u	-0.13	2.89	12.29
	v	-0.17	3.62	18.72
80	u	-0.12	3.11	13.07
	v	-0.09	3.83	20.09
76	u	-0.14	3.30	12.83
	v	0.01	4.09	21.42
72	u	-0.22	3.52	16.19
	v	-0.07	4.23	20.85
68	u	-0.21	3.83	19.67
	v	-0.24	4.38	22.30
64	u	-0.19	4.06	19.91
	v	-0.42	4.50	22.11
60	u	-0.16	4.01	20.36
	v	-0.53	4.44	18.90
56	u	-0.06	3.84	16.26
	v	-0.68	4.21	16.93
52	u	-0.09	3.49	14.91
	v	-0.83	3.91	18.43
48	u	-0.07	3.22	16.59
	v	-0.97	3.72	20.66
44	u	-0.08	3.16	17.61
	v	-1.21	3.65	19.51
40	u	-0.18	3.35	16.54
	v	-1.44	3.95	24.81
36	u	-0.33	3.64	18.78
	v	-1.88	4.57	24.37
32	u	-0.72	4.01	20.15
	v	-2.40	5.53	22.48
28	u	-1.13	4.53	22.35
	v	-3.12	6.40	25.70
24	u	-0.72	4.38	24.30
	v	-3.12	6.42	28.42
20	u	3.73	14.82	41.82
	v	1.87	17.90	47.22
16	u	10.22	29.51	71.18
	v	4.80	34.29	89.30

Table 9: Main tidal constituents of the currents at N1.

Depth (m)	Name	Frequency (cph)	Major Axis (cm/s)	Minor Axis (cm/s)	Inclination (°)	G. Phase (°)
7.2	Z_0	0.00000000	0.79	0.00	15.30	360.00
	MSf	0.00282193	0.46	-0.11	173.60	91.00
	O_1	0.03873065	0.09	-0.01	29.00	309.90
	K_1	0.04178075	0.19	0.02	160.10	177.80
	M_2	0.08051140	0.37	0.02	157.40	21.80
	S_2	0.08333334	0.15	0.06	107.30	251.00

Table 10: Main tidal constituents of the current at N2.

Depth (m)	Name	Frequency (cph)	Major Axis (cm/s)	Minor Axis (cm/s)	Inclination (°)	G. Phase (°)
18	Z_0	0.00000000	0.82	0.00	106.20	180.00
	MSf	0.00282193	0.40	-0.03	136.00	244.80
	O_1	0.03873065	0.28	-0.15	92.70	82.30
	K_1	0.04178075	0.28	-0.03	160.00	283.60
	M_2	0.08051140	0.48	-0.02	157.80	317.20
	S_2	0.08333334	0.24	0.00	135.60	104.40
13	Z_0	0.00000000	0.62	0.00	159.70	360.00
	MSf	0.00282193	0.33	-0.01	144.20	70.70
	O_1	0.03873065	0.15	-0.03	8.70	121.50
	K_1	0.04178075	0.36	0.09	154.50	349.30
	M_2	0.08051140	0.52	-0.11	170.80	38.00
	S_2	0.08333334	0.24	0.02	15.00	306.50
8	Z_0	0.00000000	1.72	0.00	150.20	360.00
	MSf	0.00282193	0.23	0.10	143.20	6.70
	O_1	0.03873065	0.10	-0.04	12.00	11.10
	K_1	0.04178075	0.12	0.07	52.50	130.30
	M_2	0.08051140	1.12	0.09	154.60	64.20
	S_2	0.08333334	0.45	-0.02	156.60	129.60
3	Z_0	0.00000000	1.70	0.00	13.80	0.00
	MSf	0.00282193	0.45	0.12	157.90	273.10
	O_1	0.03873065	0.64	0.19	136.20	159.50
	K_1	0.04178075	0.79	0.03	146.20	199.10
	M_2	0.08051140	2.35	0.35	163.90	93.50
	S_2	0.08333334	1.15	0.16	156.80	147.20

Table 11: Main tidal constituents of the currents at N3.

Depth (m)	Name	Frequency (cph)	Major Axis (cm/s)	Minor Axis (cm/s)	Inclination (°)	G. Phase (°)
20	Z_0	0.00000000	2.31	0.00	146.40	180.00
	MSf	0.00282193	0.57	-0.06	148.90	88.10
	O_1	0.03873065	0.32	0.00	152.50	342.70
	K_1	0.04178075	0.33	0.00	154.50	343.40
	M_2	0.08051140	0.72	0.04	152.20	49.20
	S_2	0.08333334	0.24	-0.07	137.00	215.00
15	Z_0	0.00000000	0.67	0.00	51.00	180.00
	MSf	0.00282193	0.83	-0.15	160.60	122.80
	O_1	0.03873065	0.18	0.01	151.60	51.00
	K_1	0.04178075	0.80	0.02	157.00	30.70
	M_2	0.08051140	1.14	-0.06	155.80	70.30
	S_2	0.08333334	0.59	0.01	168.00	118.40
10	Z_0	0.00000000	3.96	0.00	169.30	360.00
	MSf	0.00282193	0.24	-0.03	27.50	263.40
	O_1	0.03873065	0.34	0.05	124.90	105.70
	K_1	0.04178075	0.25	0.00	33.20	152.70
	M_2	0.08051140	1.19	-0.04	155.90	77.30
	S_2	0.08333334	0.65	-0.09	177.30	132.20
5	Z_0	0.00000000	2.25	0.00	156.90	360.00
	MSf	0.00282193	1.00	-0.16	0.40	66.40
	O_1	0.03873065	0.56	0.07	131.10	142.80
	K_1	0.04178075	0.77	0.06	162.70	179.60
	M_2	0.08051140	1.87	0.12	168.50	104.80
	S_2	0.08333334	1.13	-0.03	175.50	156.50
4	Z_0	0.00000000	1.13	0.00	144.00	360.00
	MSf	0.00282193	0.38	-0.26	61.30	63.90
	O_1	0.03873065	0.44	0.11	158.90	169.60
	K_1	0.04178075	1.21	0.01	170.10	167.50
	M_2	0.08051140	1.68	0.24	161.30	79.20
	S_2	0.08333334	1.10	0.11	166.40	117.20

Table 12: Main tidal constituents of the currents at N4.

Depth (m)	Name	Frequency (cph)	Major Axis (cm/s)	Minor Axis (cm/s)	Inclination (°)	G. Phase (°)
11	Z_0	0.00000000	1.60	0.00	8.90	180.00
	MSf	0.00282193	0.49	0.14	27.40	259.30
	O_1	0.03873065	0.09	0.06	86.00	80.90
	K_1	0.04178075	0.36	-0.05	4.60	240.90
	M_2	0.08051140	0.85	0.26	147.30	52.30
	S_2	0.08333334	0.39	0.15	167.60	113.10
7	Z_0	0.00000000	2.89	0.00	169.60	360.00
	MSf	0.00282193	0.41	-0.18	156.70	304.80
	O_1	0.03873065	0.20	-0.02	154.10	38.90
	K_1	0.04178075	0.30	-0.13	98.30	161.80
	M_2	0.08051140	1.11	0.14	163.70	66.20
	S_2	0.08333334	0.50	-0.01	179.30	131.80
3	Z_0	0.00000000	0.76	0.00	155.90	360.00
	MSf	0.00282193	0.61	-0.02	2.60	47.40
	O_1	0.03873065	0.29	0.13	23.00	90.20
	K_1	0.04178075	0.61	0.21	157.20	134.30
	M_2	0.08051140	1.16	0.17	167.70	94.50
	S_2	0.08333334	0.96	0.03	162.80	110.10

Table 13: Main constituents of the Tidal Currents, N5

Depth (m)	Name	Frequency (cph)	Major Axis (cm/s)	Minor Axis (cm/s)	Inclination (°)	G. Phase (°)
12.7	Z_0	0.00000000	0.39	0.00	54.70	180.00
	MSf	0.00282193	0.08	-0.01	64.50	81.80
	O_1	0.03873065	0.08	0.06	38.90	224.30
	K_1	0.04178075	0.07	-0.02	76.40	319.10
	M_2	0.08051140	0.23	-0.03	178.30	313.60
	S_2	0.08333334	0.14	-0.01	145.90	286.00

Table 14: Main constituents of the Tidal Currents, H1

Depth (m)	Name	Frequency (cph)	Major Axis (cm/s)	Minor Axis (cm/s)	Inclination (°)	G. Phase (°)
22	Z_0	0.00000000	1.04	0.00	64.00	360.00
	MSf	0.00282193	1.98	0.30	79.30	329.60
	O_1	0.03873065	0.52	-0.36	132.30	298.40
	K_1	0.04178075	0.96	0.06	60.40	154.80
	M_2	0.08051140	2.93	0.15	82.10	251.60
	S_2	0.08333334	0.57	-0.42	103.40	24.50
77	Z_0	0.00000000	0.50	0.00	10.50	180.00
	MSf	0.00282193	0.25	-0.09	127.10	159.90
	O_1	0.03873065	0.31	-0.22	137.50	290.20
	K_1	0.04178075	0.25	0.04	99.80	268.50
	M_2	0.08051140	1.06	0.33	94.80	194.40
	S_2	0.08333334	0.48	0.09	84.30	273.90

Table 15: Main tidal constituents of the currents at H2.

Depth (m)	Name	Frequency (cph)	Major Axis (cm/s)	Minor Axis (cm/s)	Inclination (°)	G. Phase (°)
96	Z_0	0.00000000	0.80	0.00	56.60	180.00
	MSf	0.00282193	1.36	-0.09	63.50	273.80
	O_1	0.03873065	0.42	-0.18	76.20	315.10
	K_1	0.04178075	0.43	-0.03	67.50	162.30
	M_2	0.08051140	0.97	0.45	74.20	149.50
	S_2	0.08333334	0.41	-0.06	47.90	191.70
64	Z_0	0.00000000	0.38	0.00	64.60	180.00
	MSf	0.00282193	1.52	0.15	65.40	272.70
	O_1	0.03873065	0.57	-0.30	127.90	323.50
	K_1	0.04178075	0.51	0.09	102.70	324.90
	M_2	0.08051140	1.80	-0.27	89.60	179.90
	S_2	0.08333334	0.59	0.07	70.90	240.00
32	Z_0	0.00000000	2.28	0.00	73.30	180.00
	MSf	0.00282193	1.81	0.05	66.80	249.40
	O_1	0.03873065	0.79	-0.48	166.00	304.10
	K_1	0.04178075	0.75	-0.30	26.00	101.10
	M_2	0.08051140	1.06	-0.05	78.00	186.60
	S_2	0.08333334	0.72	-0.29	153.90	229.70
24	Z_0	0.00000000	2.93	0.00	77.30	180.00
	MSf	0.00282193	2.33	-0.22	59.50	240.30
	O_1	0.03873065	1.05	-0.64	95.20	320.70
	K_1	0.04178075	1.00	0.06	24.90	110.00
	M_2	0.08051140	1.42	-0.32	67.40	212.50
	S_2	0.08333334	0.77	-0.08	120.30	241.60

Table 16: Tidal Height analysis of surface elevation data measured in the Harbour (MEDS).

Name	Frequency (cph)	Amplitude (cm)	Greenwich Phase (°)
Z_0	0.00000000	0.00	0.00
MSf	0.00282193	0.02	160.94
O_1	0.03873065	0.06	204.16
K_1	0.04178075	0.07	262.71
M_2	0.08051140	0.34	113.15
S_2	0.08333334	0.17	171.49

Table 17: Tidal Height analysis of surface elevation data measured in the Narrows (WLR).

Name	Frequency (cph)	Amplitude (cm)	Greenwich Phase (°)
Z_0	0.00000000	0.00	0
MSf	0.00282193	0.01	344.76
O_1	0.03873065	0.06	202.54
K_1	0.04178075	0.07	295.33
M_2	0.08051140	0.34	141.67
S_2	0.08333334	0.16	221.45

Figures

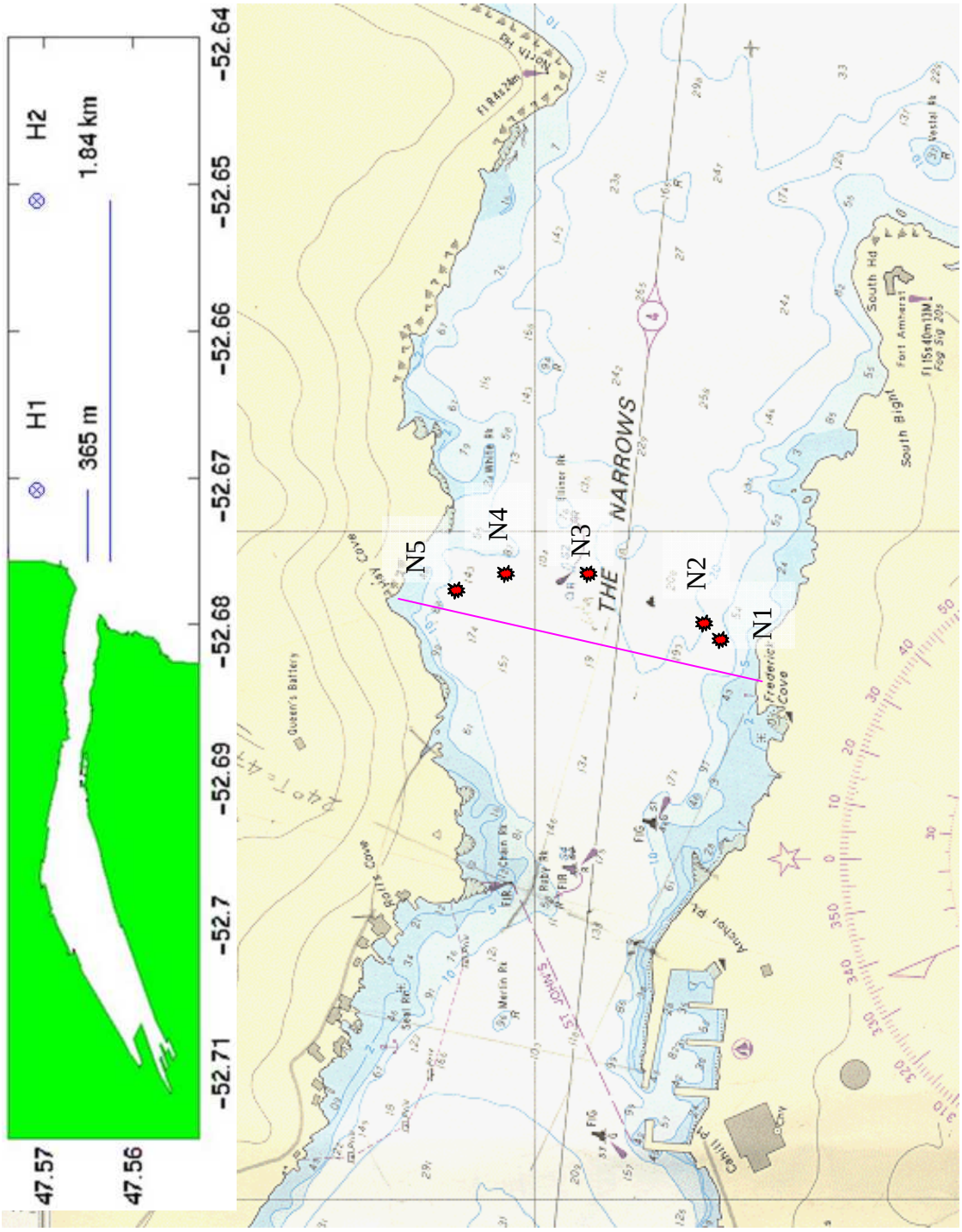

Figure 1: Topographic map of the Narrows, with moorings as red stars. Included with the inset map are the instrument mooring locations outside the Narrows and the distance from the coast to the mooring.

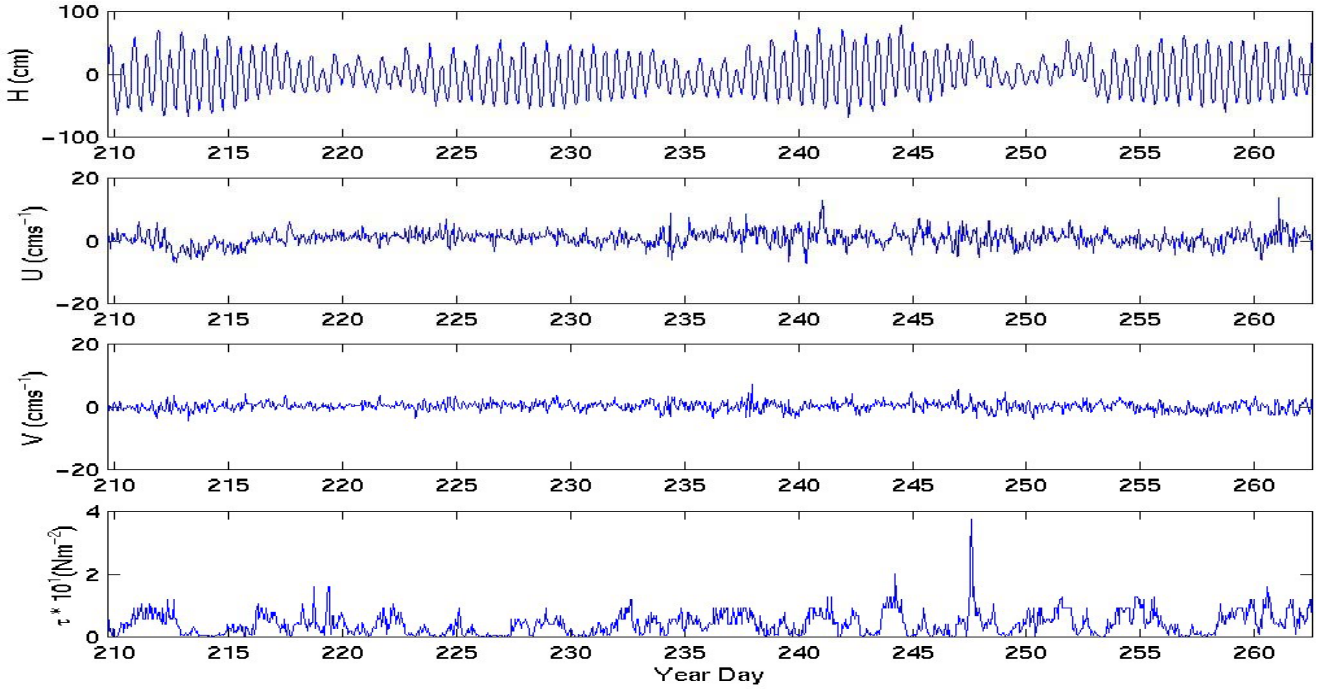

Figure 2: The raw times series of the u component and v components of the S4 current meter at N1 in cm s^{-1}. Included are the surface elevation in cm, and the wind stress in Nm^{-2}.

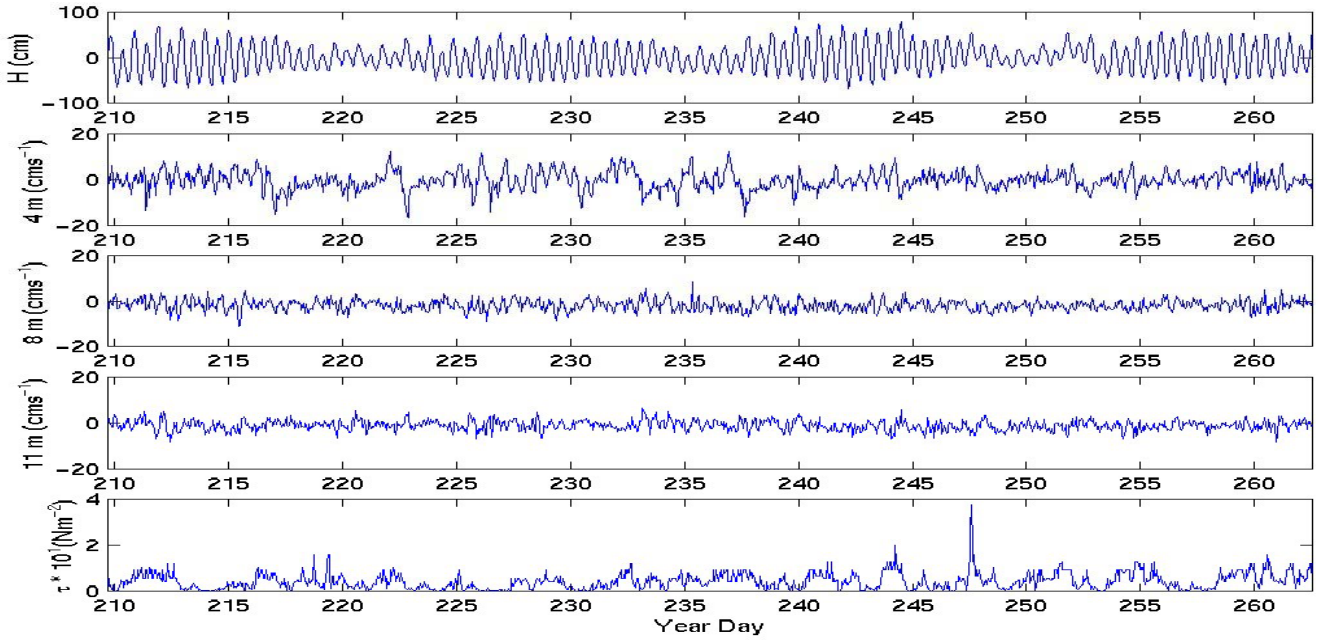

A

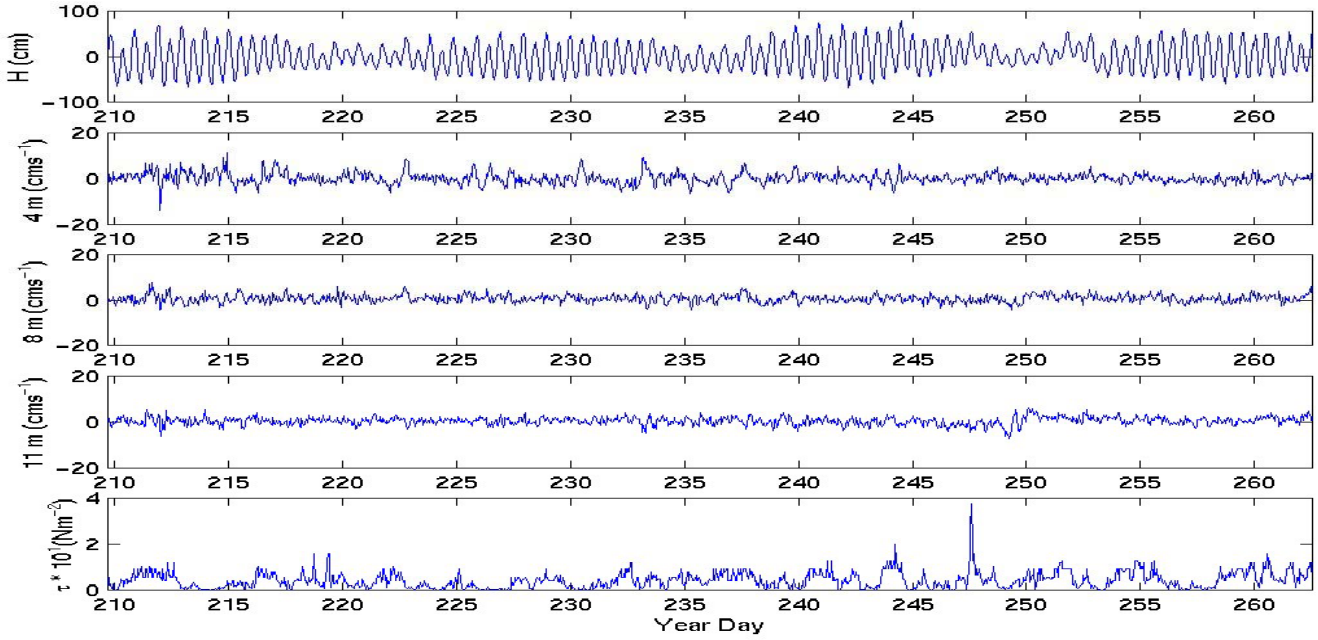

B

Figure 3: The raw times series of the u component (A) and v component of selected depths from the ADCP at N2 in cm s^{-1}. Included are the surface elevation in cm, and the wind stress in N m^{-2}.

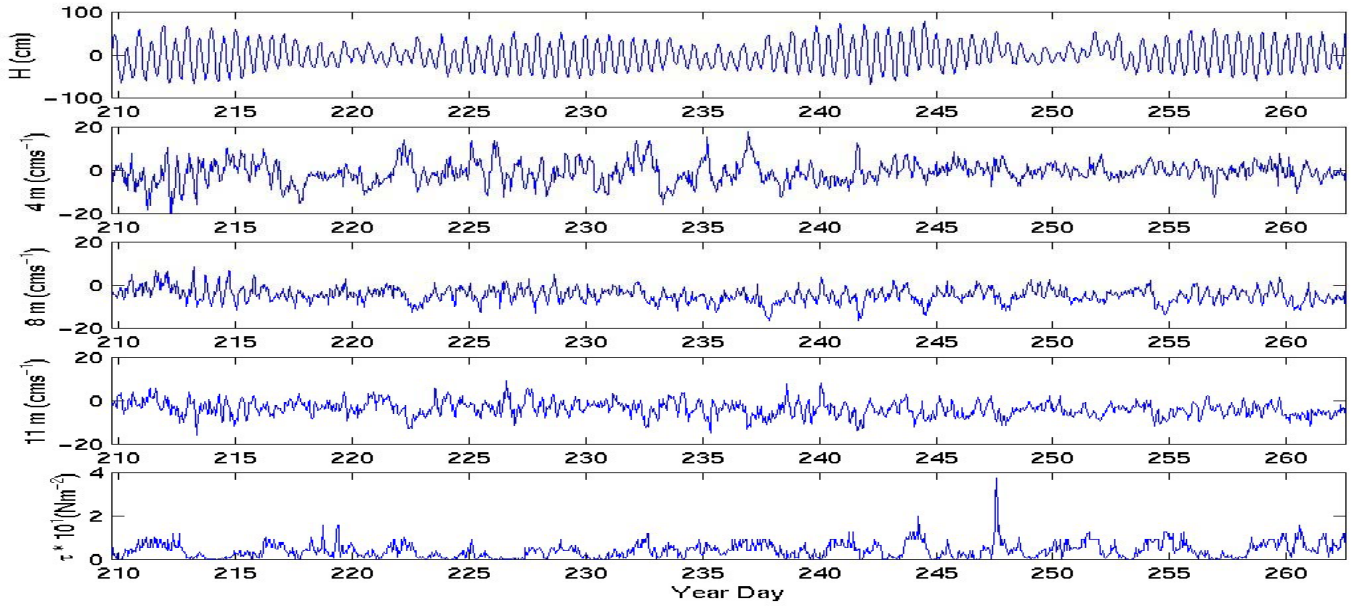

A

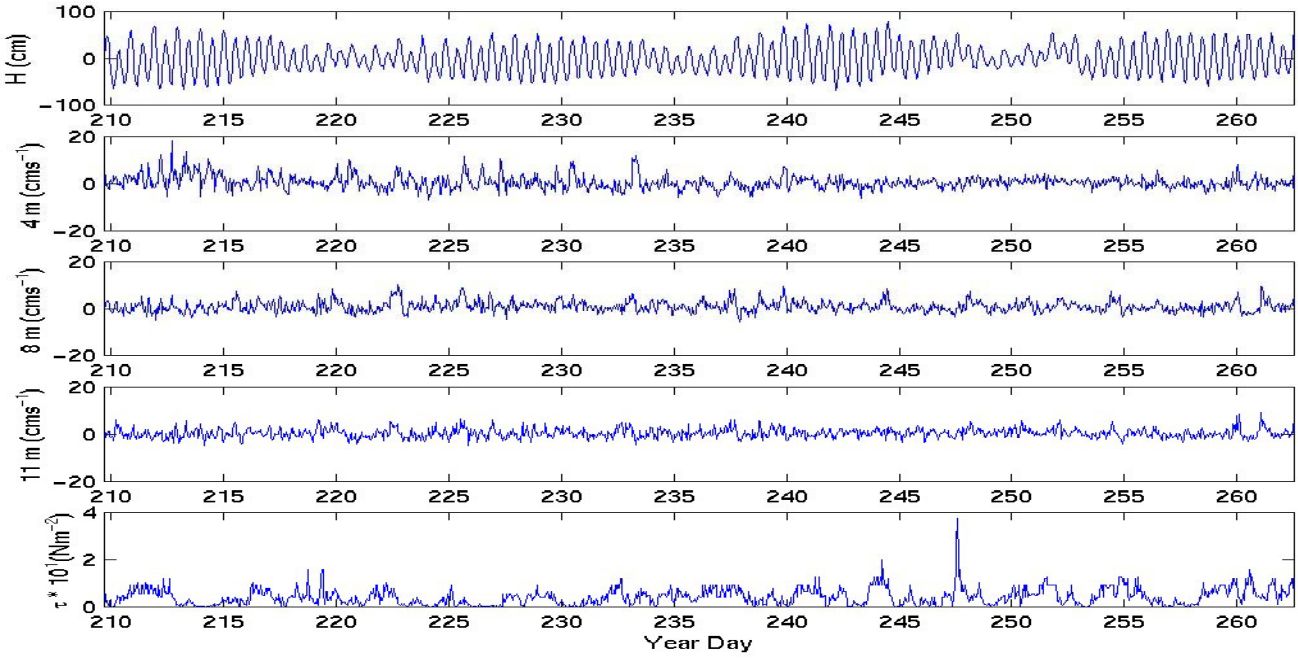

B

Figure 4: The raw times series of the u component (A) and v component of selected depths from the ADCP at N3 in cm s^{-1}. Included are the surface elevation in cm, and the wind stress in N m^{-2}.

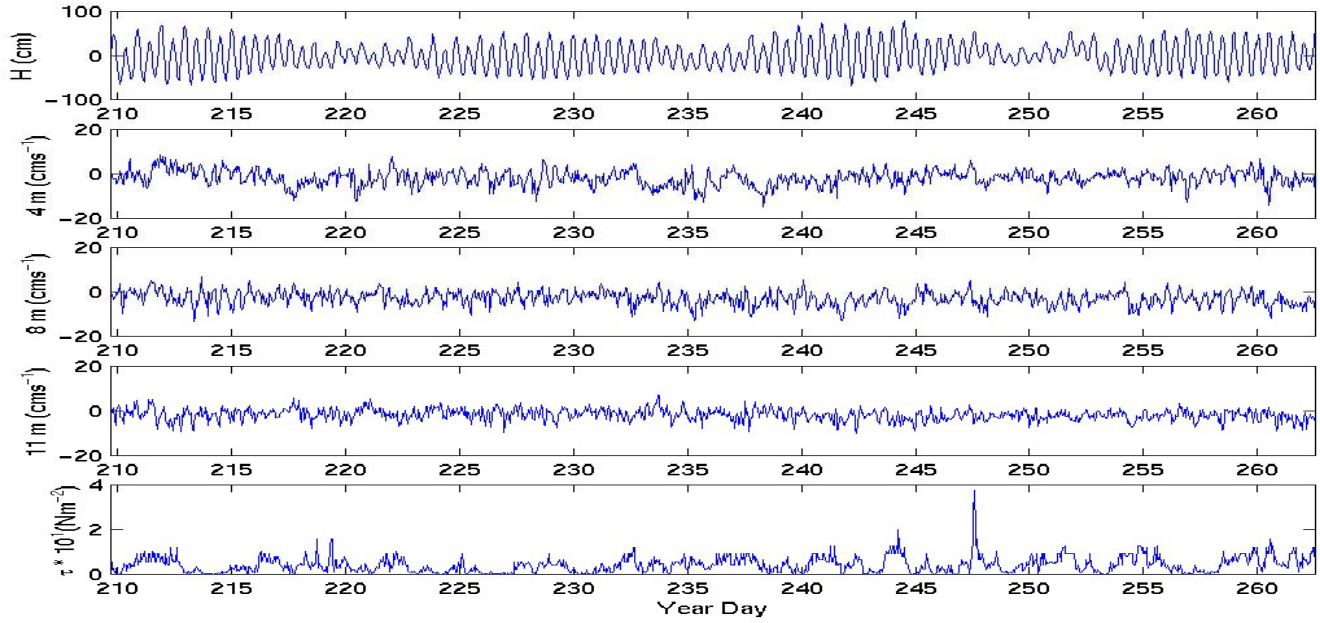

A

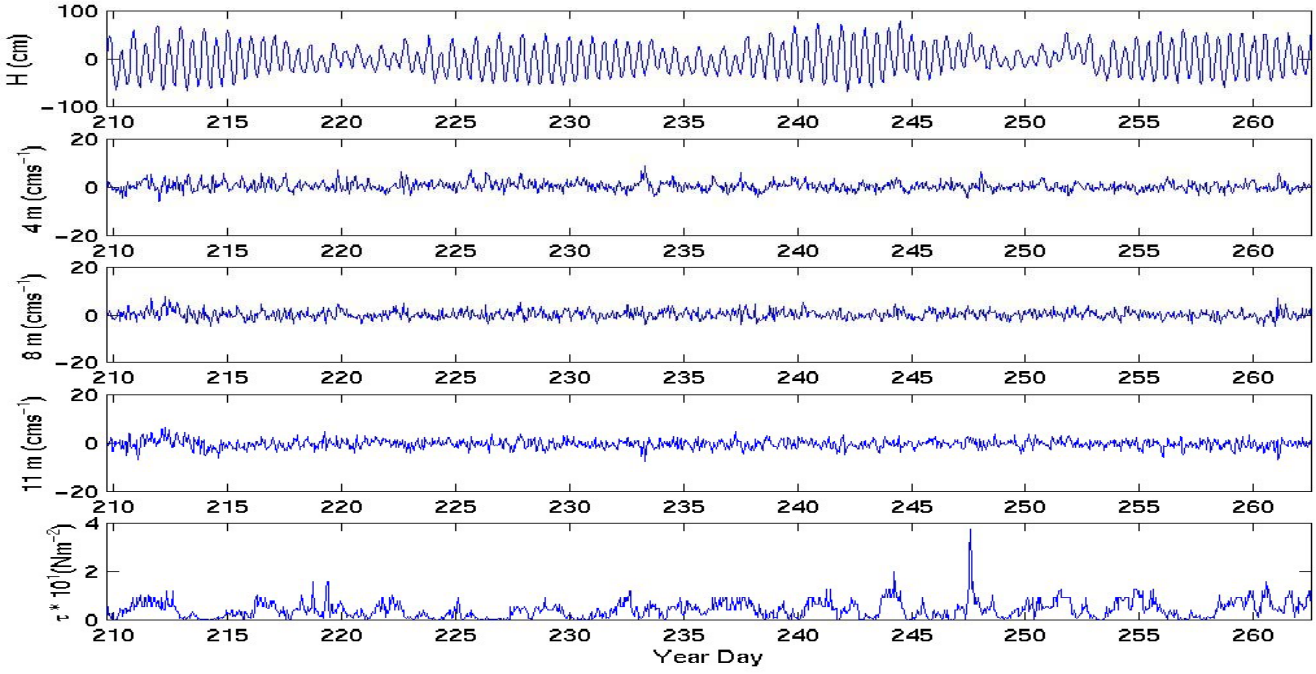

B

Figure 5: The raw times series of the u component (A) and v component of selected depths from the ADCP at N4 in cm s^{-1}. Included are the surface elevation in cm, and the wind stress in N m^{-2}.

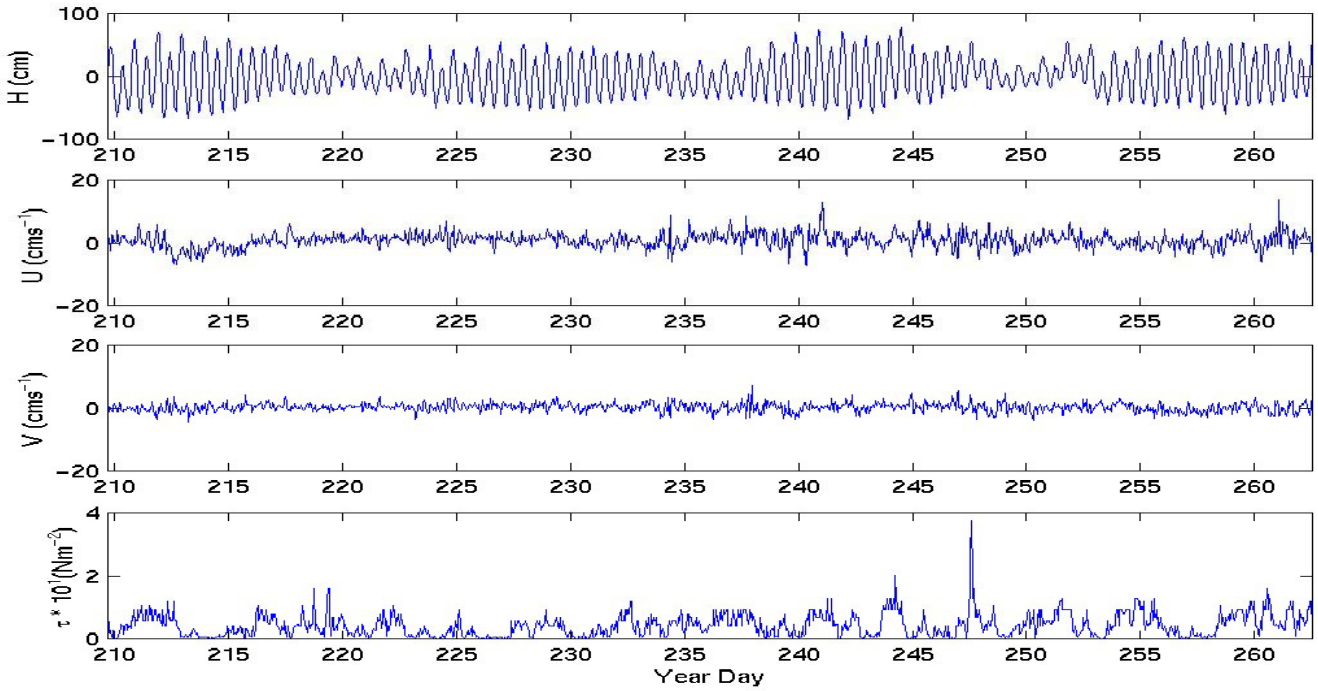

Figure 6: The raw times series of the u component and v components of the S4 current meter at N5 in cm s^{-1}. Included are the surface elevation in cm, and the wind stress in Nm^{-2}.

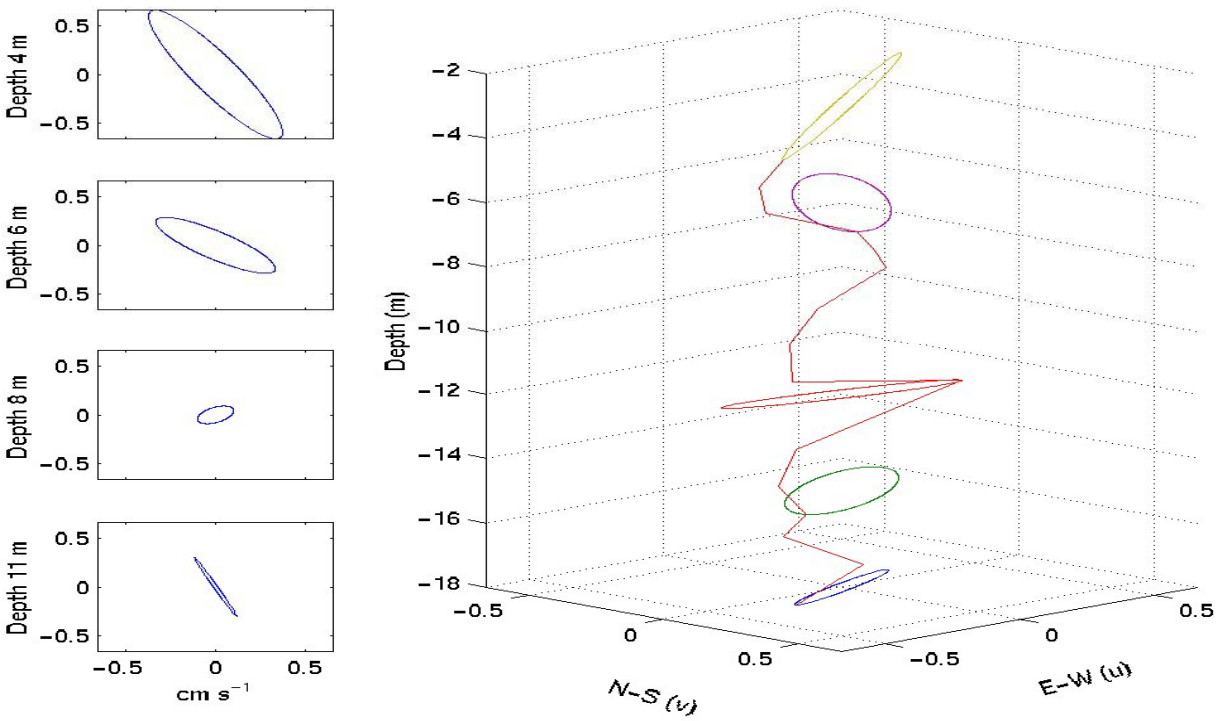

A

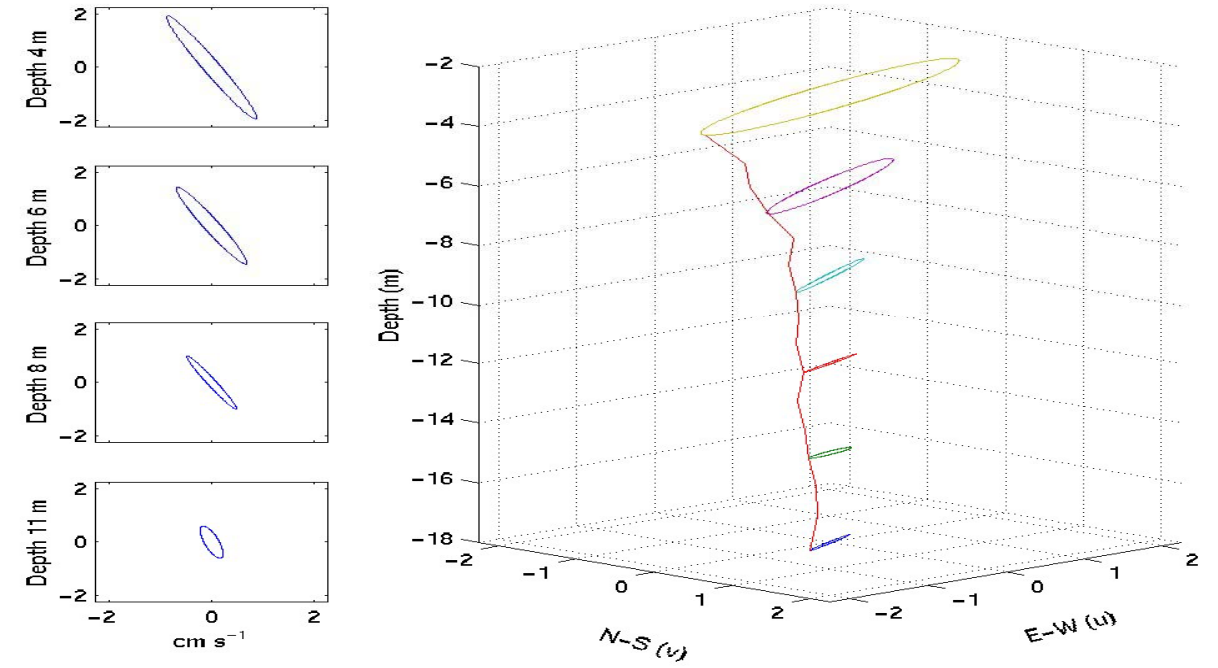

B

Figure 7: The tidal ellipses at the K_1 (A) and M_2 (B) frequencies, determined by Foreman's analysis at N2. Here, E-W and N-S are the axes as rotated 10 clockwise from Earth Axes.

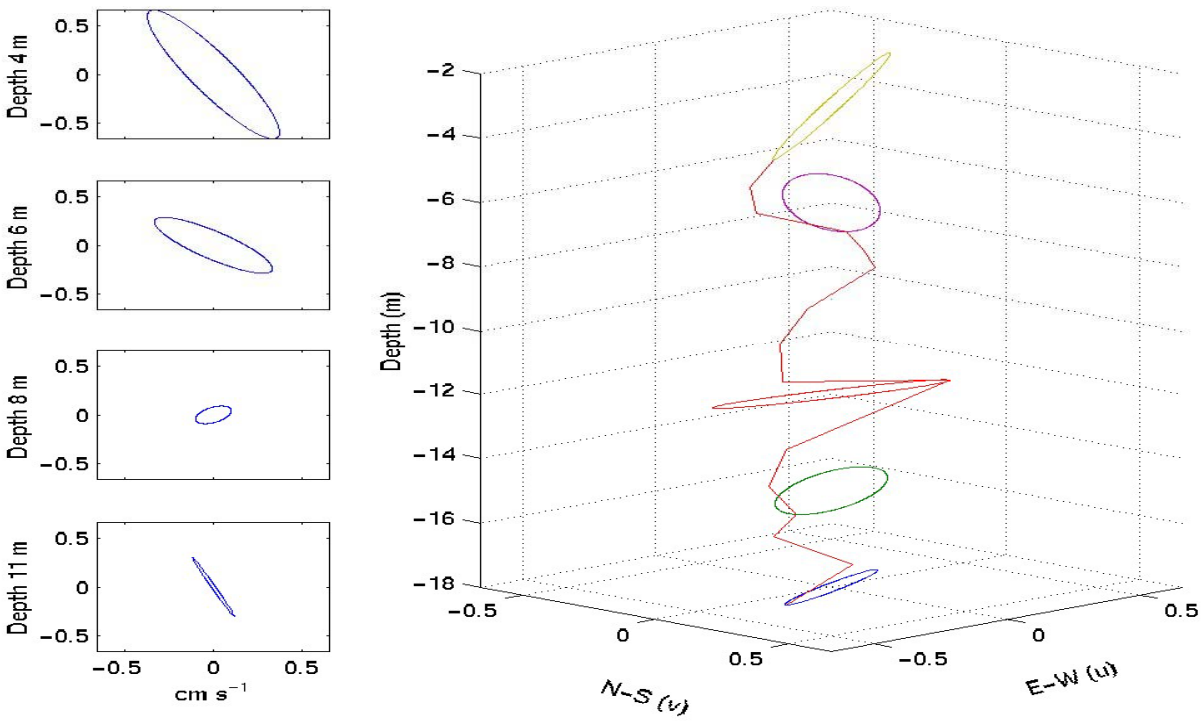

A

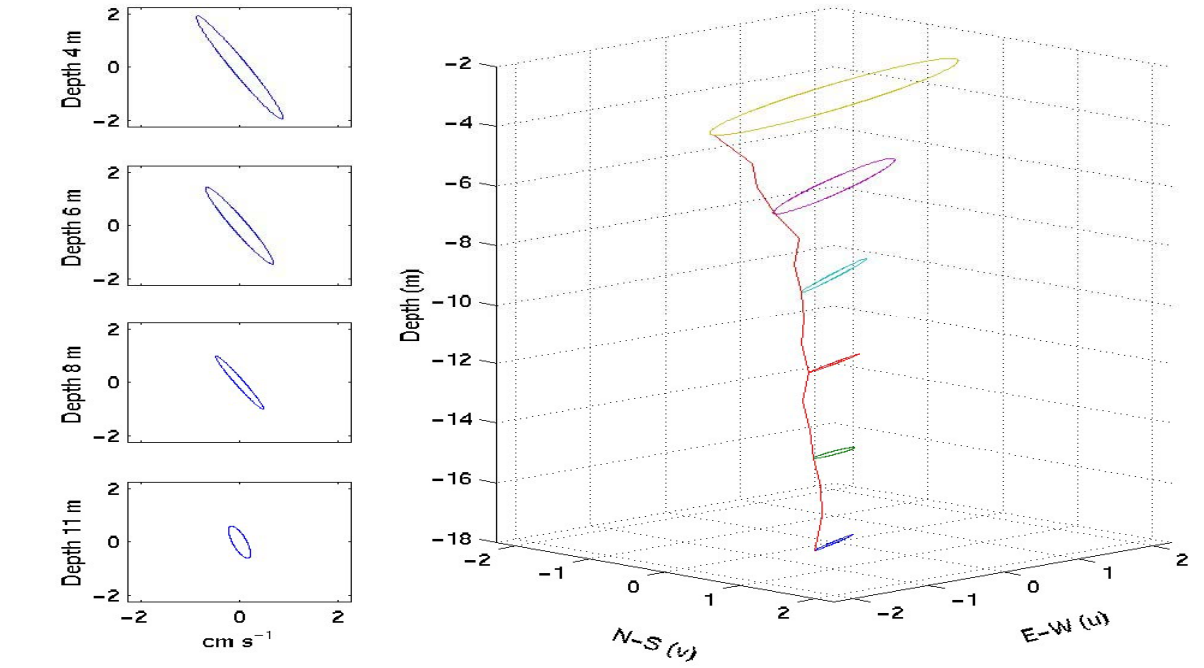

B

Figure 8: The tidal ellipses at the K_1 (A) and M_2 (B) frequencies, determined by Foreman's analysis at N3. Here, E-W and N-S are the axes as rotated 10 clockwise from Earth Axes.

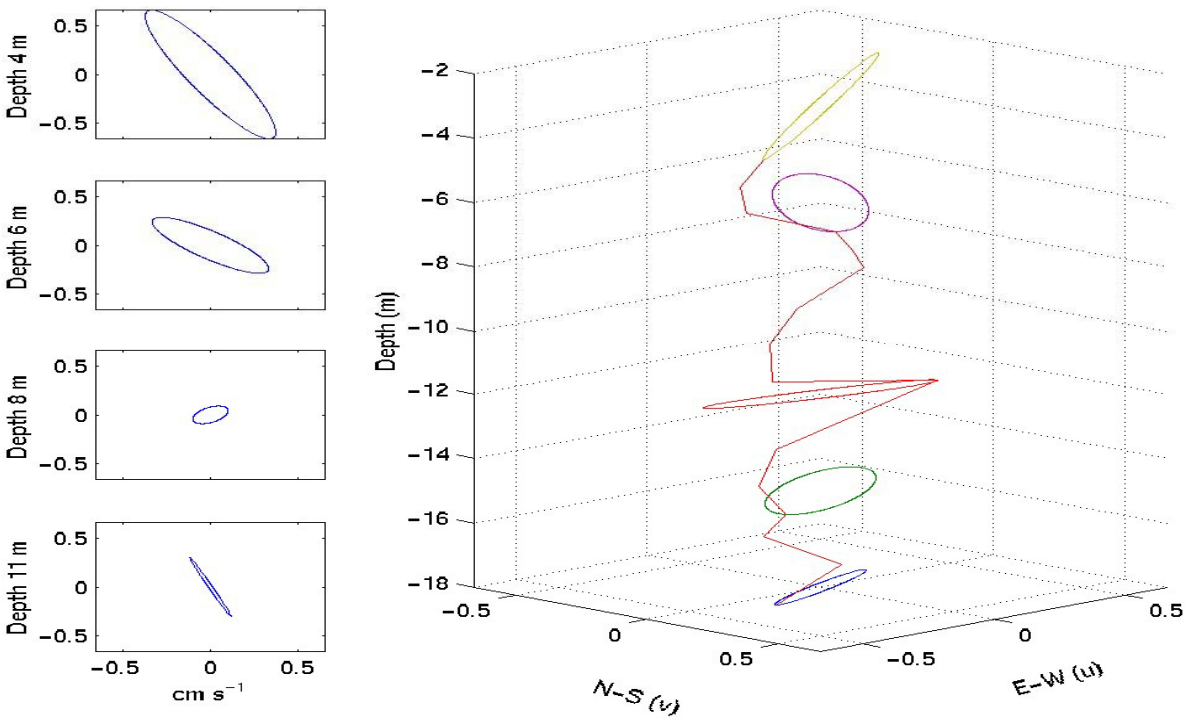

A

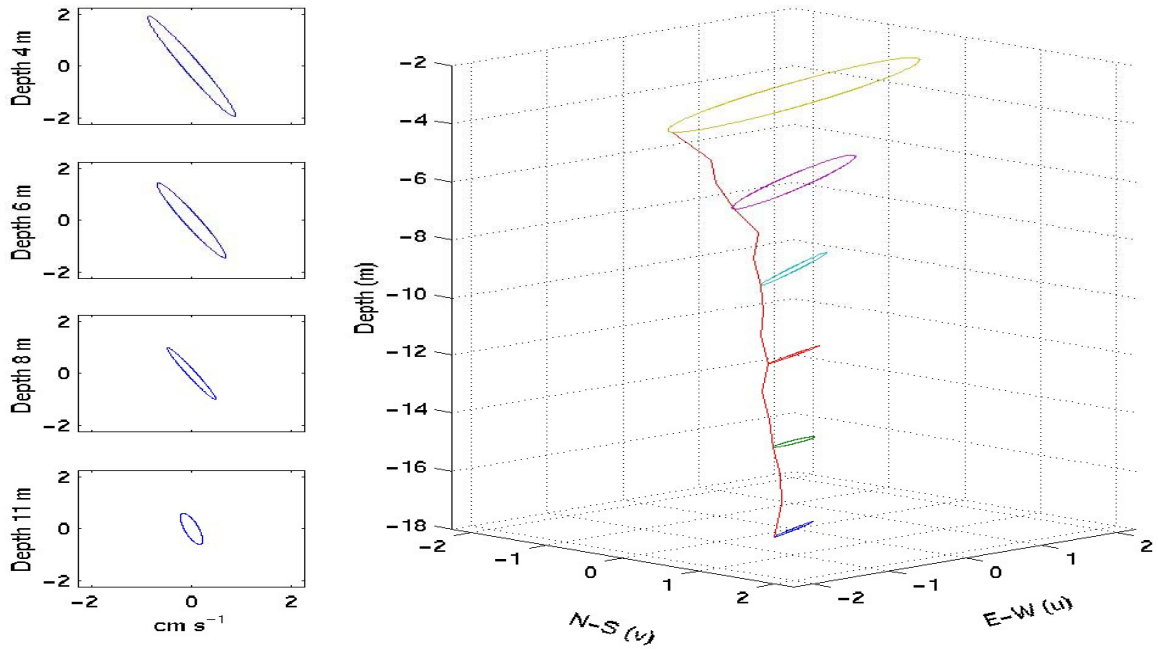

B

Figure 9: The tidal ellipses at the K_1 (A) and M_2 (B) frequencies, determined by Foreman's analysis at N4. Here, E-W and N-S are the axes as rotated 10 clockwise from Earth Axes.

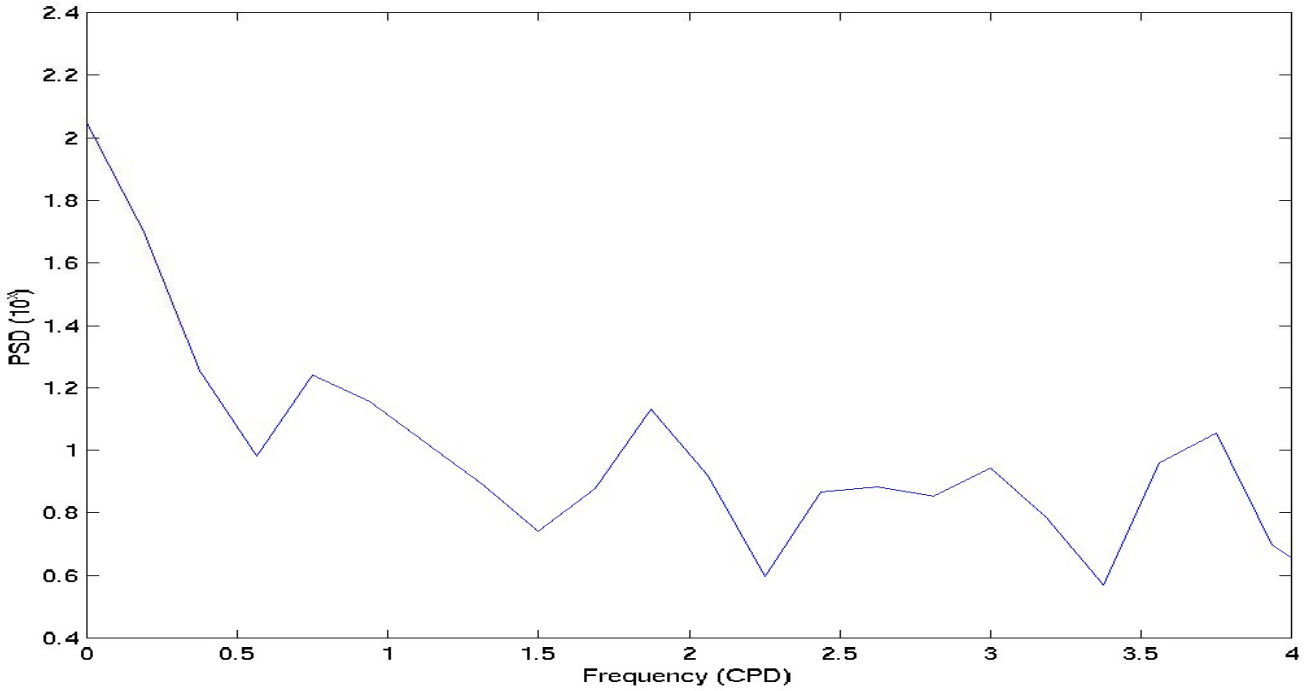

Figure 10: Power Spectral Density of the In/Out current time series from N1.

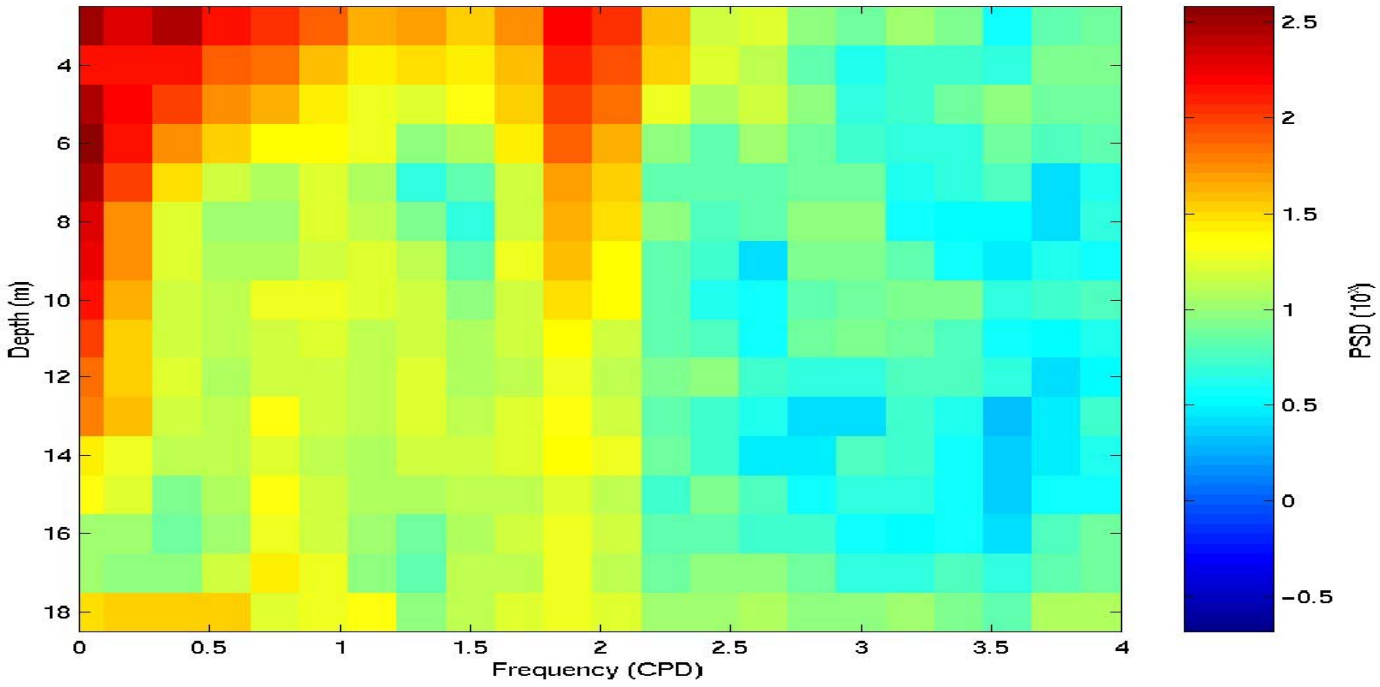

Figure 11: Power Spectral Density for the current at each depth bin measured by the ADCP at N2 along the In/Out axes.

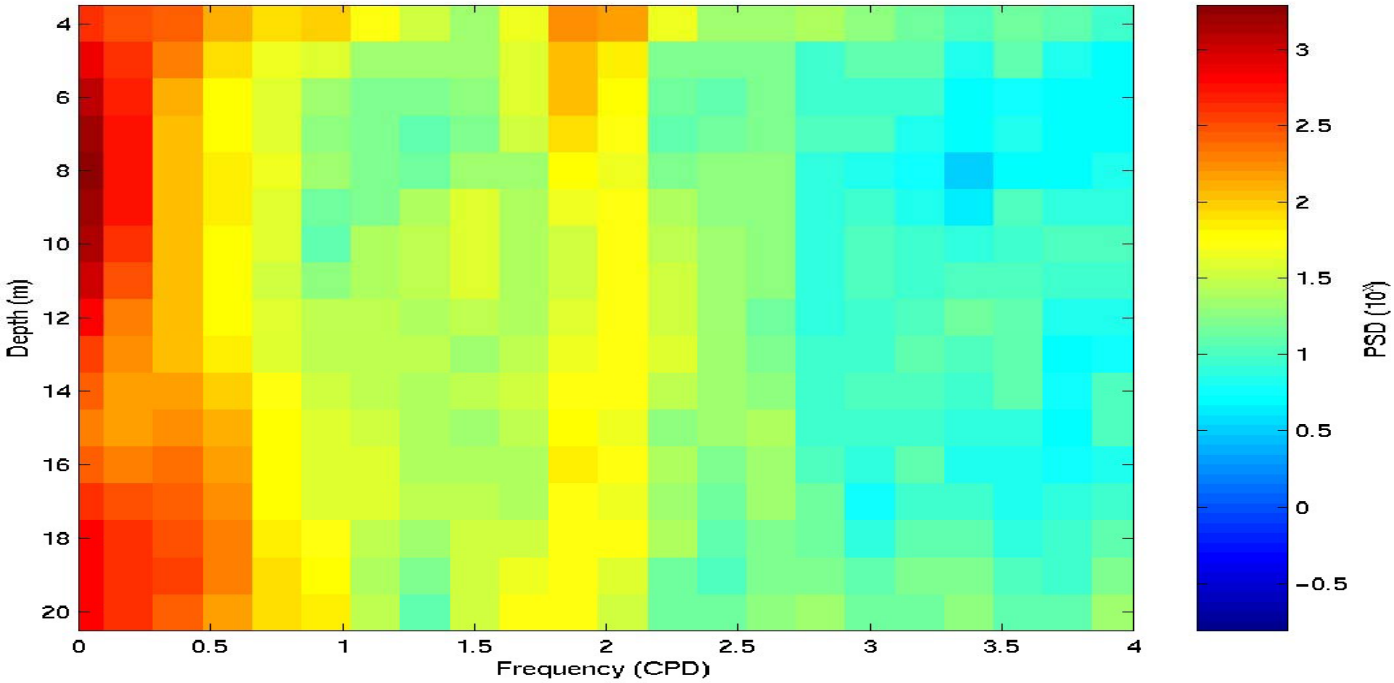

Figure 12: Power Spectral Density for the current at each depth bin measured by the ADCP at N3 along the In/Out.

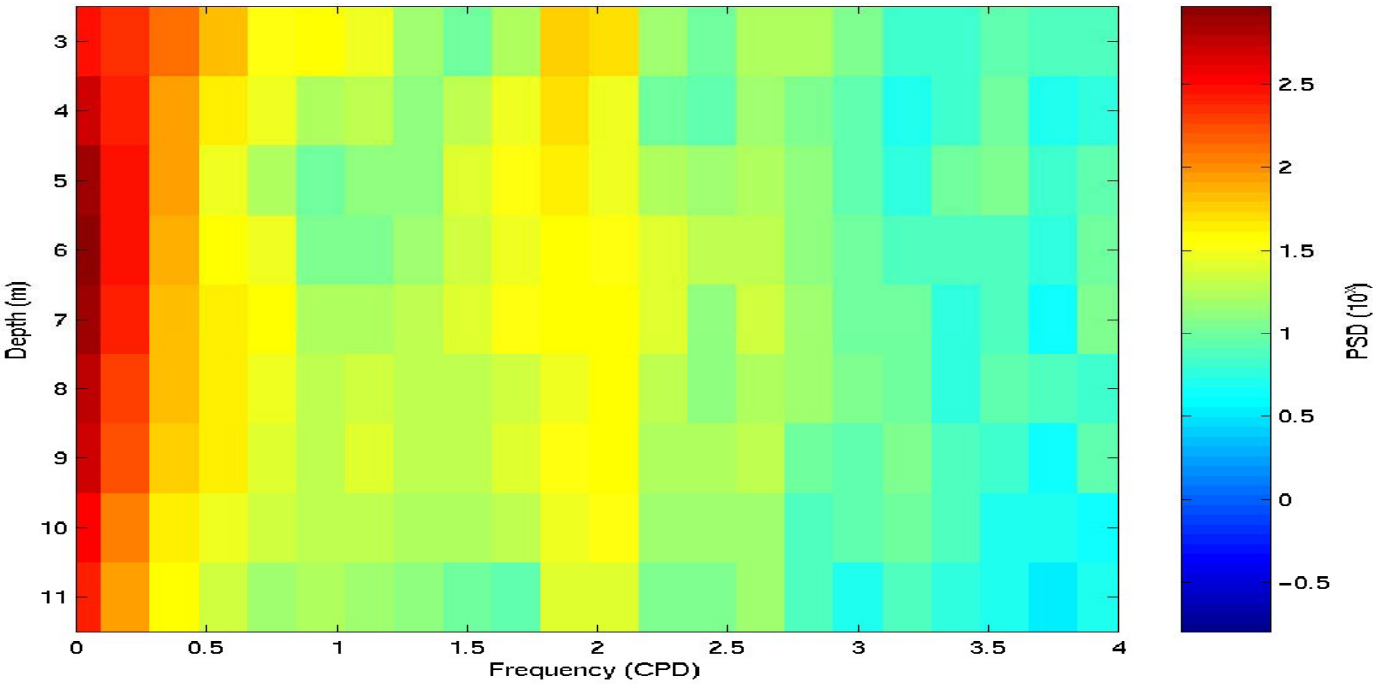

Figure 13: Power Spectral Density for the current at each depth bin measured by the ADCP at N4 along the In/Out.

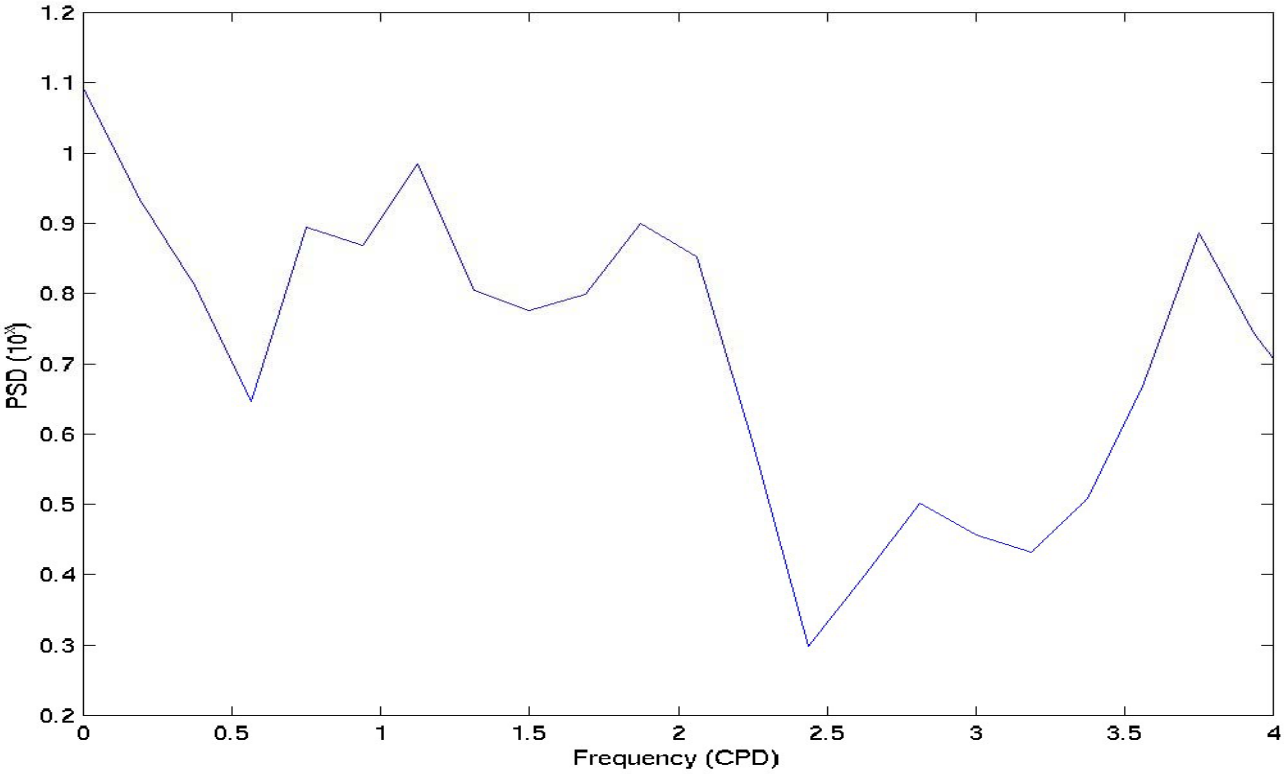

Figure 14 : Power Spectral Density of the In/Out current time series from N5.

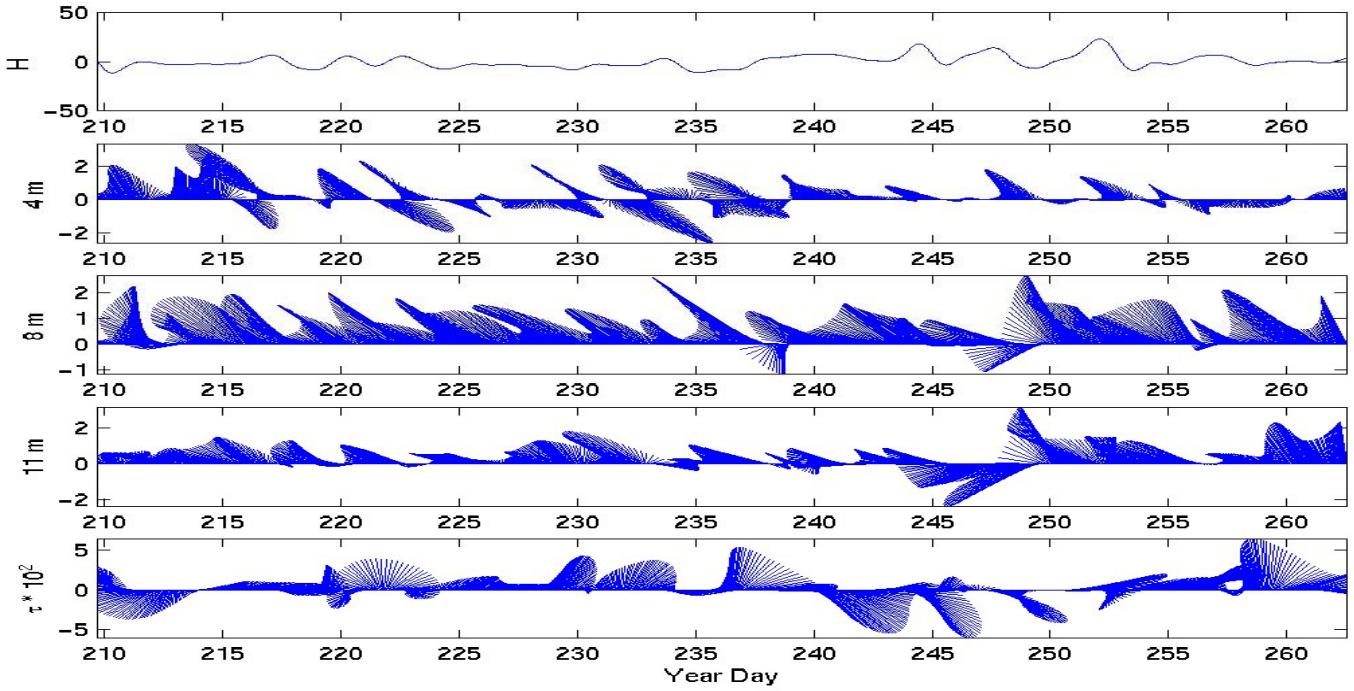

Figure 15: Subtidal current vector diagram for selected depths at N2.

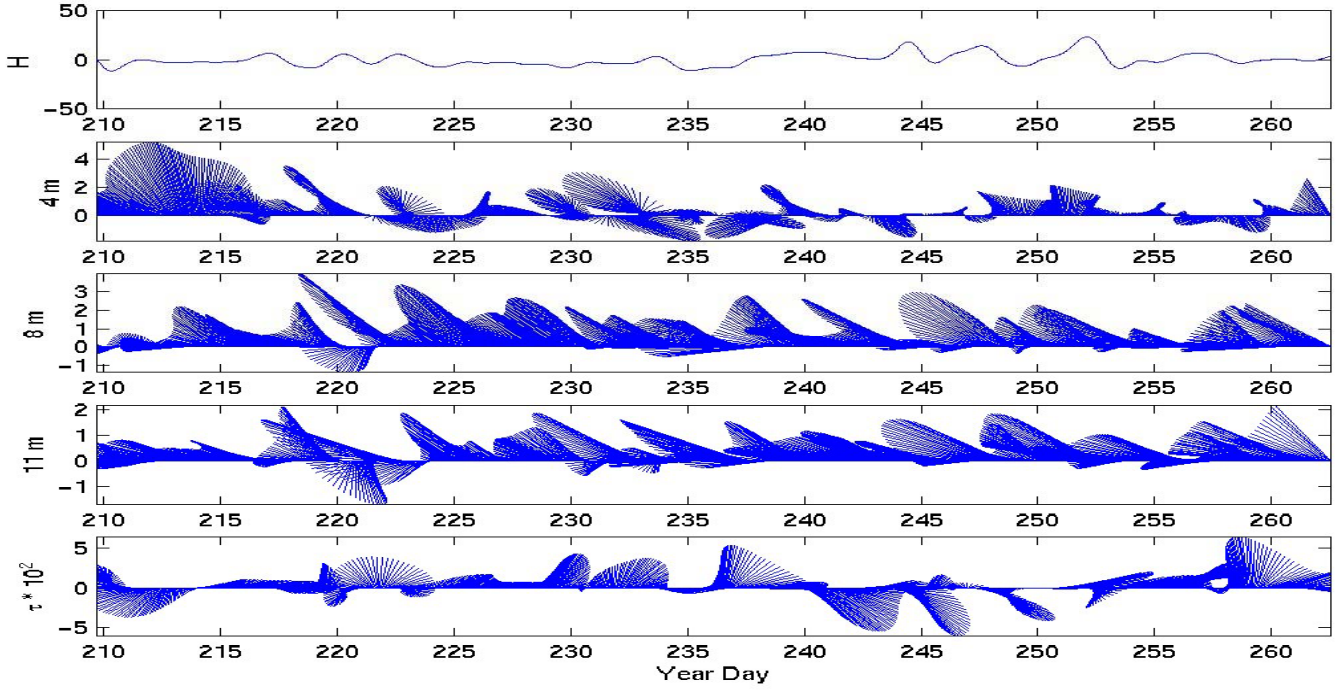

Figure 16: Subtidal current vector diagram for selected depths at N3.

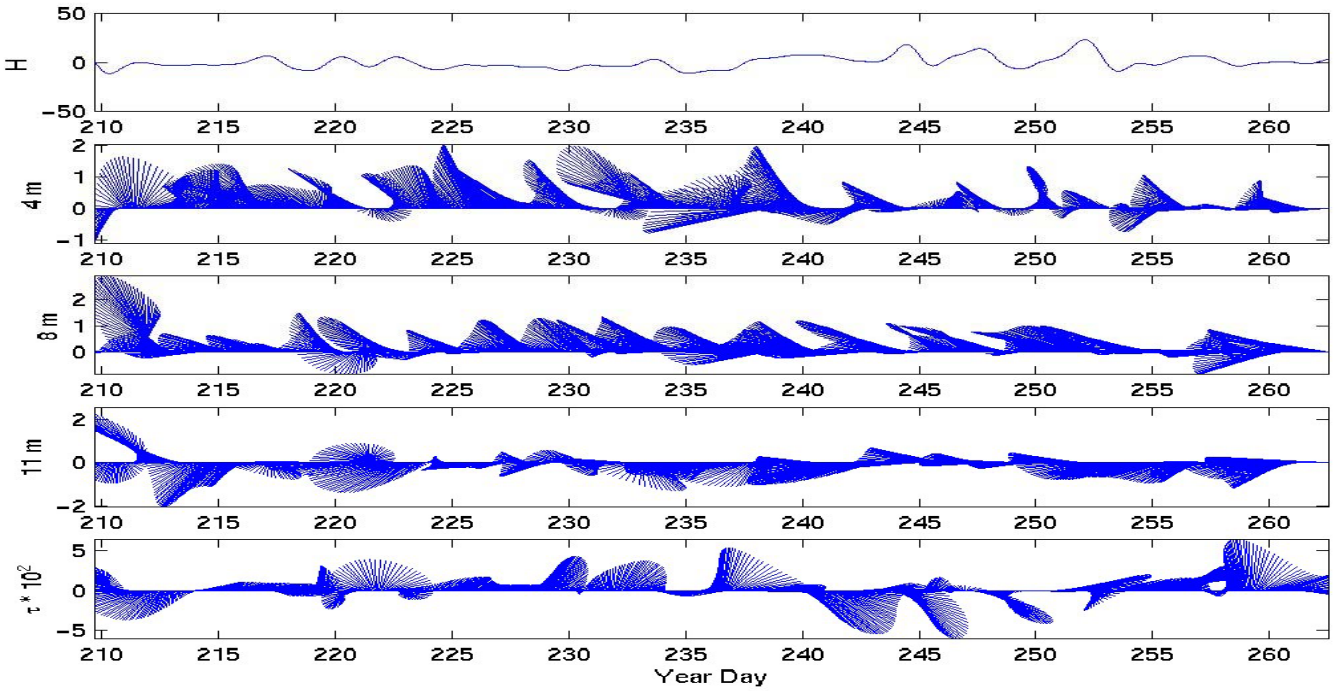

Figure 17: Subtidal current vector diagram for selected depths at N4.

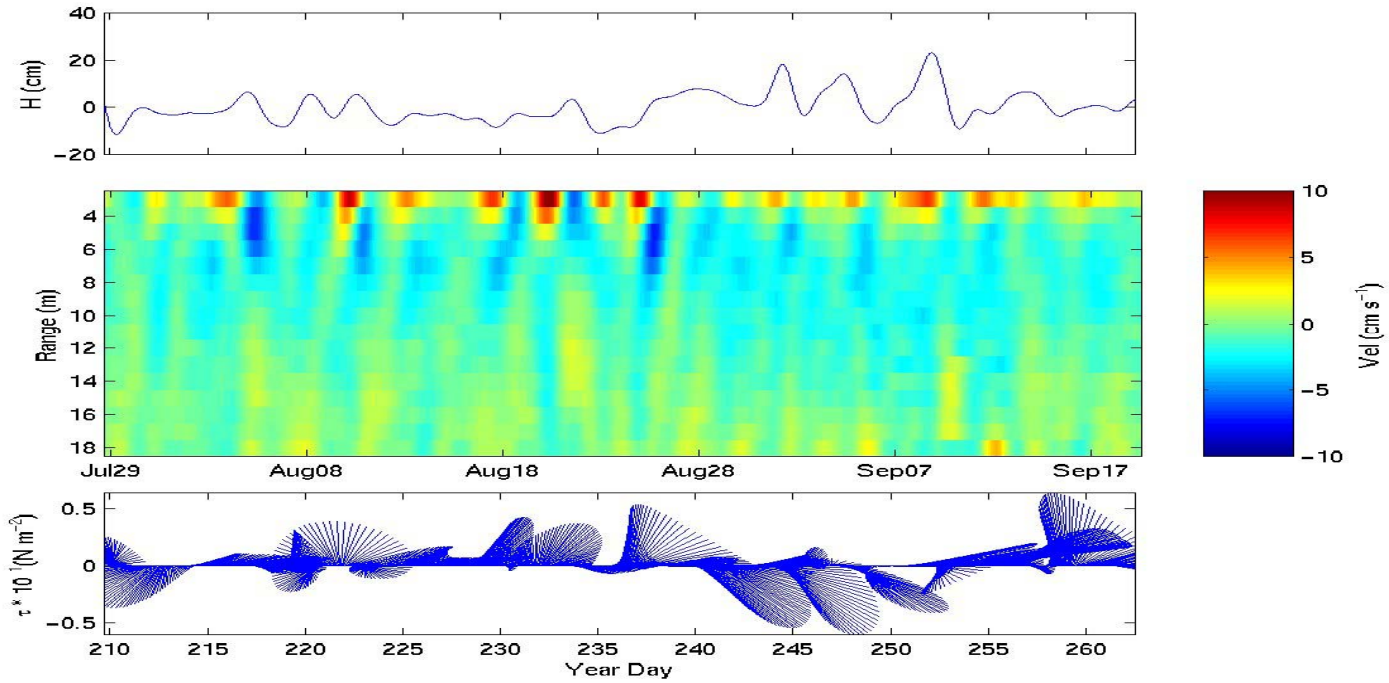

Figure 18: Subtidal In(-)/Out(+) velocities at all depths from N2.

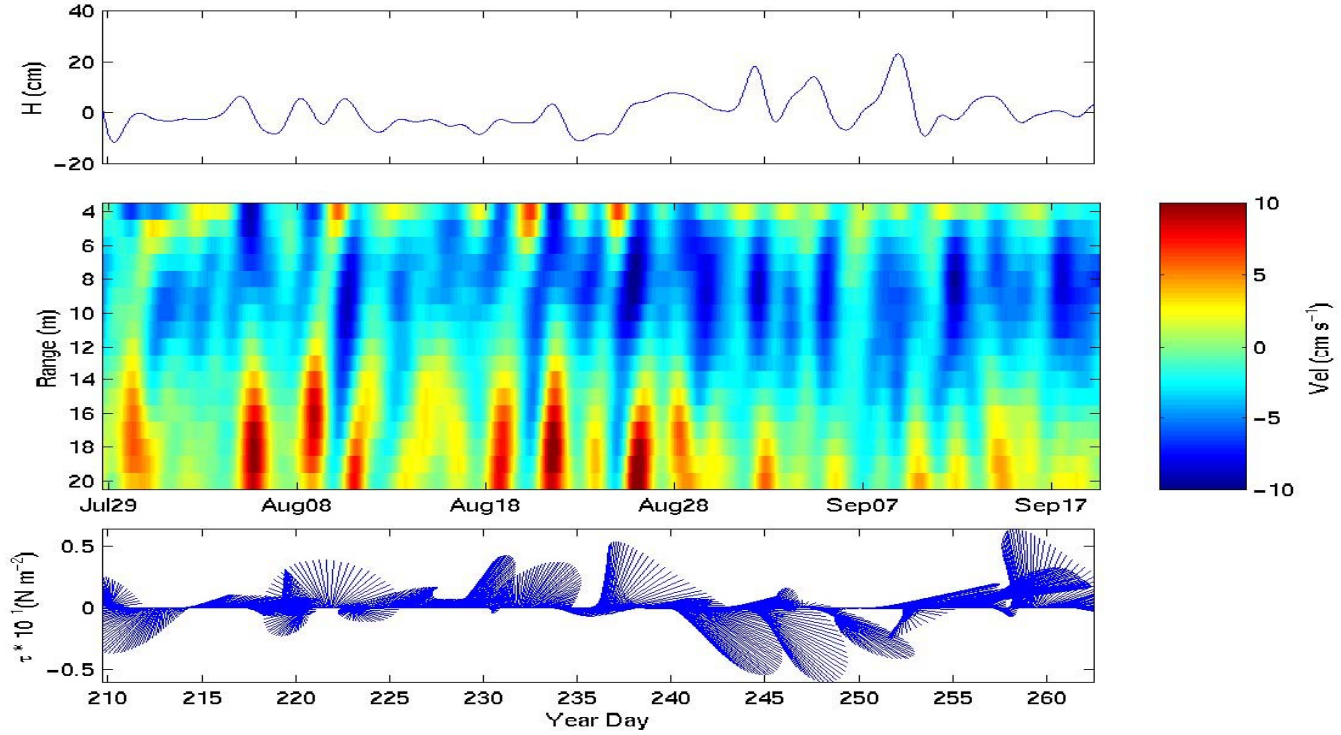

Figure 19: Subtidal In(-)/Out(+) velocities at all depths from N3.

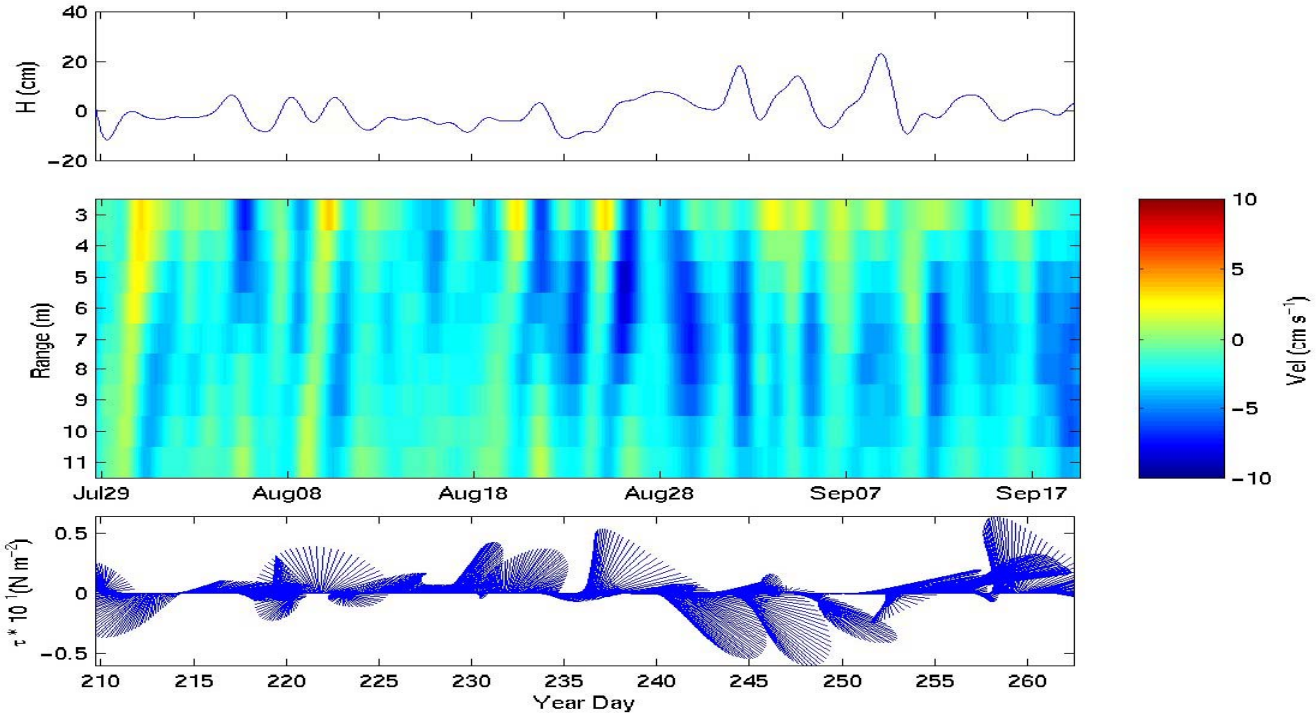

Figure 20: Subtidal In(-)/Out(+) velocities at all depths from N4.

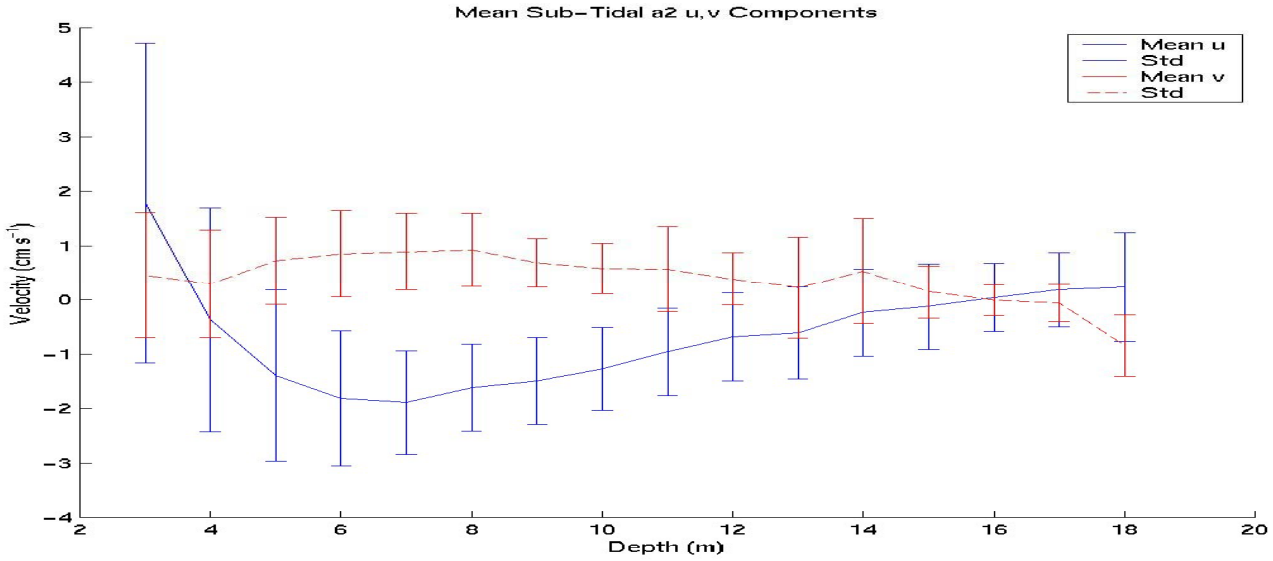

Figure 21: Profile plot of the mean along (blue solid) and cross (red dashed) channel velocity measured by the ADCP at N2. The error bars are one standard deviation in length.

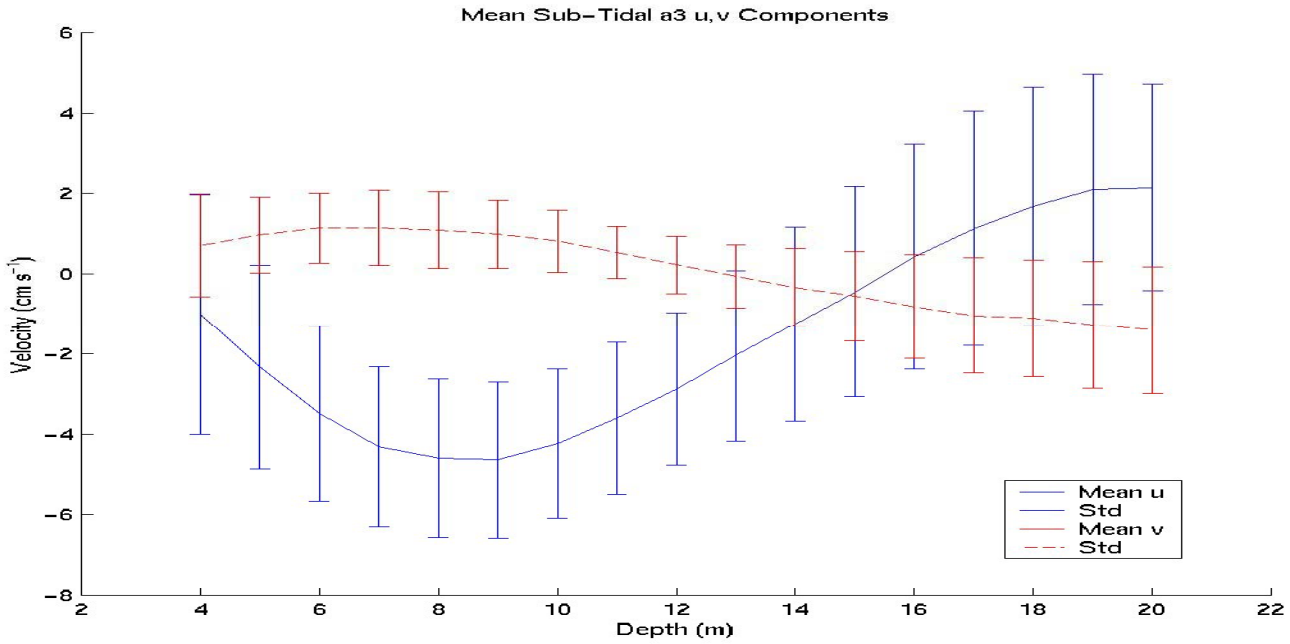

Figure 22: Profile plot of the mean along (blue solid) and cross (red dashed) channel velocity measured by the ADCP at N3. The error bars are one standard deviation in length.

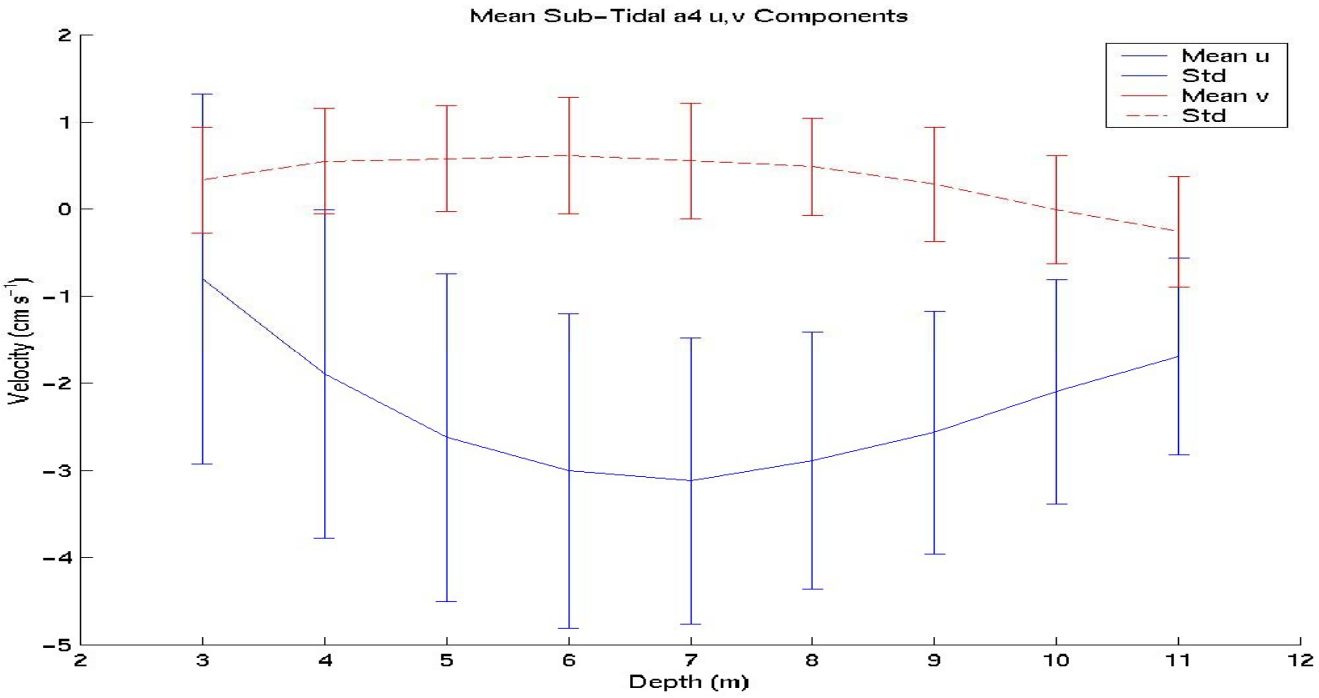

Figure 23: Profile plot of the mean along (blue solid) and cross (red dashed) channel velocity measured by the ADCP at N4. The error bars are one standard deviation in length.

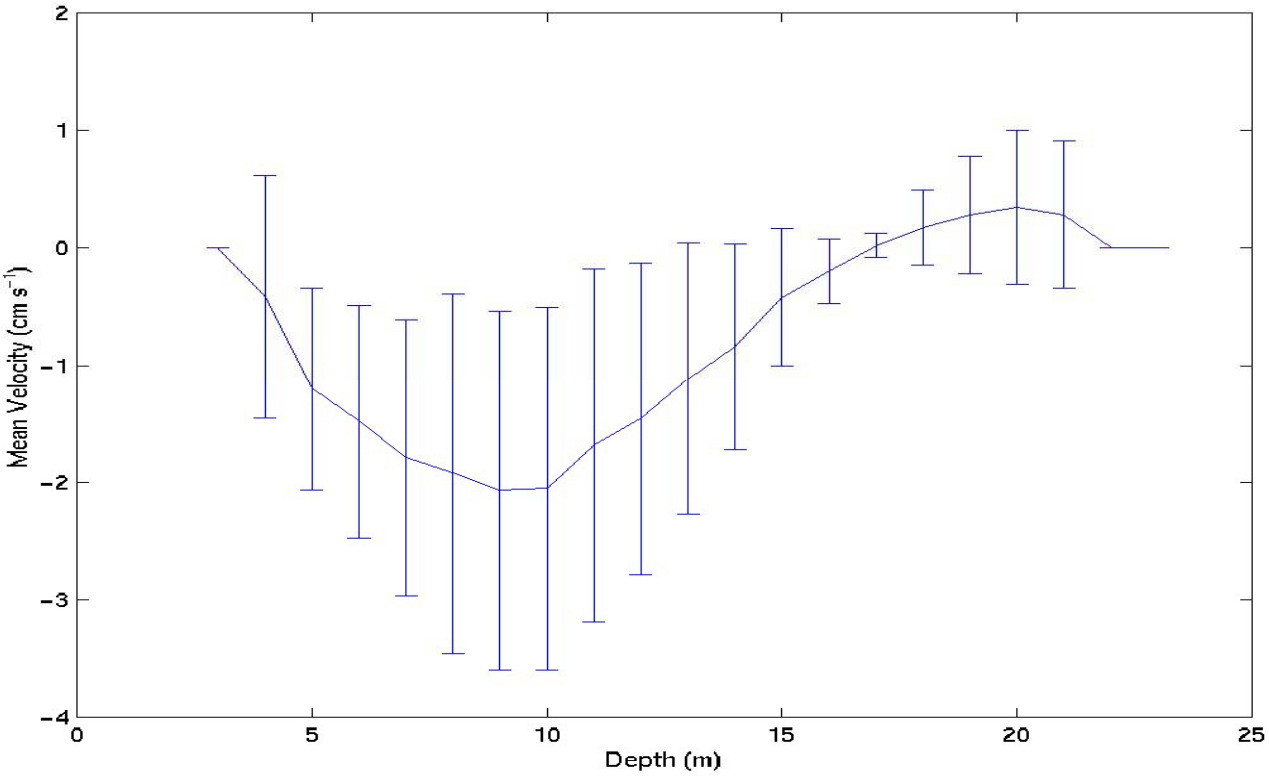

Figure 24: Mean velocity in each depth bin, determined from the interpolated velocity field. The size of the vertical bars is equal to one standard deviation in the mean velocity field.

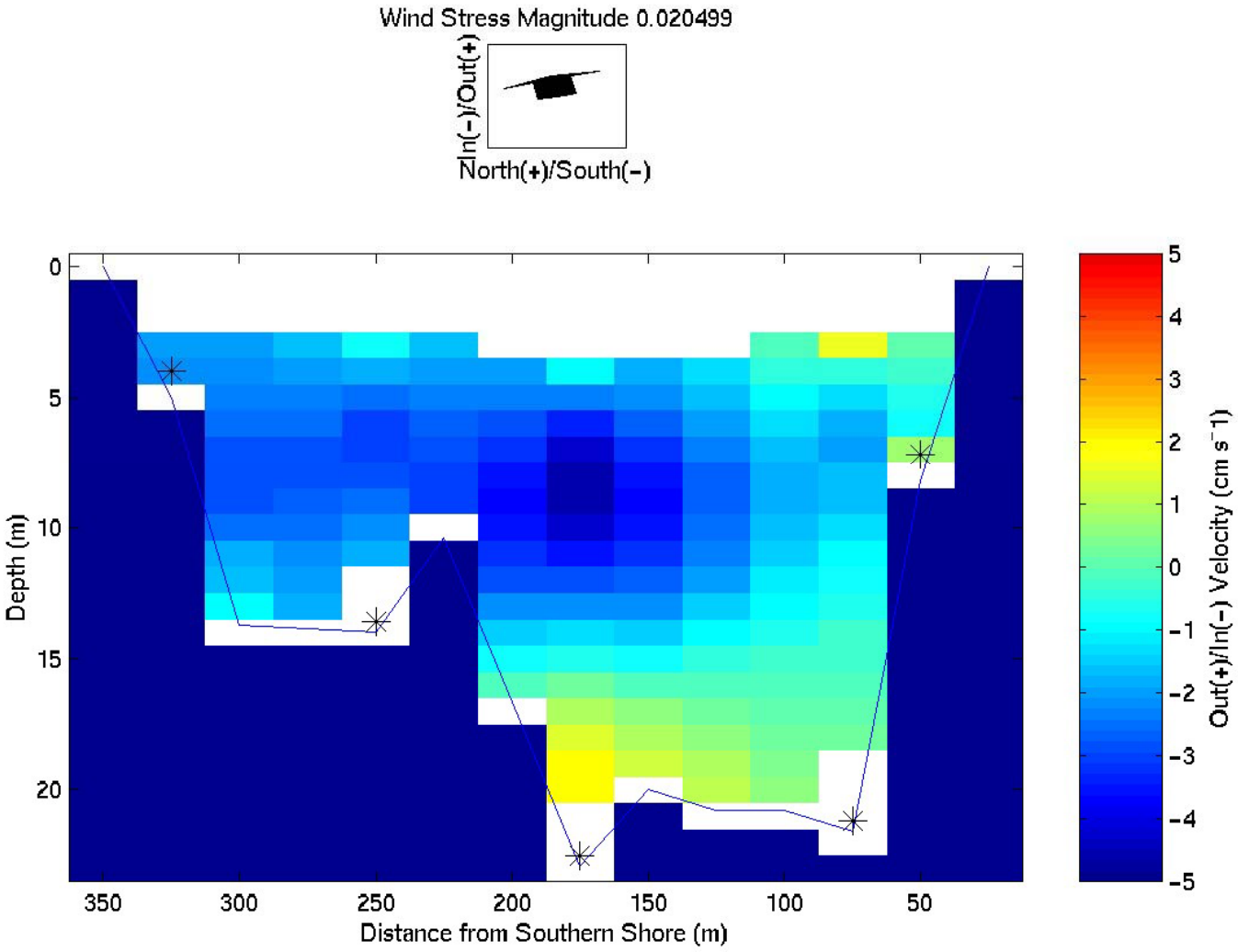

Figure 25: The mean wind vector and mean interpolated velocity across the channel. Red (+) implies flow out of harbour while blue (-) is into harbour. Perspective is looking out of Narrows to North Atlantic

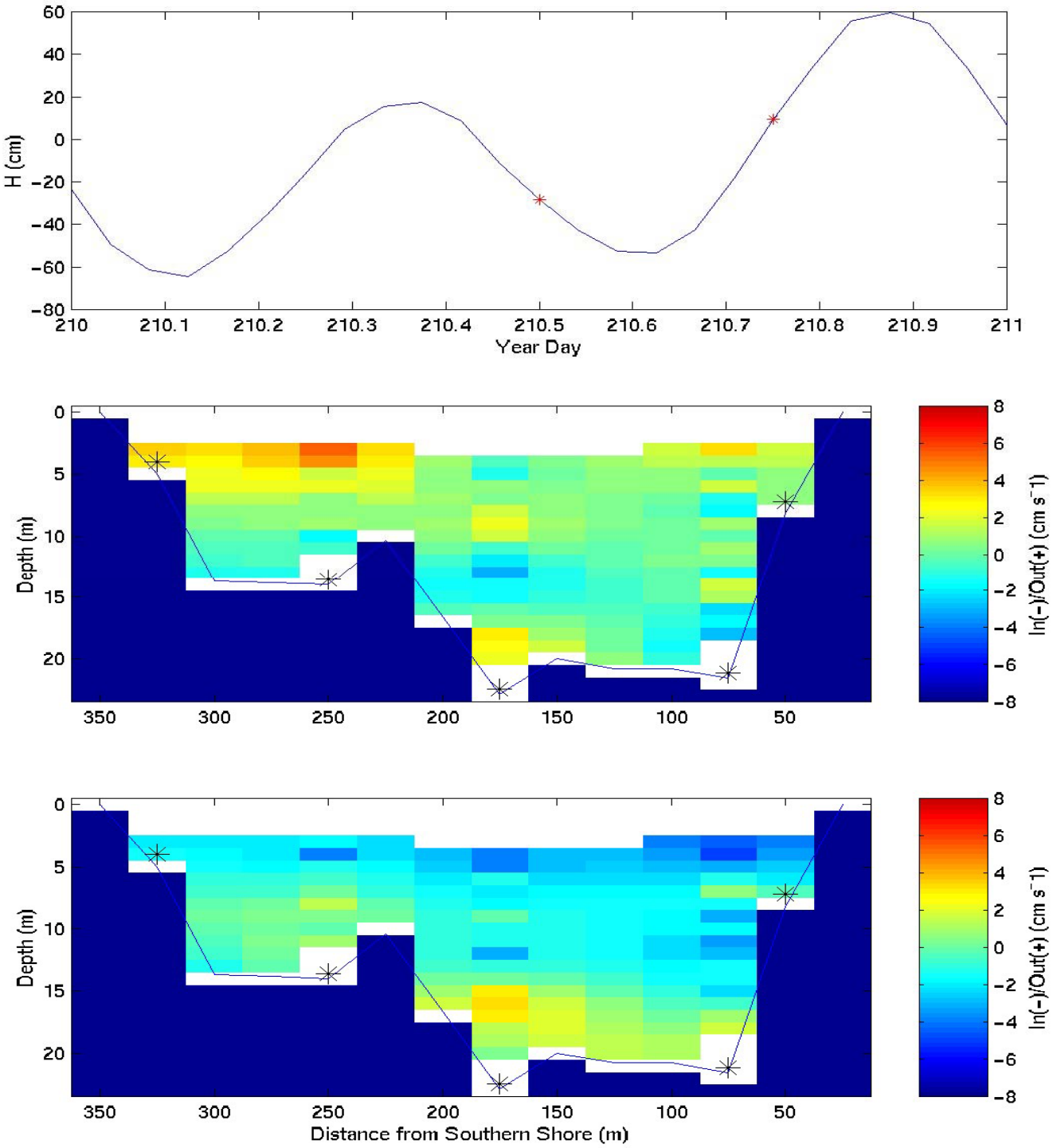

Figure 26: The surface elevation for year day 210 to 211, in cm, along with a typical interpolated velocity field during ebb (centre) and flood (bottom) tides. Red (+) implies flow out of harbour while blue (-) is into harbour. Perspective is looking out of Narrows to North Atlantic.

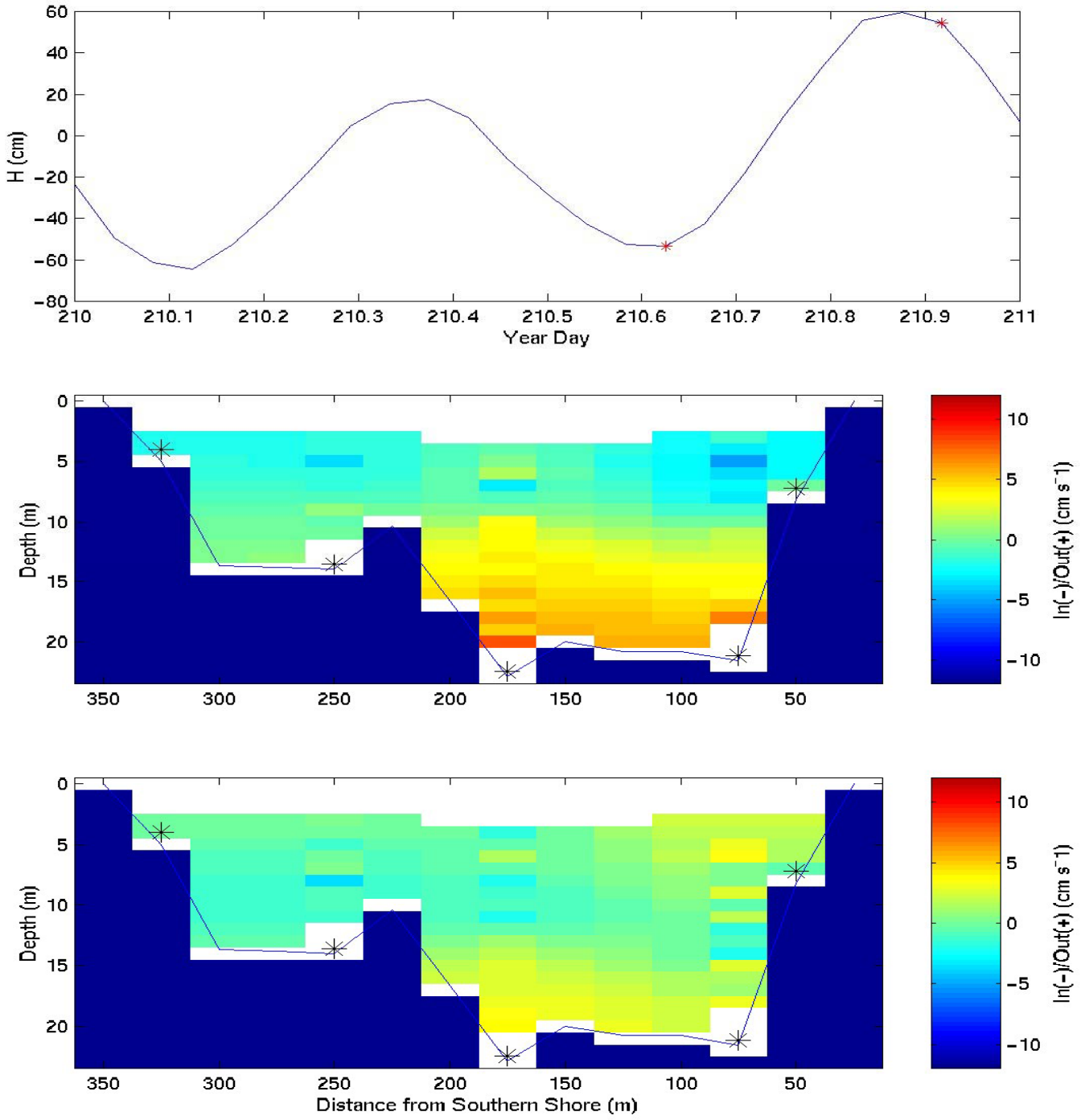

Figure 27: The surface elevation for year day 210 to 211, in cm, along with a typical interpolated velocity field during peak ebb (centre) and peak flood (bottom) tides. Red (+) implies flow out of harbour while blue (-) is into harbour. Perspective is looking out of Narrows to North Atlantic.

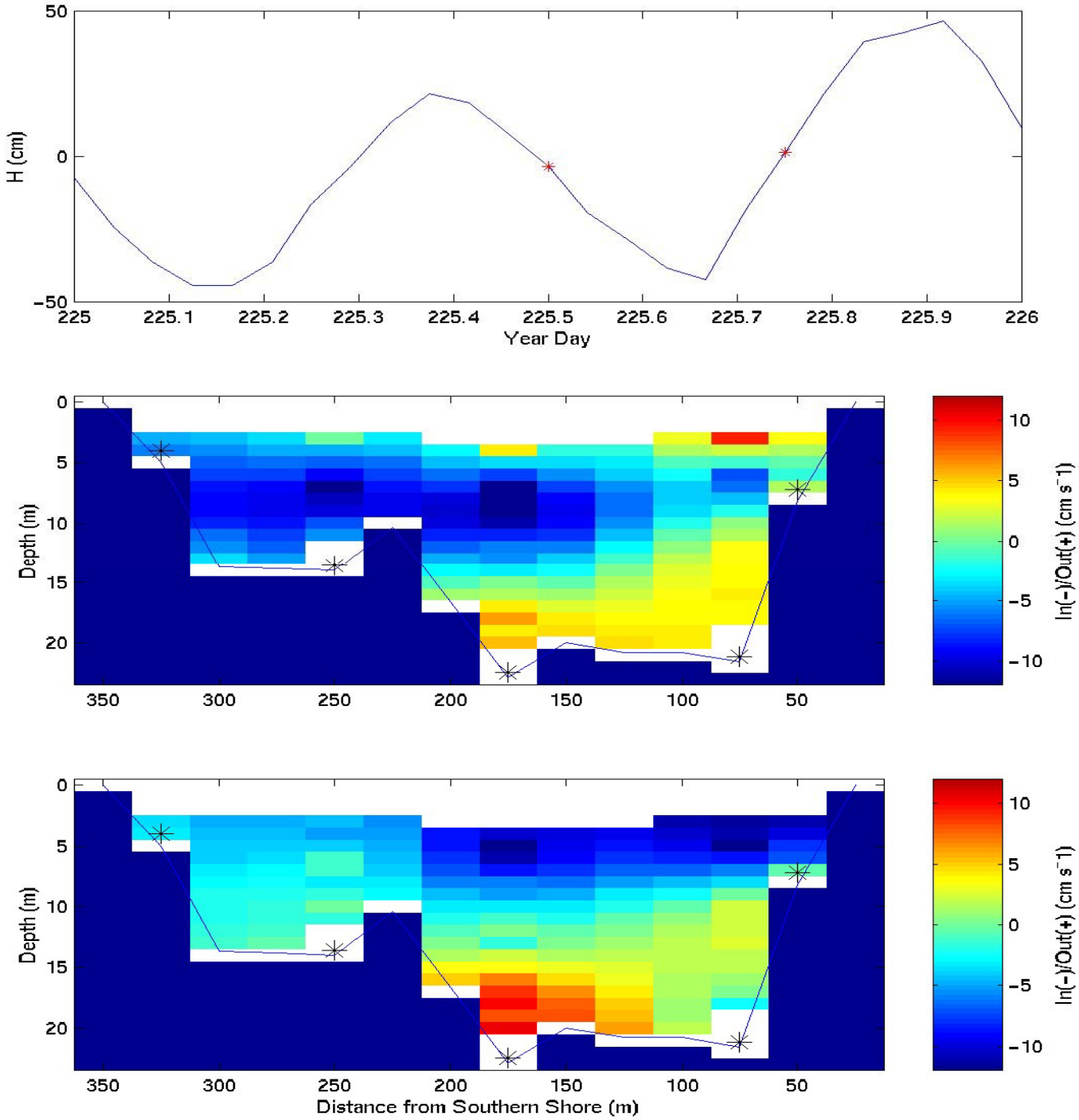

Figure 28: The surface elevation for year day 225 to 226, in cm, along with a typical interpolated velocity field during ebb (centre) and flood (bottom) tides. Red (+) implies flow out of harbour while blue (-) is into harbour. Perspective is looking out of Narrows to North Atlantic.

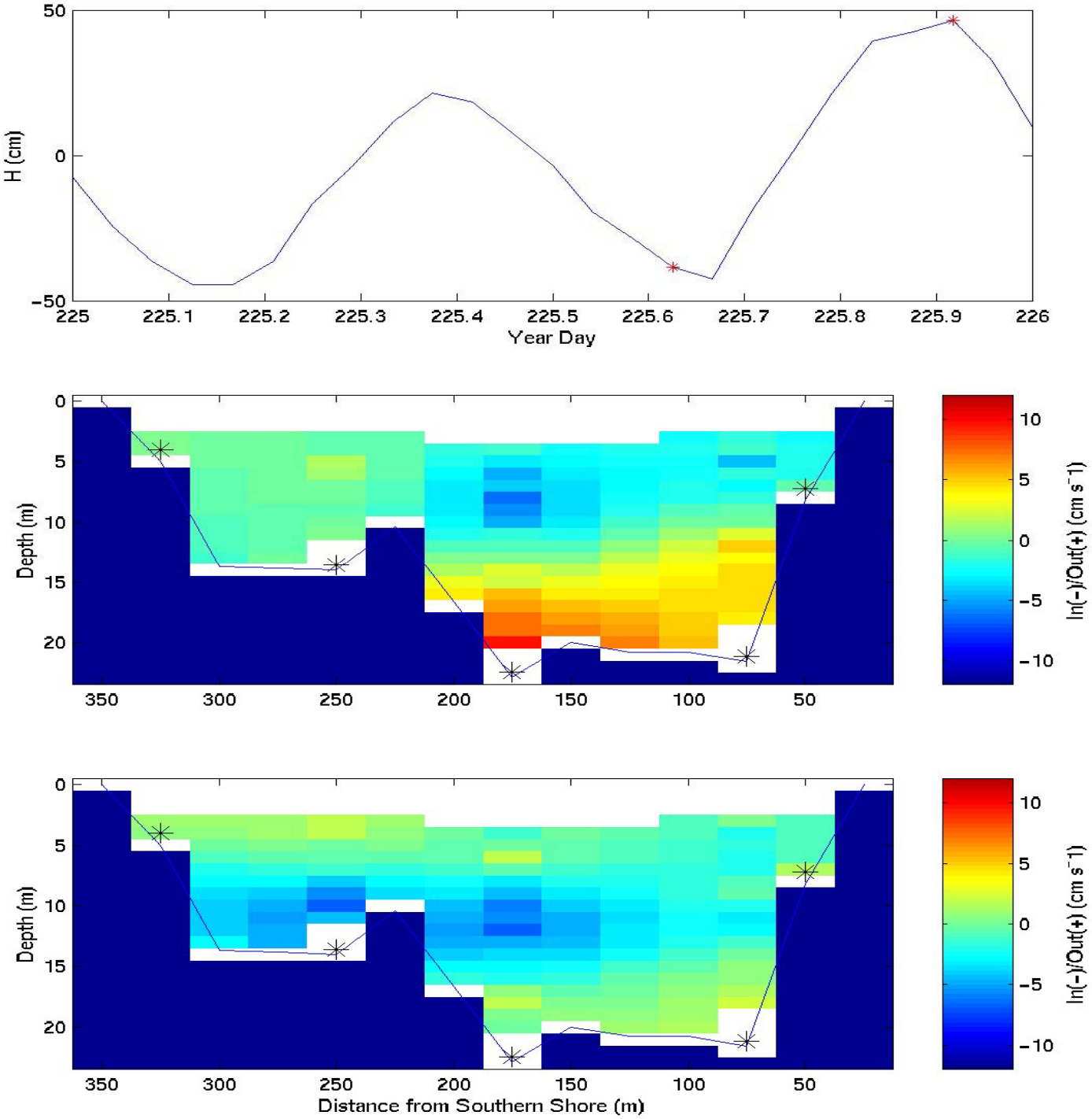

Figure 29: The surface elevation for year day 225 to 226, in cm, along with a typical interpolated velocity field during peak ebb (centre) and peak flood (bottom) tides. Red (+) implies flow out of harbour while blue (-) is into harbour. Perspective is looking out of Narrows to North Atlantic.

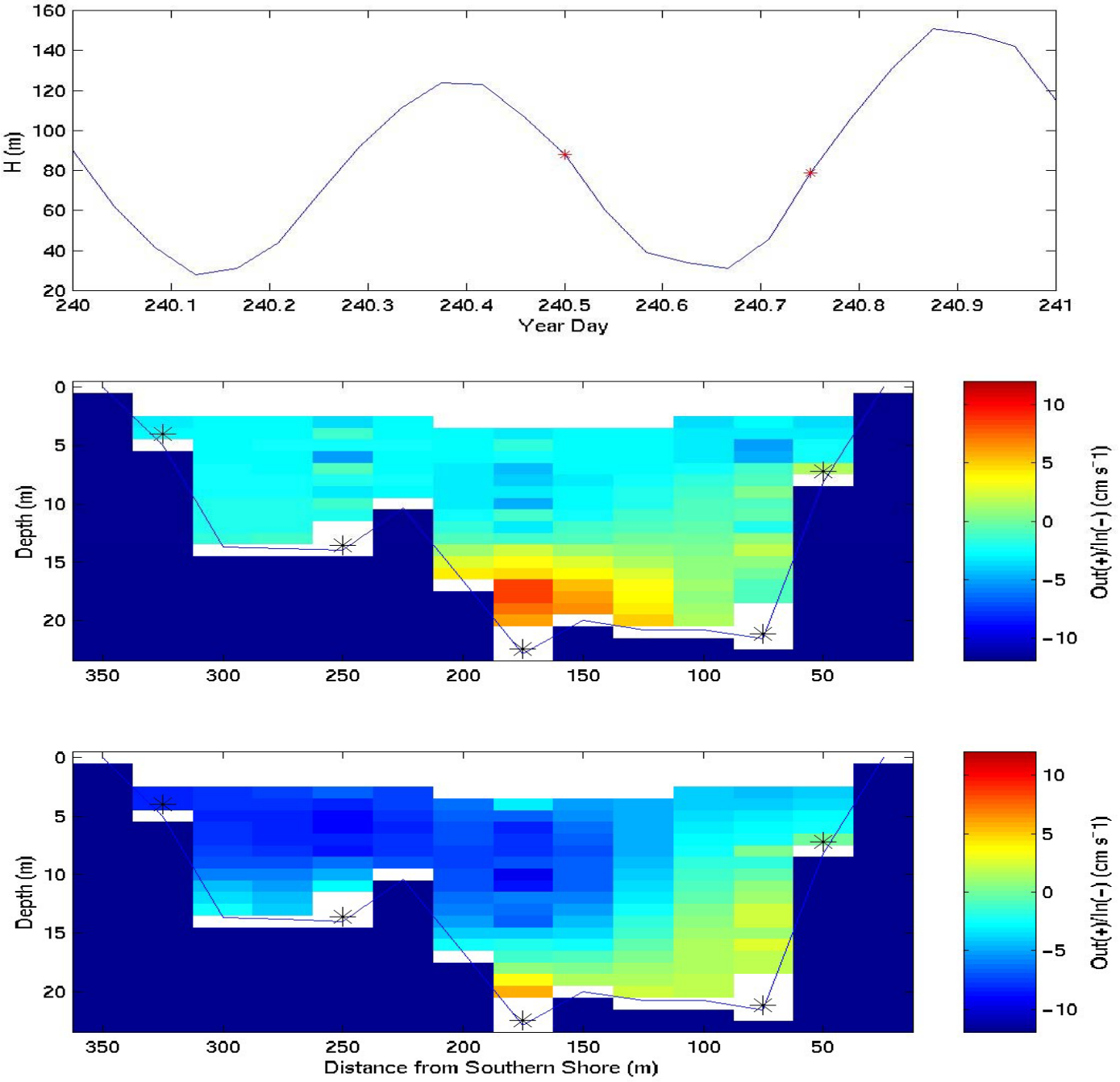

Figure 30: The surface elevation for year day 240 to 241, in cm, along with a typical interpolated velocity field during ebb (centre) and flood (bottom) tides. Red (+) implies flow out of harbour while blue (-) is into harbour. Perspective is looking out of Narrows to North Atlantic.

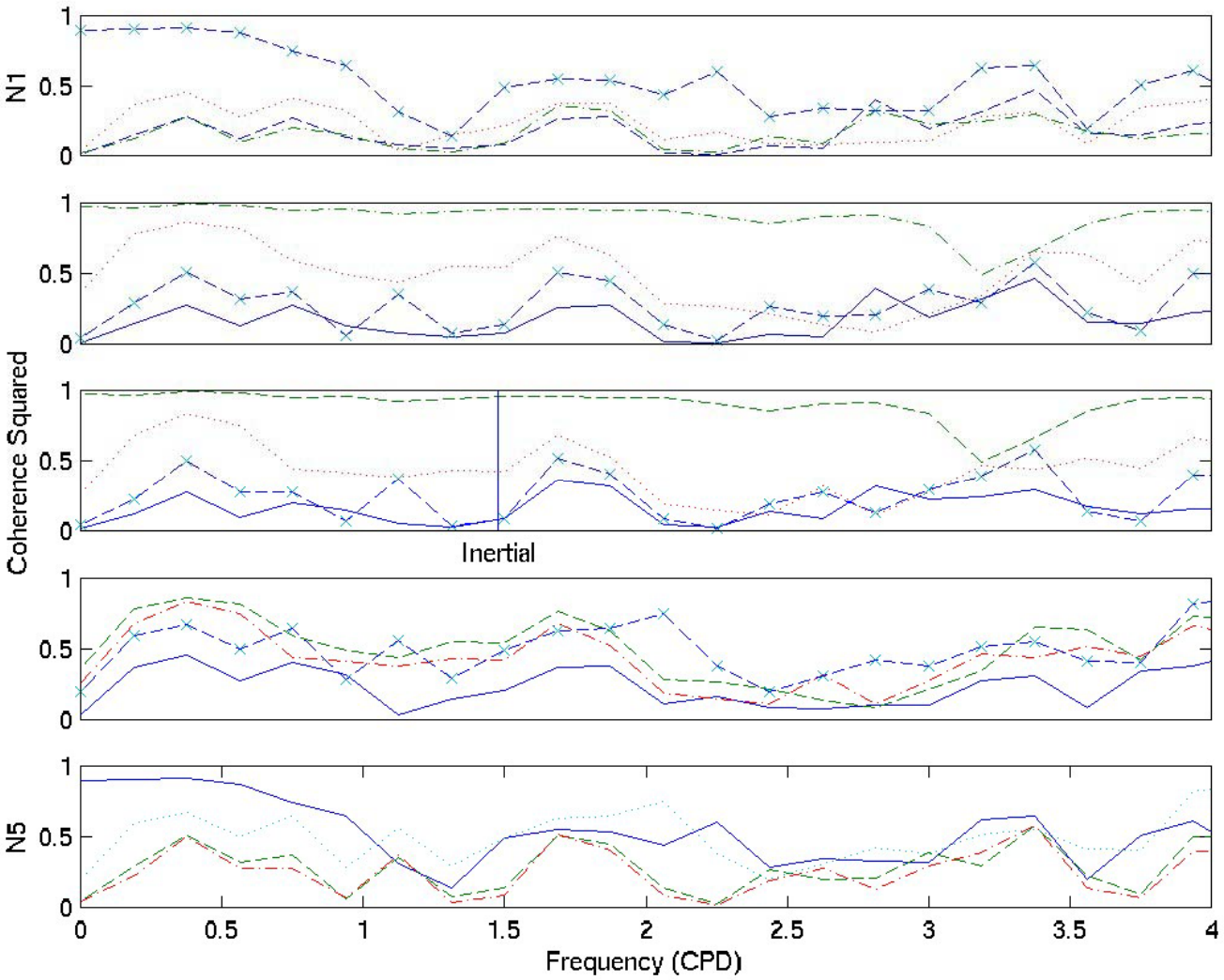

Figure 31: Each axes displays the coherence squared analysis comparing the temperature recorded at that mooring location to the temperature recorded at the other four locations (solid, N1; dashed, N2; dash-dot, N3; dotted, N4; solid-x, N5).

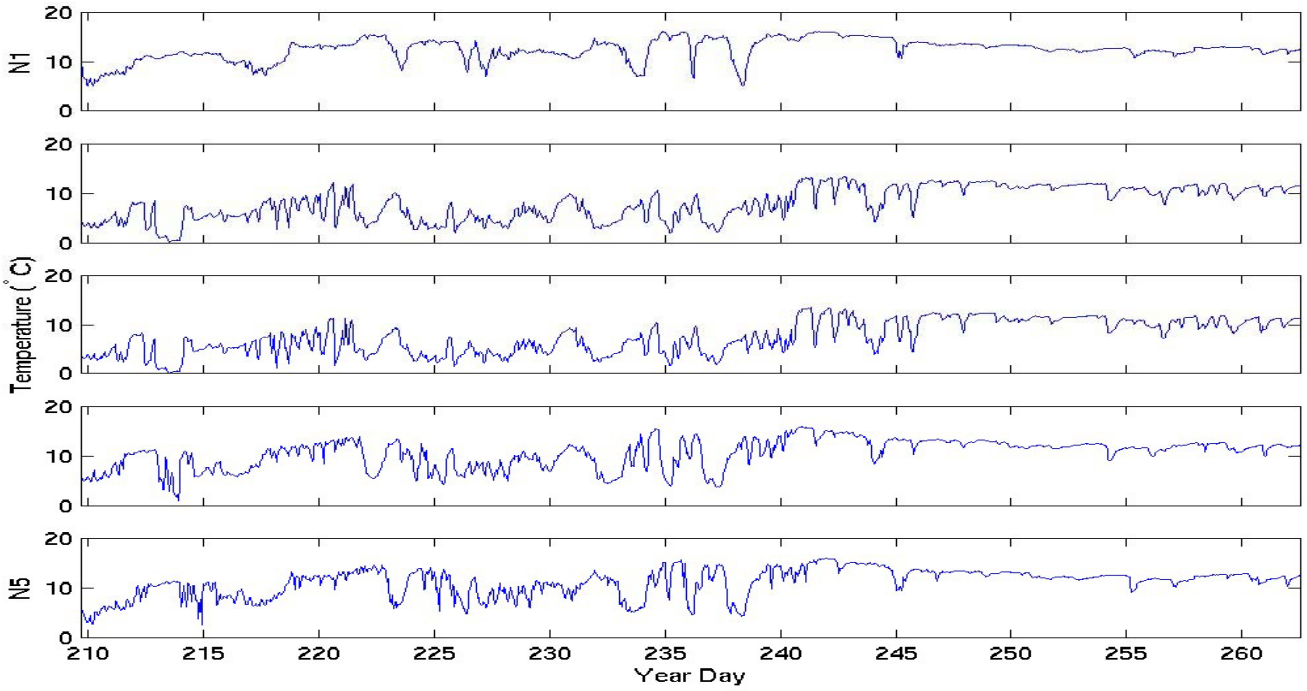

Figure 32: The temperature as recorded at each mooring location in the Narrows (N1 to N5 from top to bottom).

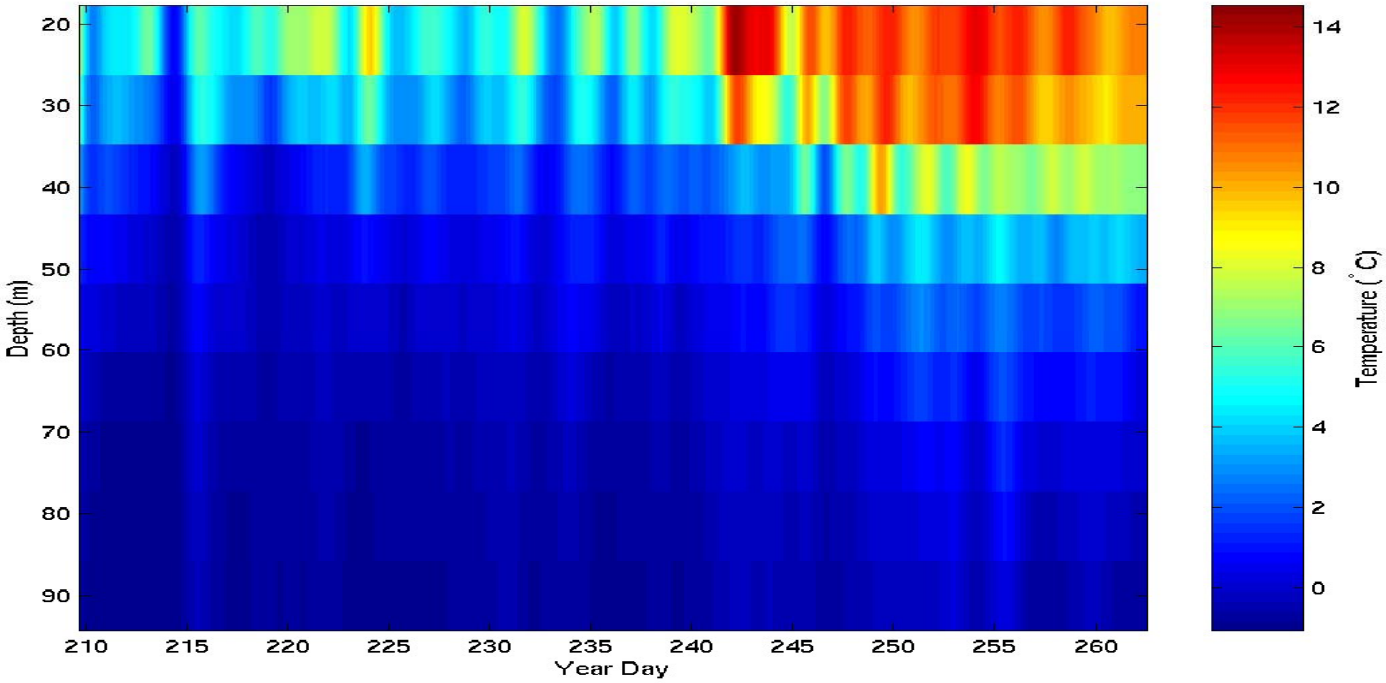

Figure 33: The temperature as recorded at mooring location H1, filtered to remove all but the subtidal signal.

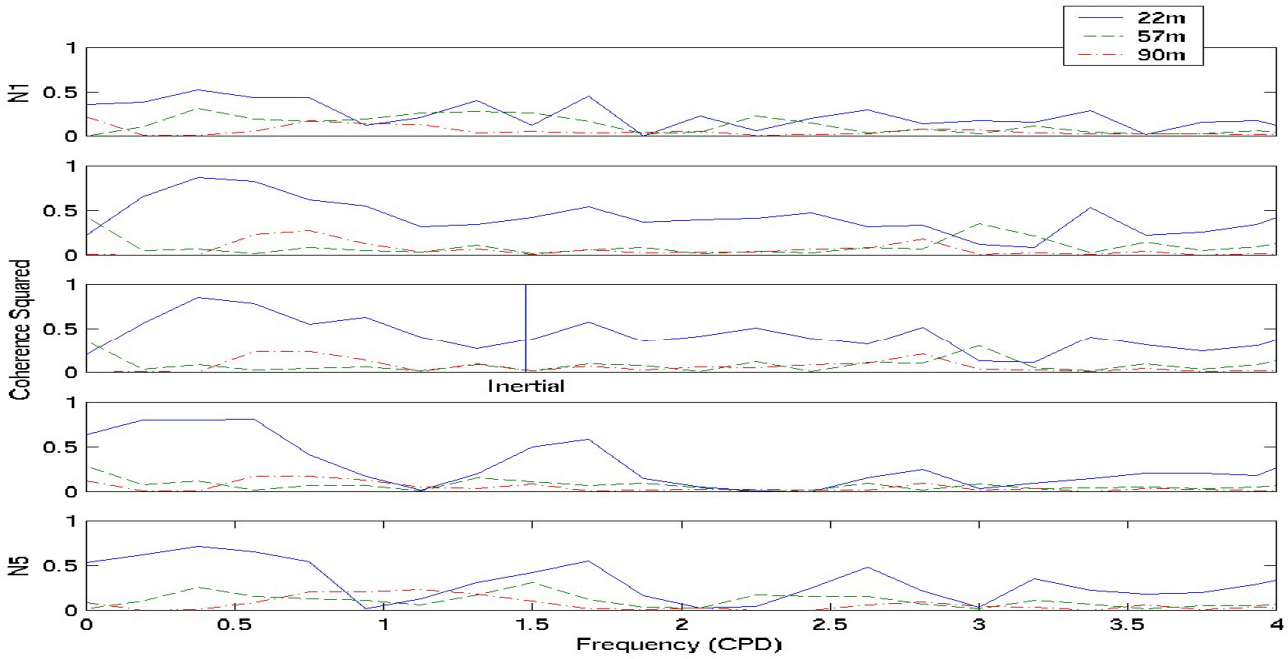

Figure 34: Each axis displays the coherence square analysis comparing the measured temperature at each mooring location (N1 to N5 top to bottom) to the temperature measured at depths of 22 m (solid) 57 m (dashed) and 90 m (dash dot) from the Vemco's at H1.

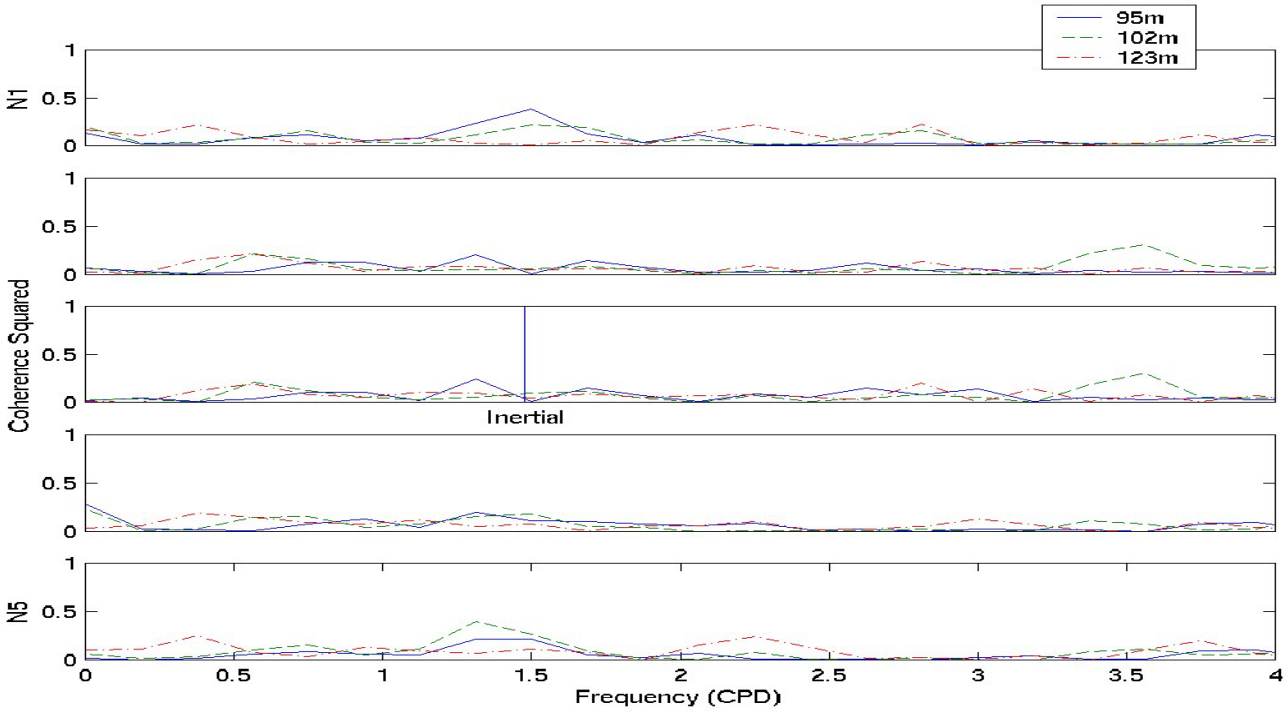

Figure 35: Each axis displays the coherence square analysis comparing the measured temperature at each mooring location (N1 to N5 top to bottom) to the temperature measured at depths of 95 m(solid), 102 m (dashed) and 123 m (dash dot) from the Vemco's at H2.

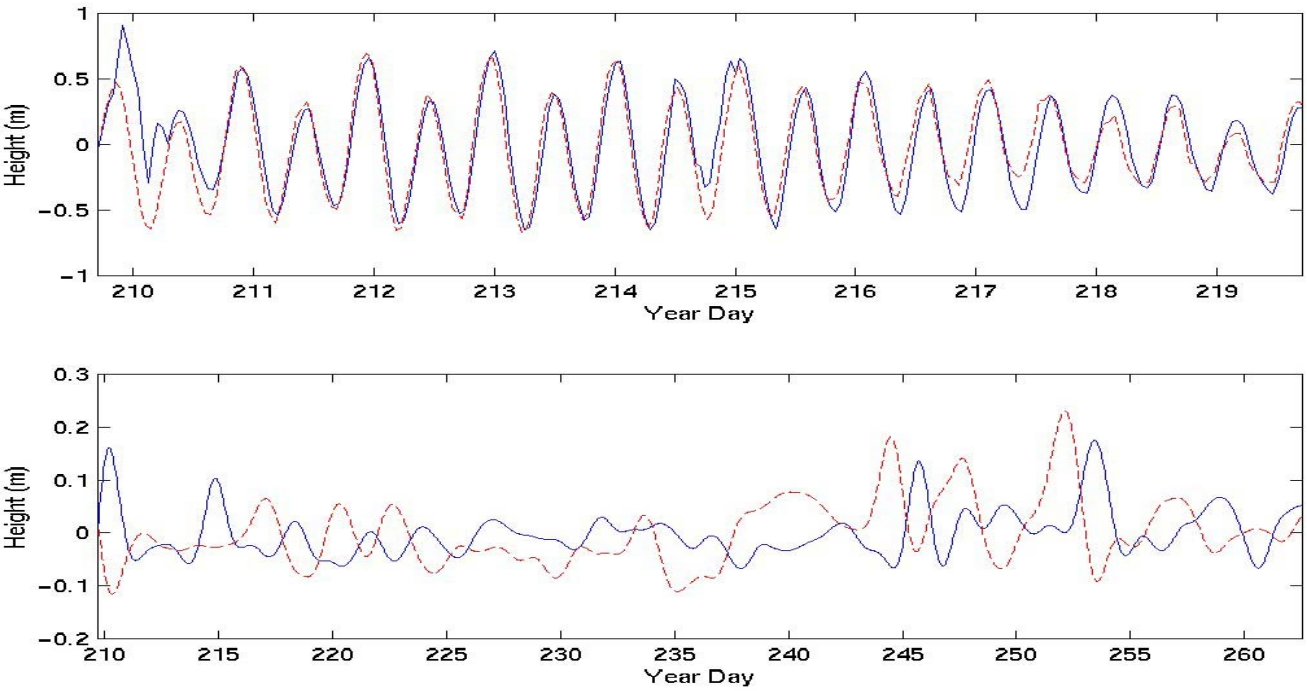

Figure 36: Surface elevation recorded by the tide gauge at N5 (solid), and by MEDS dashed). The upper plot shows a 10 day period using the unfiltered data, while the lower plot shows only the sub-tidal surface elevation.

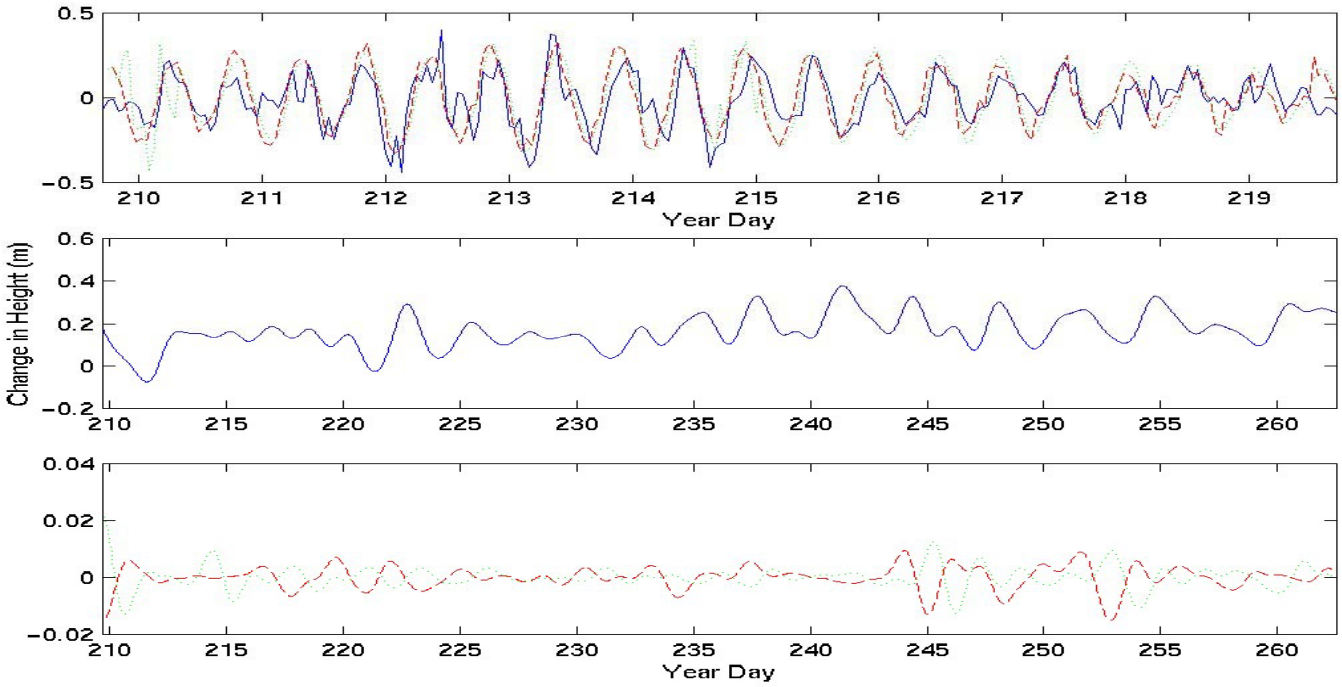

Figure 37: The change in surface elevation as calculated from the interpolated velocity data (solid), the tide gauge (red dashed) and the MEDS (green dash dot). The upper plot presents the change in elevation using the raw data, while the lower plot shows the filtered sub-tidal change using the velocity data.

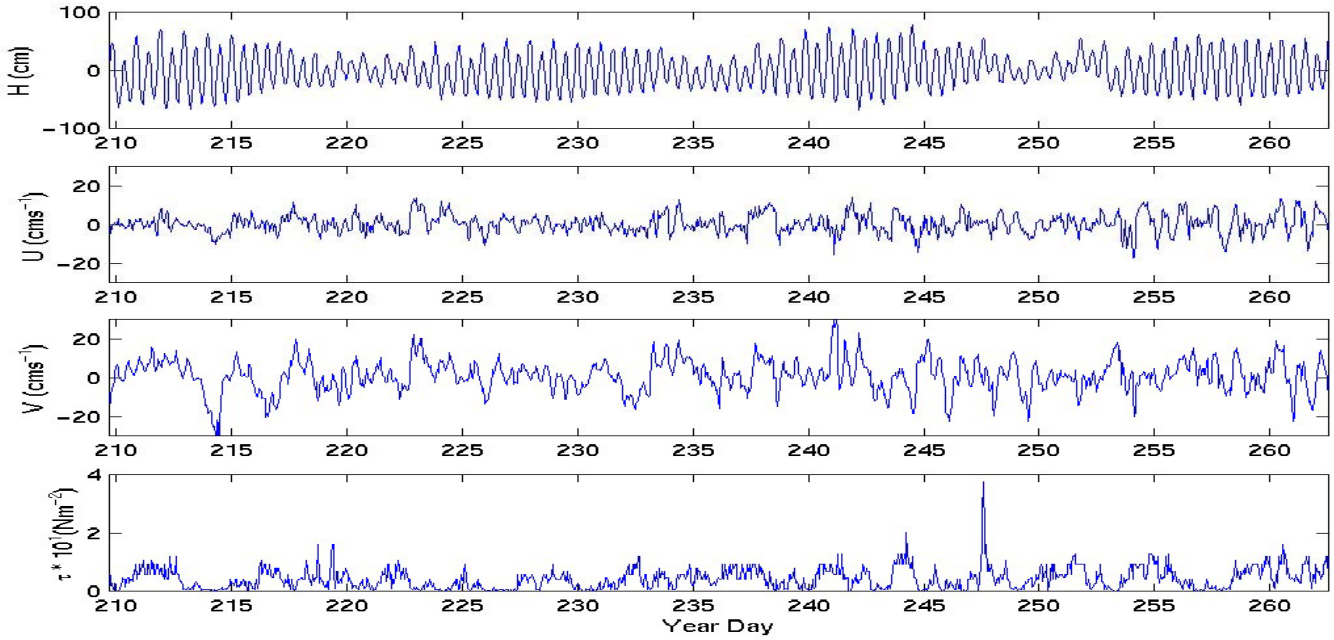

Figure 38: The raw times series of the u component and v components of the S4 current meter at H1 in cm s^{-1}. Included are the surface elevation in cm, and the wind stress in Nm^{-2}.

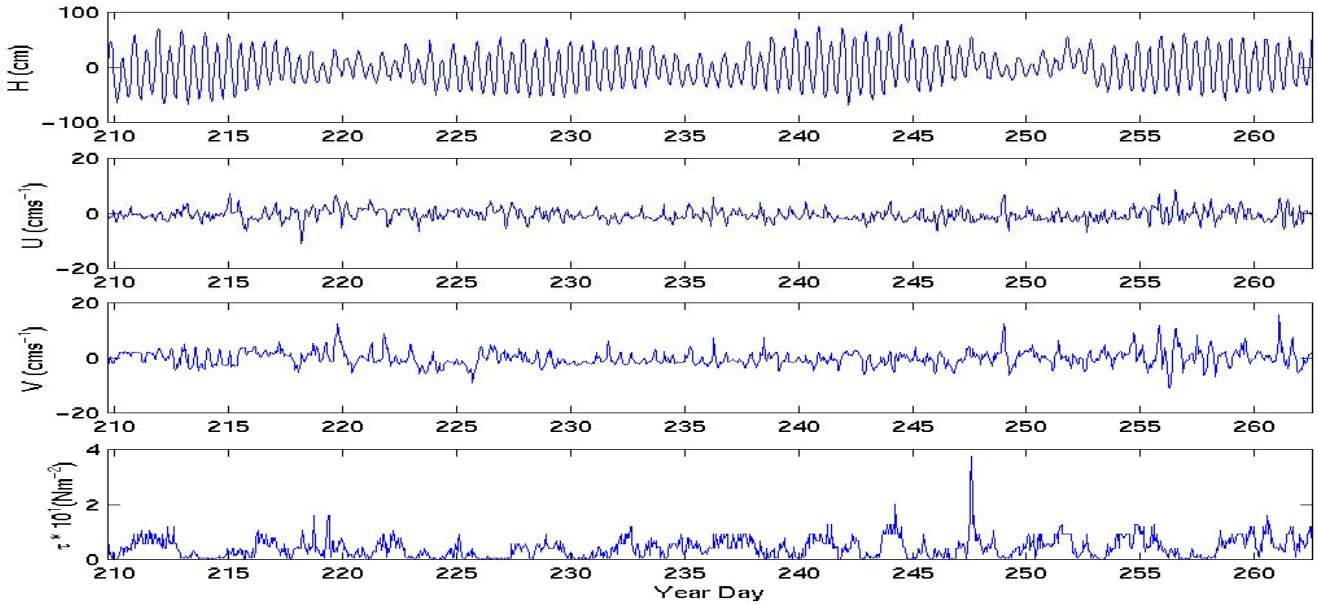

Figure 39: The raw times series of the u component and v components of the RCM current meter at H1 in cm s^{-1}. Included are the surface elevation in cm, and the wind stress in N m^{-2}.

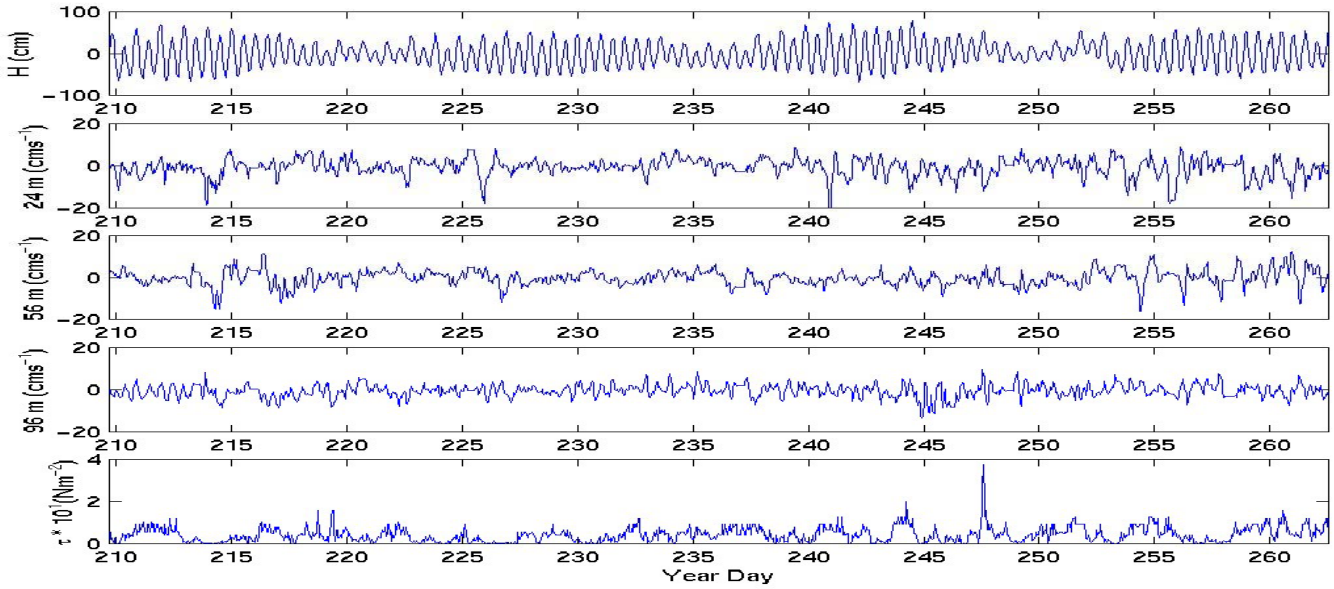

A

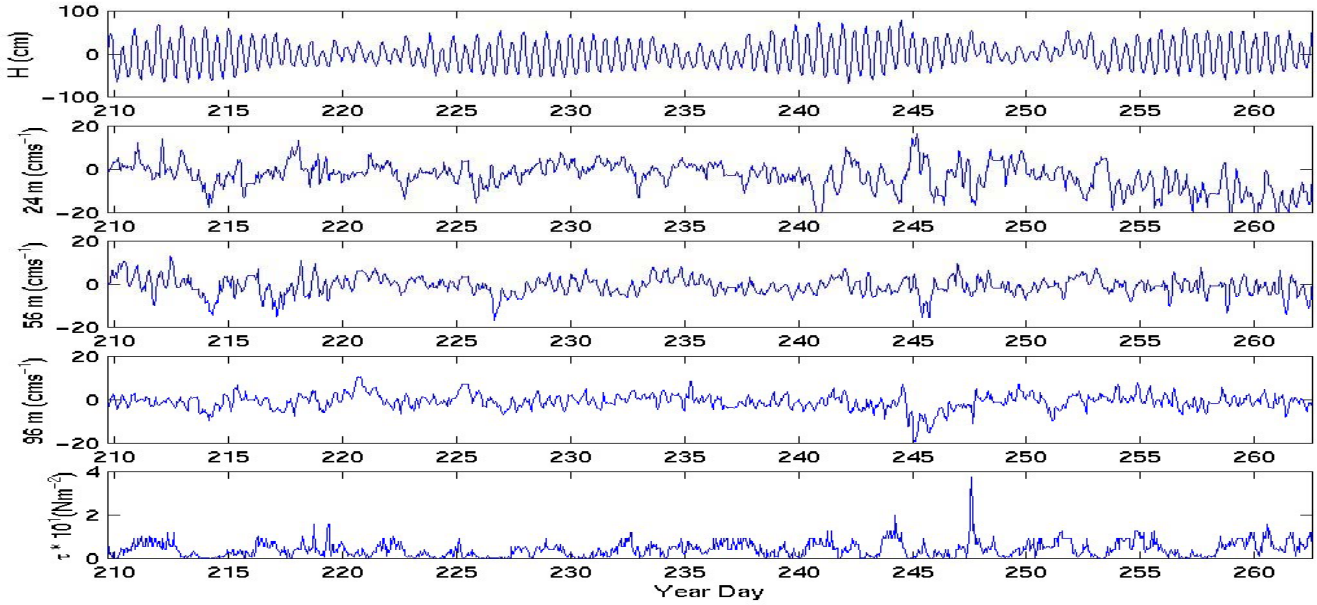

B

Figure 40: The raw times series of the u component (A) and v component of selected depths from the ADCP at H2 in cm s^{-1}. Included are the surface elevation in cm, and the wind stress in N m^{-2}.

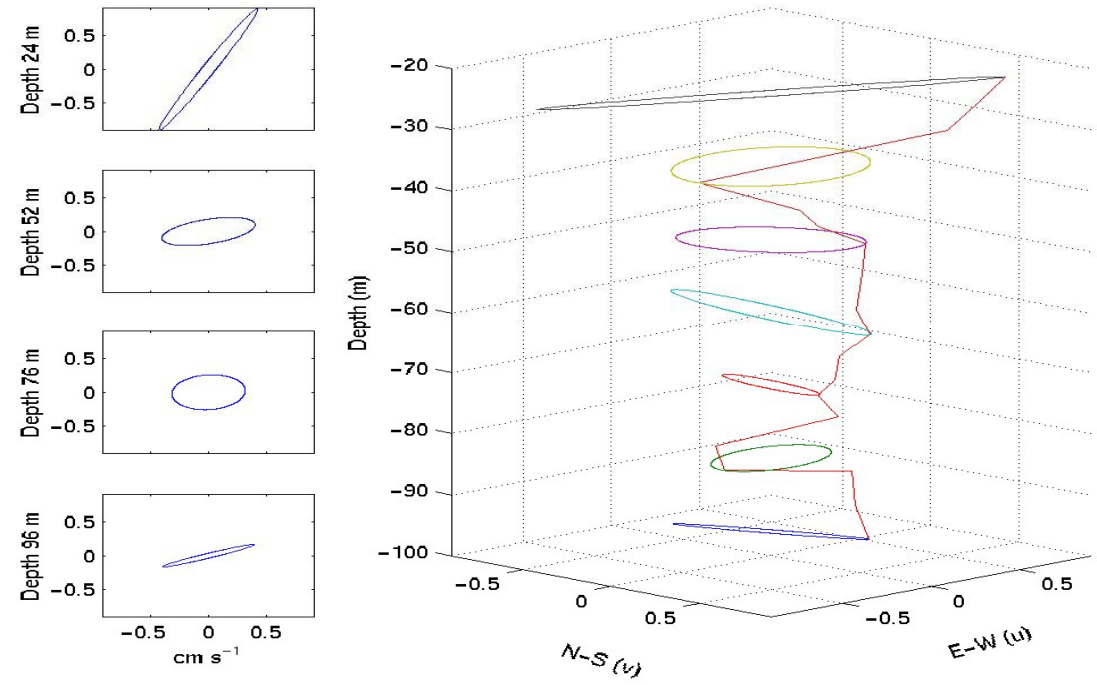

A

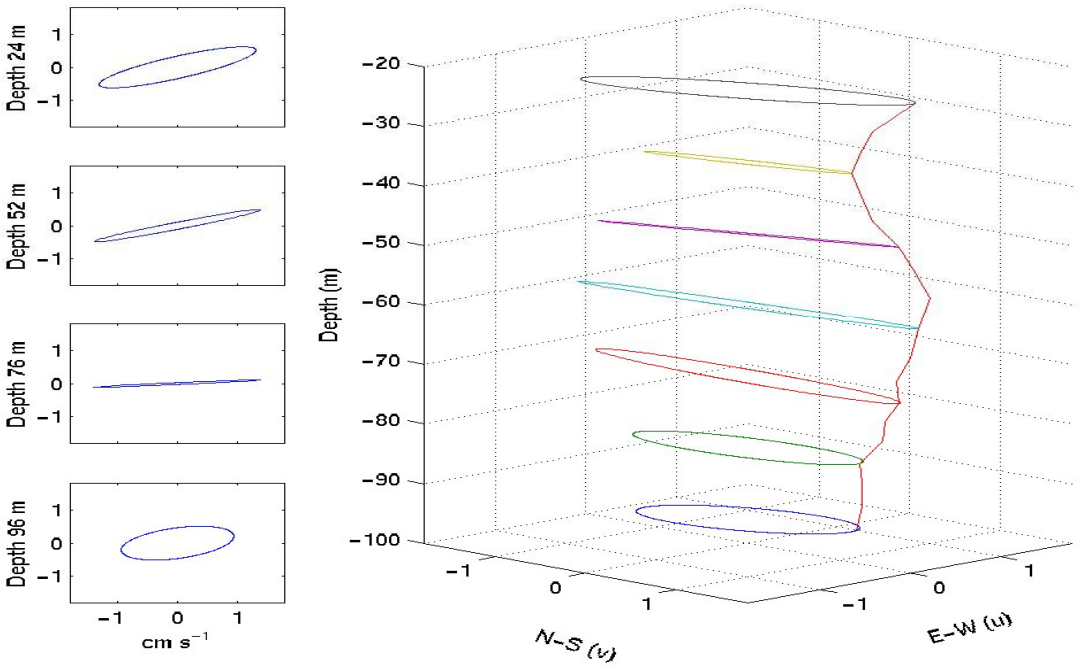

B

Figure 41: The tidal ellipses at the K_1 (A) and M_2 (B) frequencies, determined by Foreman's analysis at H2. Here, E-W and N-S are the Earth Axes.

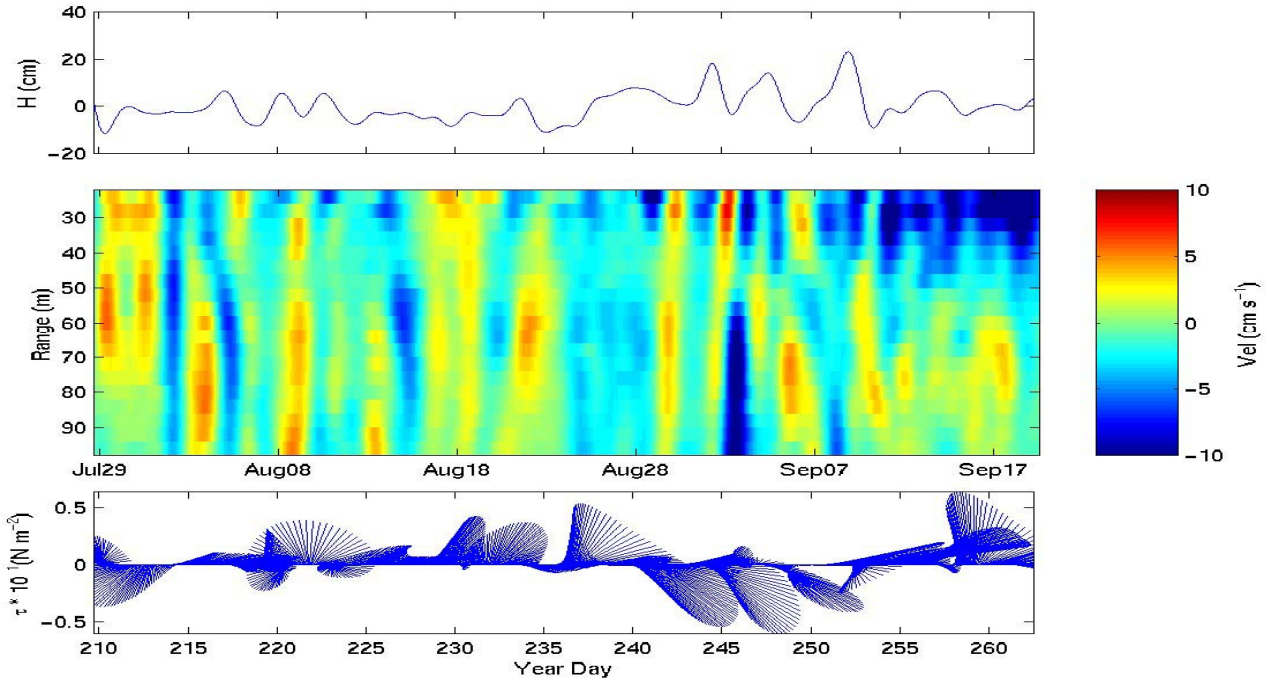

Figure 42: Subtidal current velocity for the u (East/West) component measured at H2.

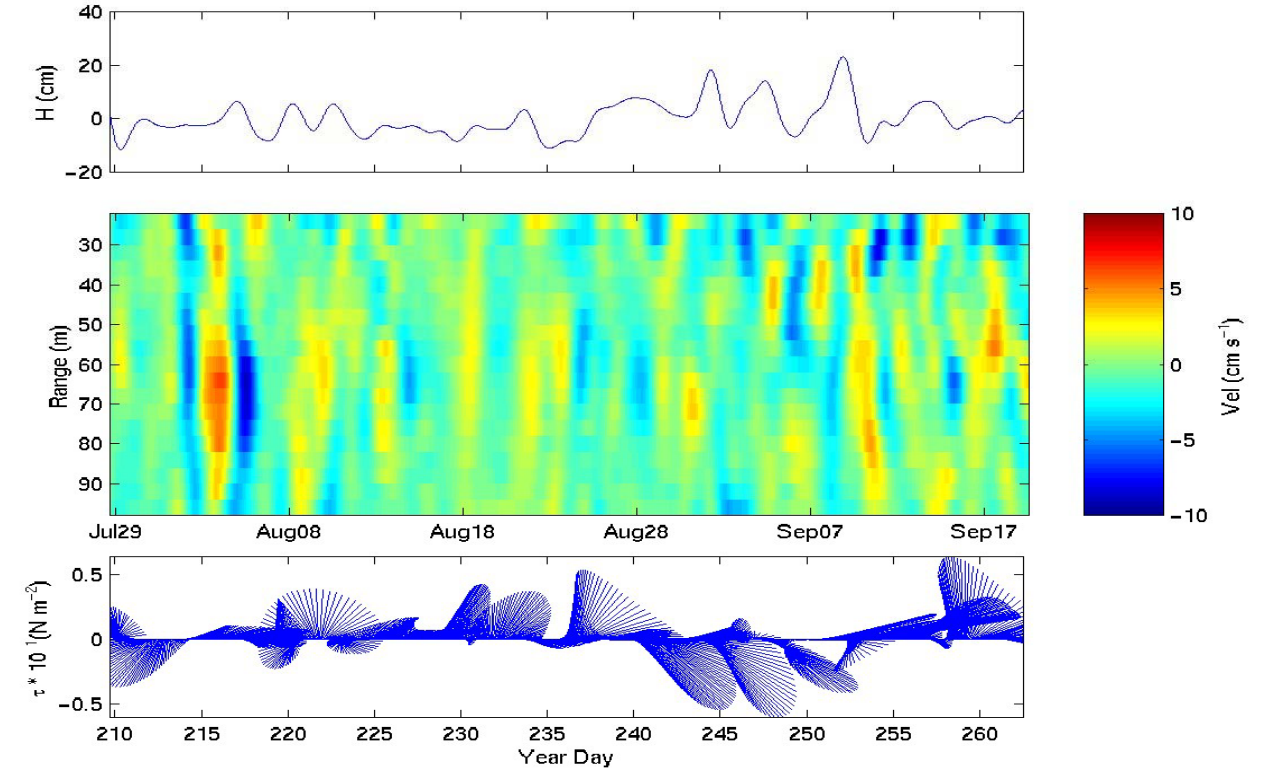

Figure 43: Subtidal current velocity for the v (North/South) component measured at H2.

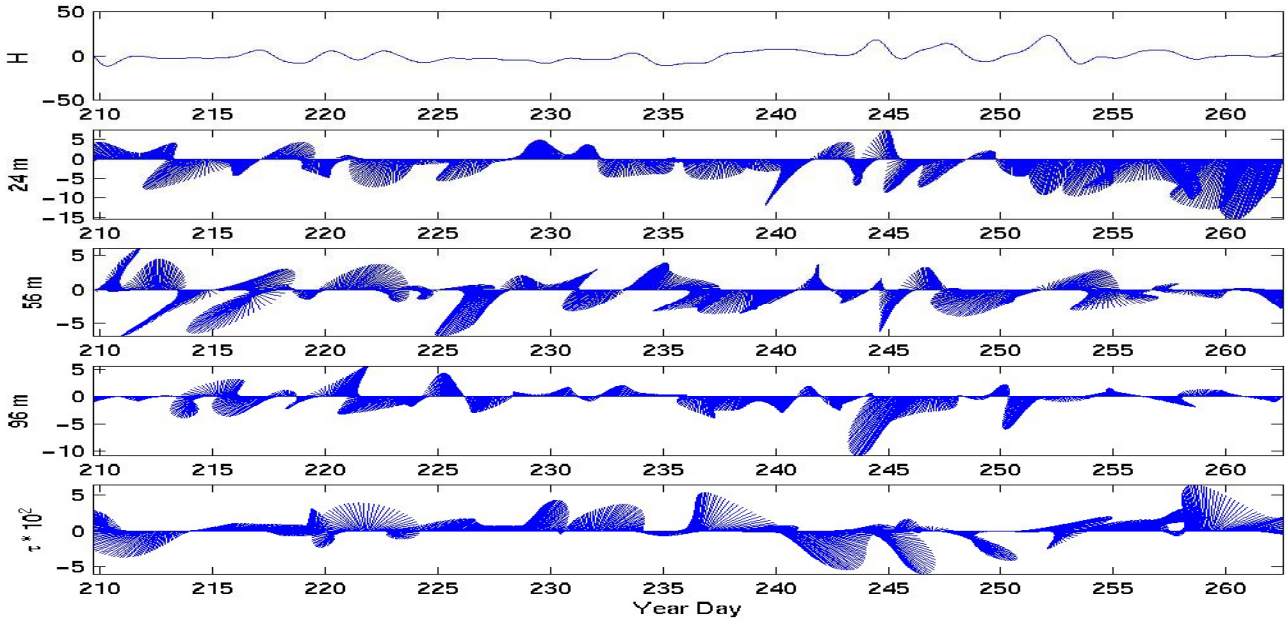

Figure 44: Subtidal current velocities at selected depths from H2.

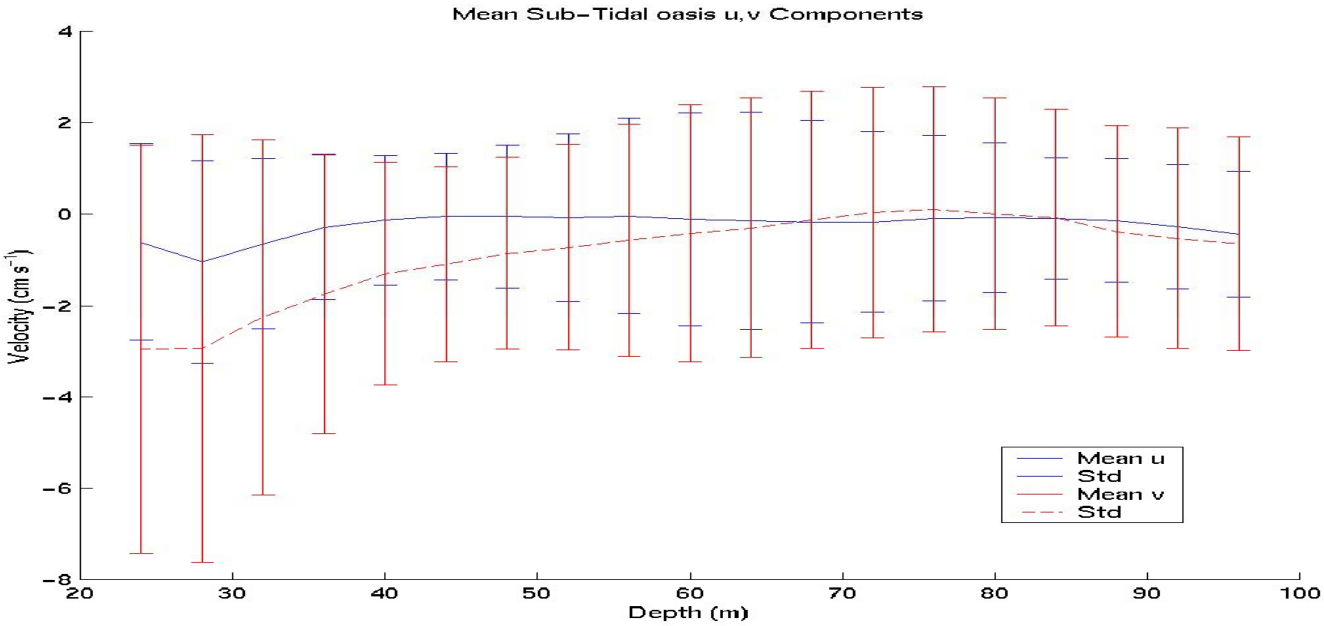

Figure 45: Mean velocity of East/West (blue) and North/South (red dashed) components measured by the ADCP at H2. The error bars are one standard deviation in length.

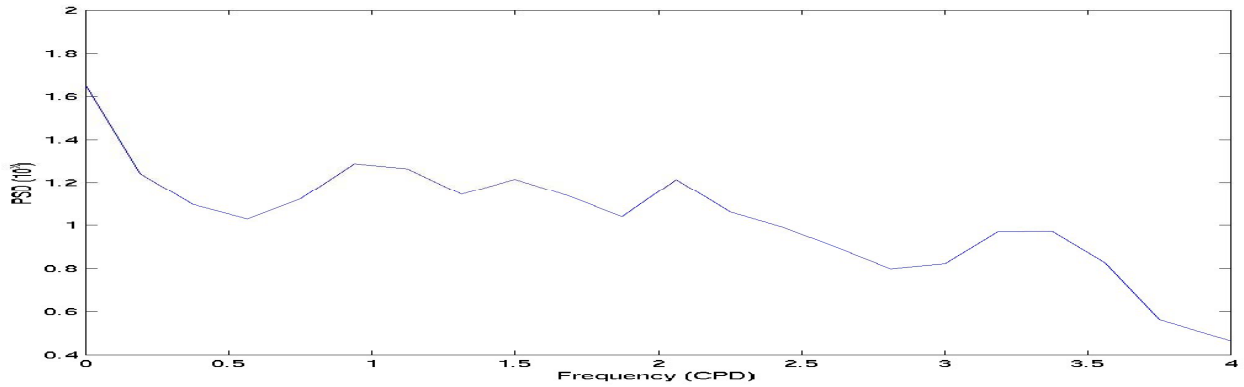

Figure 46: Power Spectral Density of the In/Out current time series from the S4 at H1.

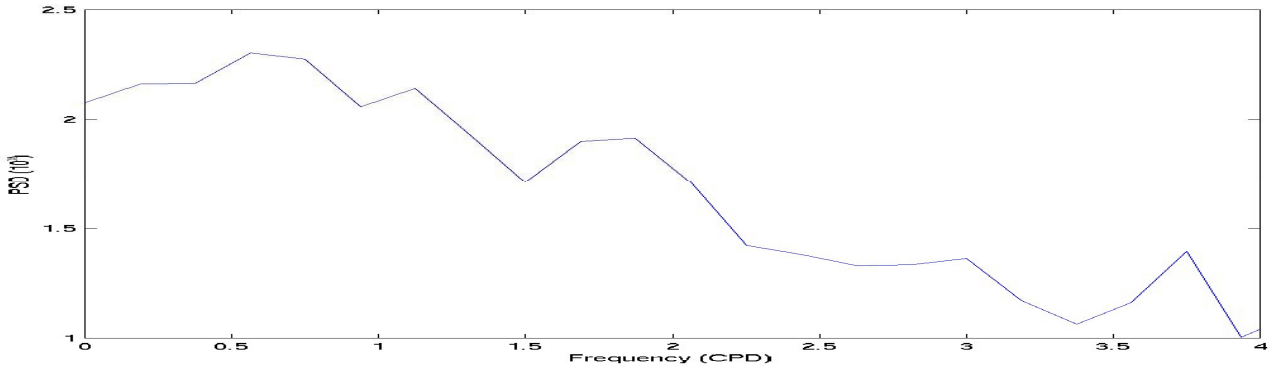

Figure 47: Power Spectral Density of the In/Out current time series from RCM at H1.

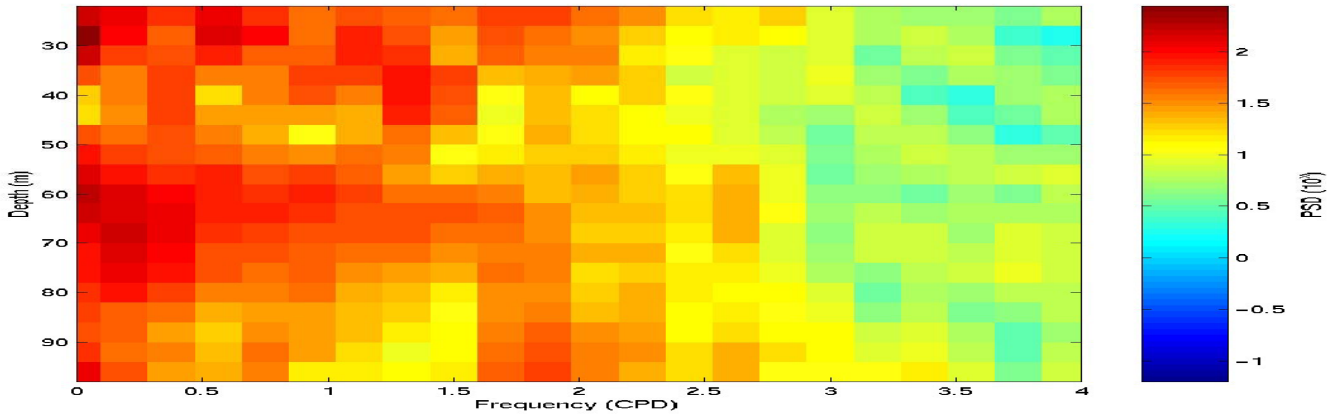

Figure 48: Power Spectral Density for the current at each depth bin measured by the ADCP at H2 along the In/Out.

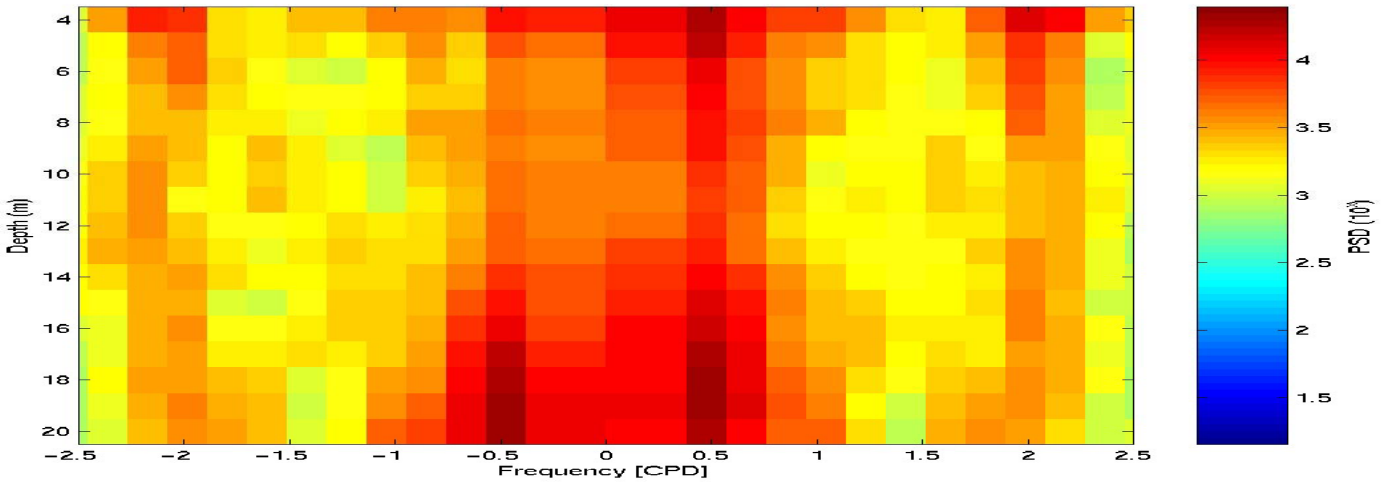

A

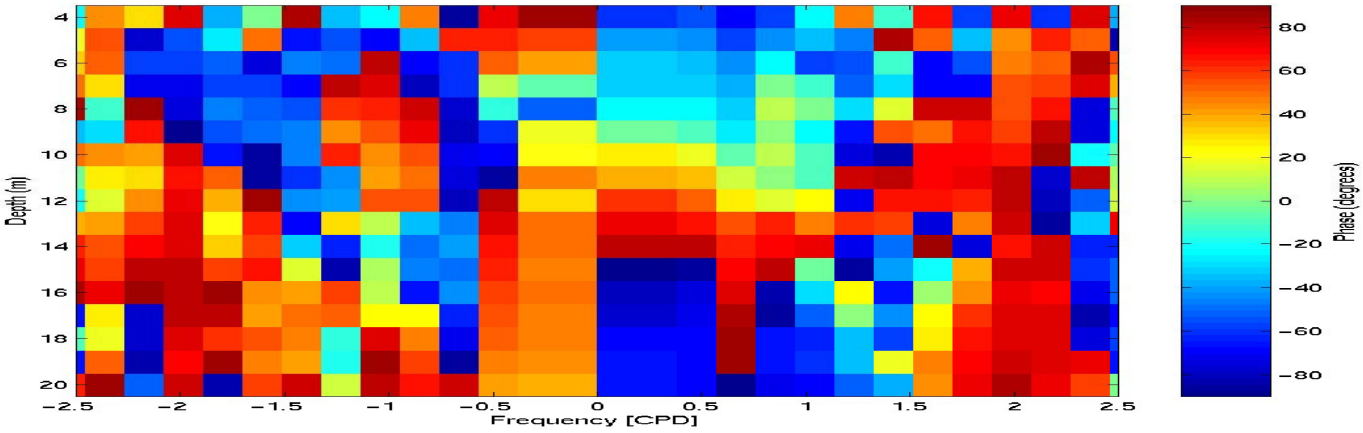

B

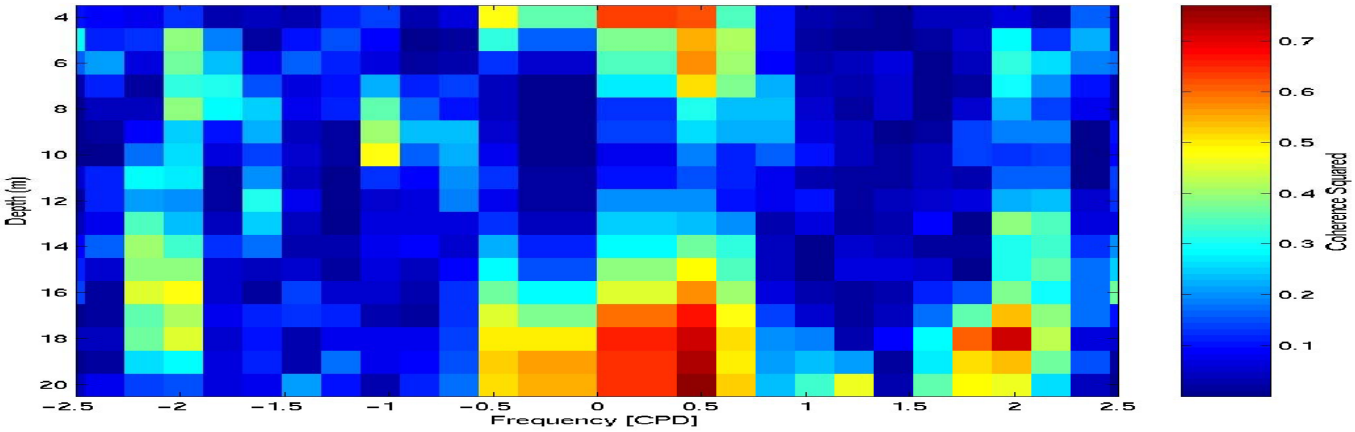

C

Figure 49: Rotary auto spectra (A) from the ADCP current velocities recorded at N3, inner coherence squared (B) between N3 and the S4 at H1 (depth 22 m), and the inner phase (C) between N3 and S4 at H1.

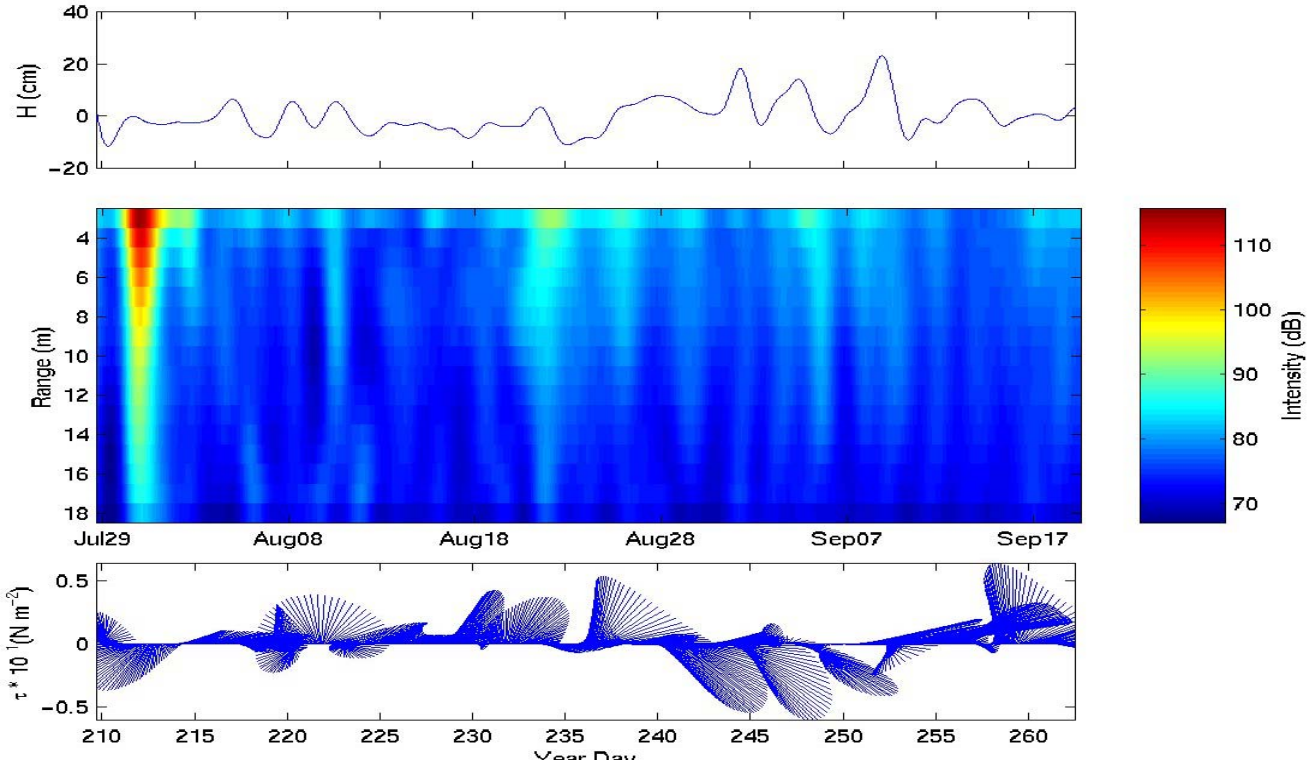

Figure 50: Subtidal backscatter intensity from N2. Included are the surface elevation (cm) and the magnitude of the wind stress (N m^{-2}).

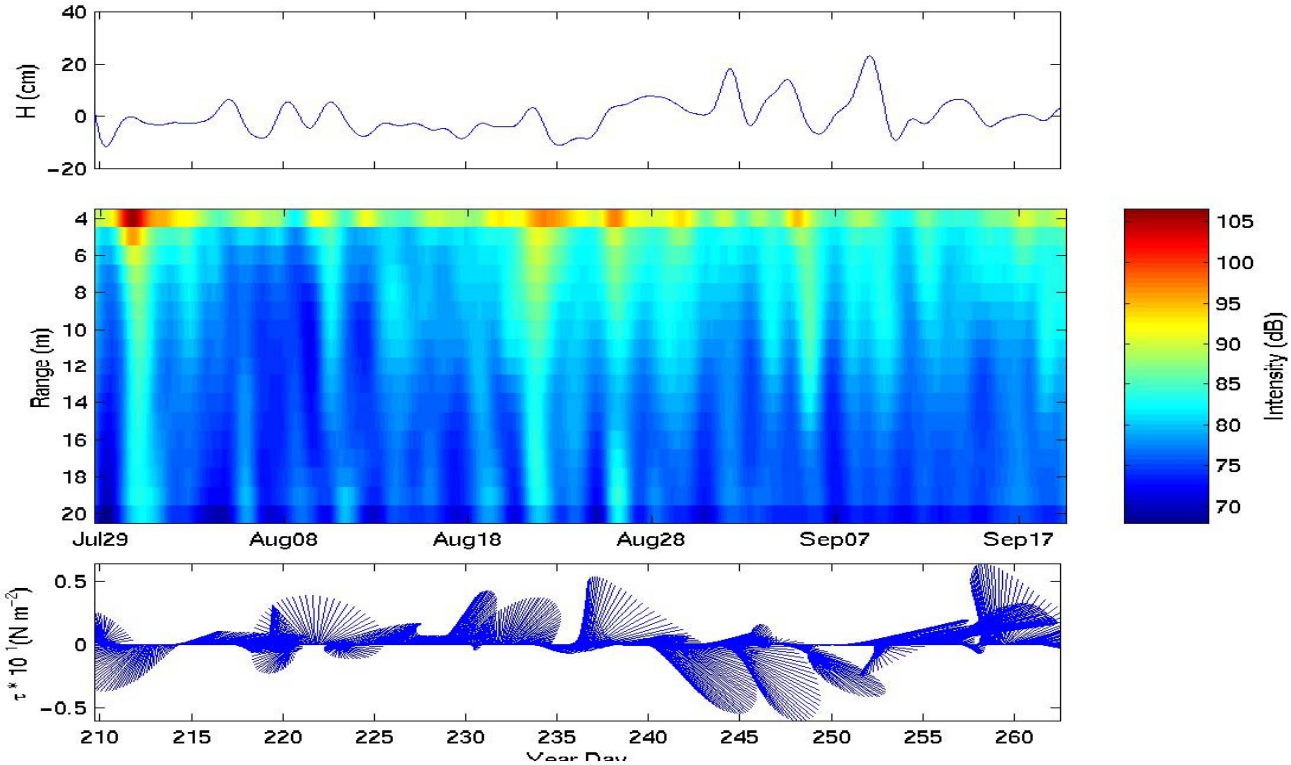

Figure 51: Subtidal backscatter intensity from N3. Included are the surface elevation (cm) and the magnitude of the wind stress (N m^{-2}).

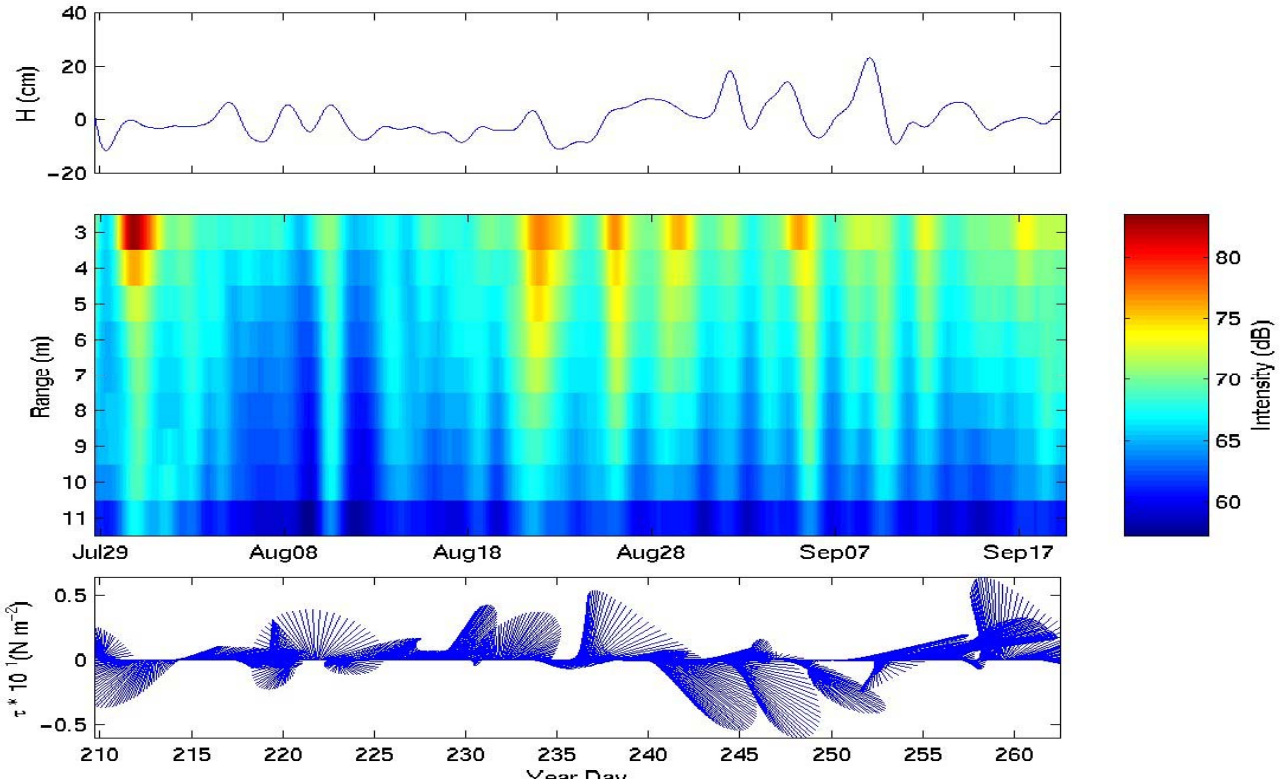

Figure 52: Subtidal backscatter intensity from N4. Included are the surface elevation (cm) and the magnitude of the wind stress (N m^{-2}).

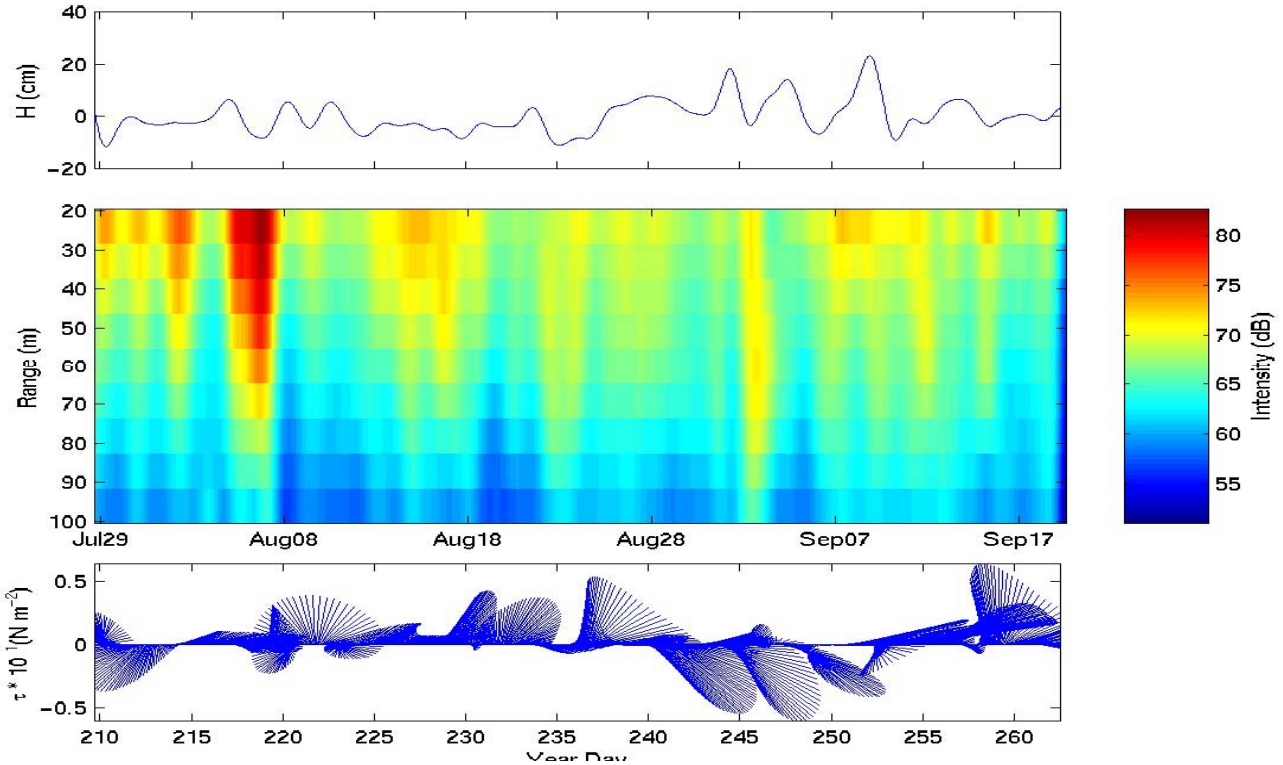

Figure 53: Subtidal backscatter intensity from H2. Included are the surface elevation (cm) and the magnitude of the wind stress (N m^{-2}).

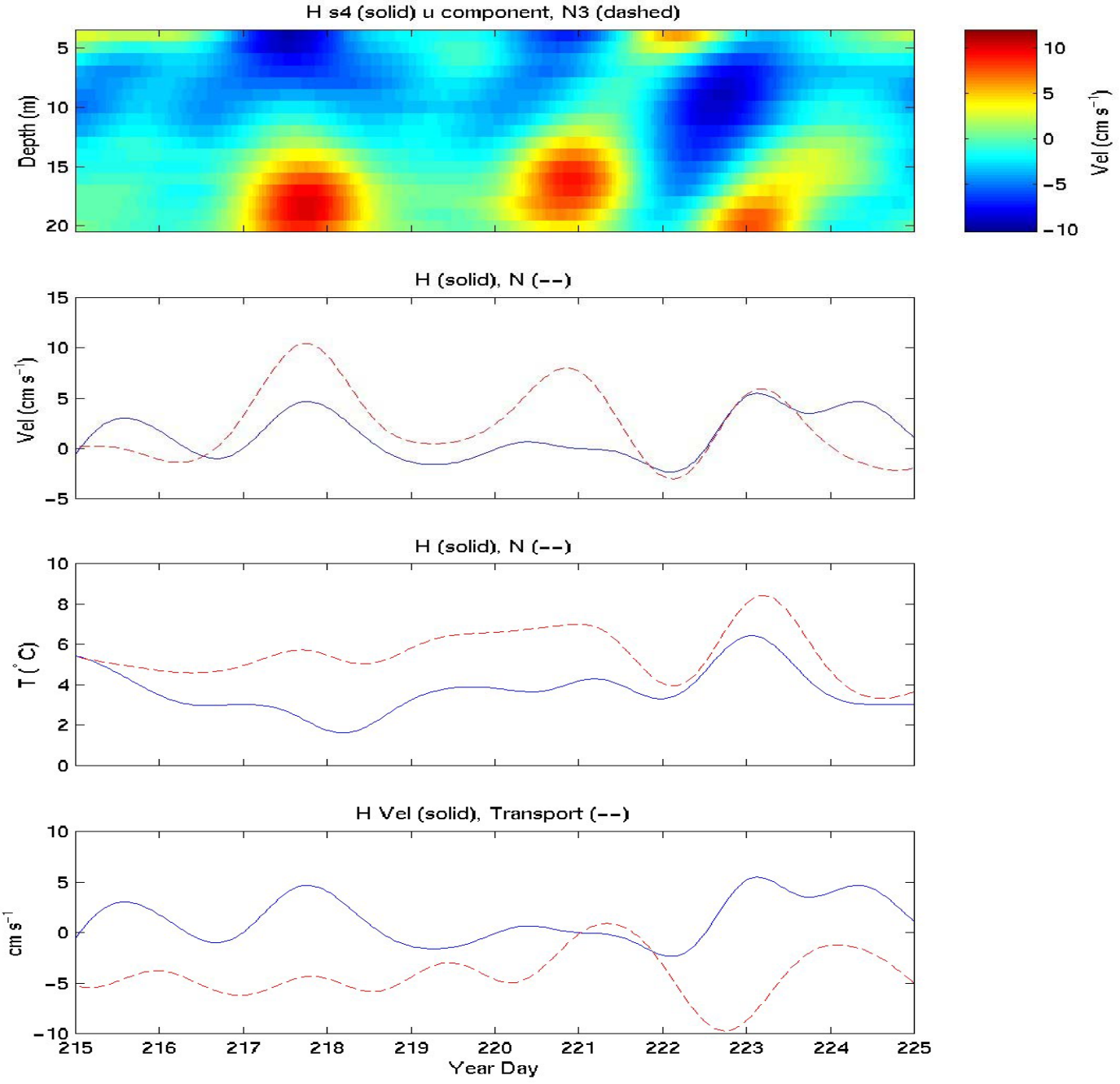

Figure 54: Effect of external forcing on the Narrows for year day 215 to 225. Subtidal current time series of the u component measured at N3 (a). The along channel velocity at 18 m depth from N3 (red) overlaid on the East/West velocity measured by the S4 (blue) at H1 (b). The temperature measured by the ADCP at N3 (red) with the temperature measured by the S4 at H1 (blue) (c). One tenth of the calculated transport (red) with the East/West component of velocity at H1 (blue) (d).

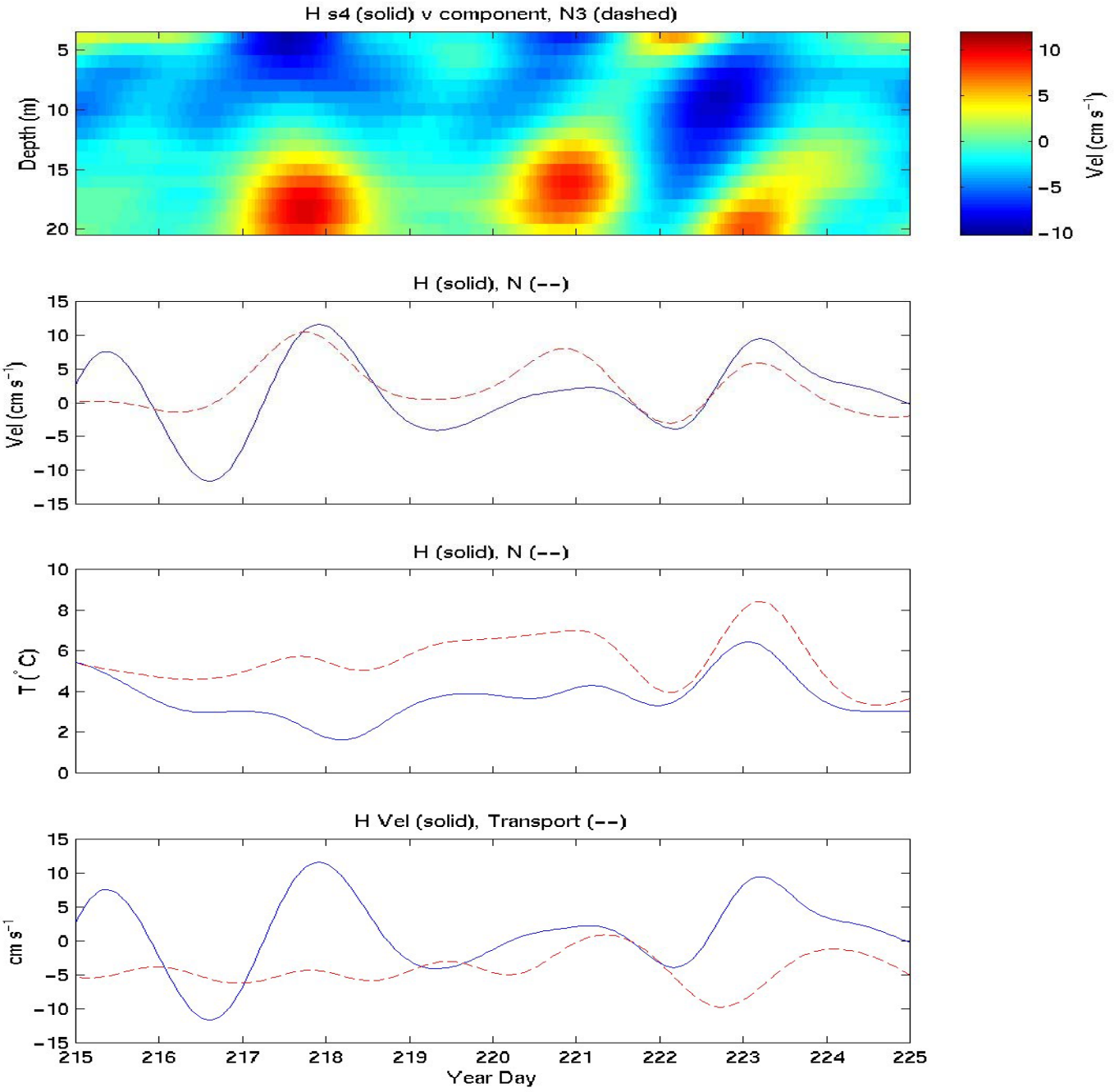

Figure 55: Effect of external forcing on the Narrows for year day 215 to 225. Subtidal current time series of the u component measured at N3 (a). The along channel velocity at 18 m depth from N3 (red) overlaid on the North/South velocity measured by the S4 (blue) at H1 (b). The temperature measured by the ADCP at N3 (red) with the temperature measured by the S4 at H1 (blue) (c). One tenth of the calculated transport (red) with the North/South component of velocity at H1 (blue) (d).

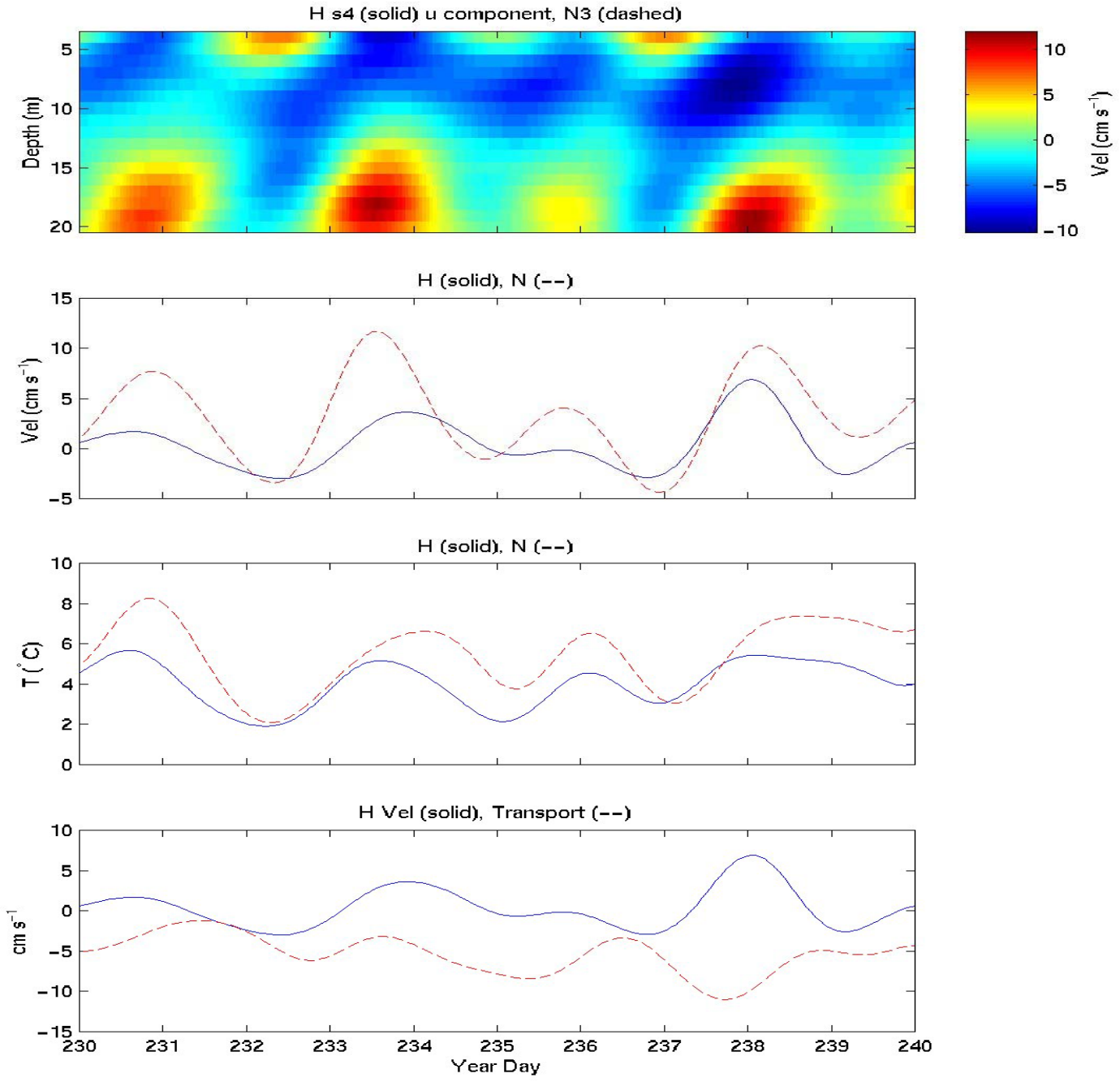

Figure 56: Effect of external forcing on the Narrows for year day 230 to 240. Subtidal current time series of the u component measured at N3 (a). The along channel velocity at 18 m depth from N3 (red) overlaid on the East/West velocity measured by the S4 (blue) at H1 (b). The temperature measured by the ADCP at N3 (red) with the temperature measured by the S4 at H1 (blue) (c). One tenth of the calculated transport (red) with the East/West component of velocity at H1 (blue) (d).

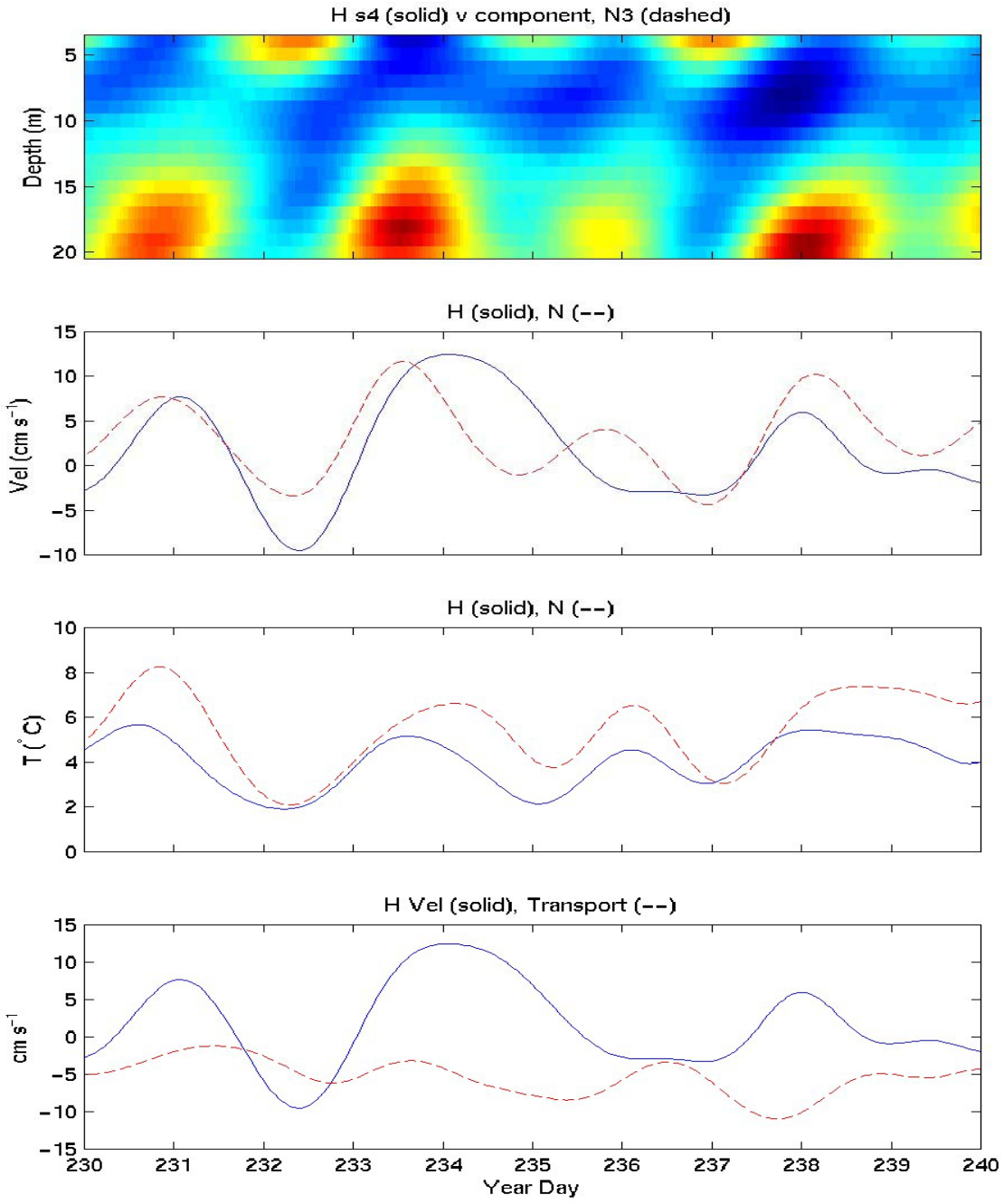

Figure 57: Effect of external forcing on the Narrows for year day 230 to 240. Subtidal current time series of the u component measured at N3 (a). The along channel velocity at 18 m depth from N3 (red) overlaid on the North/South velocity measured by the S4 (blue) at H1 (b). The temperature measured by the ADCP at N3 (red) with the temperature measured by the S4 at H1 (blue) (c). One tenth of the calculated transport (red) with the North/South component of velocity at H1 (blue) (d).